6-25-2010

Bidirectional mode-locked fiber ring laser

Alexandre Bittencourt de Pinho e Braga

Follow this and additional works at: https://digitalrepository.unm.edu/ose_etds

Bidirectional Mode-Locked
Fiber Ring Laser

by

Alexandre Bittencourt de Pinho e Braga

B.S., Optical Engineering, University of Arizona, 1998
M.S., Electrical Engineering, University of Arizona, 2000

DISSERTATION

Submitted in Partial Fulfillment of the
Requirements for the Degree of

Doctor of Philosophy
Optical Sciences and Engineering

The University of New Mexico

Albuquerque, New Mexico

May, 2010

ALEXANDRE BITTENCOURT DE PINHO E BRAGA
_____
Candidate

OSE - PHYSICS AND ASTRONOMY
_____
Department

This dissertation is approved, and it is acceptable in quality
and form for publication:

Approved by the Dissertation Committee:

_____, Chairperson

_____

_____

_____

_____

_____

_____

_____

_____

ii
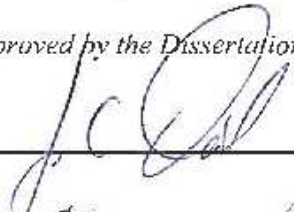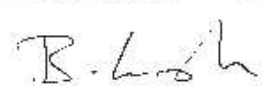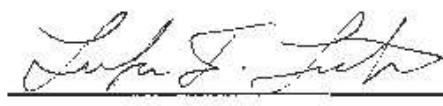
Dedication

I dedicate this dissertation to all those who shared with me the burden for all the years of my work in pursue of this degree. To my parents, for their encouragement and support. To Daniela, Tatsuo and Akira, for all the inspiring moments.

"A journey of a thousand miles begins with a single step." – Confusius

Acknowledgments

It is impossible to dissociate the success of this project from the people who so eagerly contributed, both professionally and emotionally, to its realization. The outcomes of this endeavor would have never become possible without the help of those who, during all my years of struggle, became essential in their support of the project. Therefore, I would like to take a few lines to mention some of these very special people. For instance, I can not thank enough senior engineer Ron Kay, of the CHTM's electronic shop, whose so persistent counseling has helped me in so many occasions find my way in the electronics world. I also could not forget to mention the students from Dr. Jain's group, including himself, for the allowances of equipment and all the help troubleshooting fiber optics. A very special thanks is also due to Dr. Shay, from Kirkland Air Force Base, Albuquerque, for his assistance with the splicing of some polarization maintaining fibers. I would also like to thank all my colleagues at the Diels' group for their support, and, in particular, to Xuan Luo and Koji Masuda. A special thanks is also due to some former members, such as Ladan Arissian, for her enormous motivating support, Andreas Velten, Mikael Hosatte, Olivier Challus, Marta Navarro, and Thien Trang Dang, from whom I have inherited the project, and to whom I owe a great piece of gratitude for the promptness of her email responses to the millions of questions I had. Furthermore, a want to show some appreciation for the members of my defense's committee - Dr. Ganesh Balakrishnan, Dr. Luke Lester, and Dr. Keith Lidke - for taking the time to review this manuscript, and providing useful feedback. Finally, and most important of all, I would like to thank my adviser, and friend, Professor Jean-Claude Diels, for his patience, guidance, encouragements, opportunity to succeed, and for never giving up on me[1].

---

[1]Through all the ups and downs of the project.

Bidirectional Mode-Locked Fiber Ring Laser

by

Alexandre Bittencourt de Pinho e Braga

ABSTRACT OF DISSERTATION

Submitted in Partial Fulfillment of the
Requirements for the Degree of

Doctor of Philosophy
Optical Sciences and Engineering

The University of New Mexico

Albuquerque, New Mexico

May, 2010

Bidirectional Mode-Locked Fiber Ring Laser

by

Alexandre Bittencourt de Pinho e Braga

B.S., Optical Engineering, University of Arizona, 1998

M.S., Electrical Engineering, University of Arizona, 2000

Ph.D., Optical Sciences and Engineering, University of New Mexico, 2010

Abstract

In modern day world, advances in technology are constantly pushing the limits of improvement in measurement accuracy. With each passing year, government agencies and contract companies increase investment in research of high precision, ultra sensitive, instruments. Over the last decade, advancements in ultrashort time scale optics have moved the field of metrology to the quantic realm. At this new scientific frontier, mode-locked lasers, with ultra sensitive phase measurement capabilities, have been playing an increasingly significant role. Among these highly sophisticated systems, mode-locked fiber lasers have been extensively explored in an unidirectional mode, while bidirectional remains a promising source for applications with considerable space for experimental innovation. In this project, efforts have been made to contribute to the scientific achievements in this area, with the implementation of

an innovative approach for bidirectional mode-locking of fiber lasers, as a potential source for intra-cavity phase interferometry. It consists of a passively driven active mechanism that both stabilizes the laser and controls the location of the crossing points of the counter-circulating pulses. For that purpose, the idea has been developed in both a theoretical and experimental level, with the design, construction, and testing of a fiber ring laser scheme capable of producing stable and independent (frequency unlocked) bidirectional pulses. In this manuscript, the description of the research is presented in seven separate chapters. The first chapter provides an overview of the project itself, the advantages of the controlling mechanism and the importance and practical applications of bidirectional mode-locked fiber lasers. Chapter two introduces the theoretical background necessary to understand pulse propagation in a nonlinear, birefringent, gain saturated optical fiber. In chapter three, the passive mechanism behind bidirectional mode-locking is detailed. Chapter four deals with the system's modeling and computer simulation, and chapter five explains the functional aspects of the self-regenerative system used to stabilize and control the laser pulsing. Chapter six describes the experimental setup itself, and presents the measured data results. Finally, chapter seven summarizes all the work done, emphasizing the consequences of the experimental findings, and laying out the foundations for future work.

Contents

Contents

Contents

Contents

List of Figures

List of Tables

Glossary

CW In capital letters, it stands for Continuous wave.

cw In lowercase letters, it stands for clockwise.

ccw Counter-clockwise.

EDF Erbium-doped fiber. A specialty type of fiber doped with Er^{+3} ions, and used as distributed gain medium in fiber optics systems.

DSF Dispersion-Shifted Fiber. A type of fiber specially designed to have its zero dispersion wavelength (frequency) value shifted from its normal value, which is located near 1.33μm.

ECL Emitter coupled logic circuit. An electronics technological standard used in high speed, low voltage level, circuitry.

$FWHM$ Full width at half maximum. A figure of merit used to assess the width of a pulse, whether given in time, space, or spectral domain.

NPR Nonlinear polarization rotation. A combined effect of self and cross phase modulation, that results in a intensity dependent rotation of a mode's state of polarization.

PBS Polarization beam splitter. A device that splits incoming light into its orthogonal polarization components.

Glossary

PC
Polarization controller. A device that mechanically modifies the state of polarization of the fiber's propagating mode.

PLL
Phase-Locked Loop. A self-stabilizing circuit architecture vary popular in telecommunications applications. It is used to track and regenerate signal frequencies or as frequency synthesizers.

PMF
Polarization maintaining fiber. A specialty type of fiber designed to maintain the state of polarization (SOP) of a propagating mode, by using a highly birefringent medium that split its "slow" and "fast" axis' orthogonal components, so that when linearly polarized light, aligned to either axis, is launched into the fiber, it comes out of it with its SOP unchanged.

SMF
Single mode fiber. A fiber that can only propagate a single mode for wavelengths $\lambda \geq 2\pi\sqrt{n_c^2 - n_{cl}^2}/V$, where V is known as the fiber's "vee" number (typically 2.45 for fused silica), and a, n_c, and n_{cl}, its core radius, core index, and cladding index, respectively.

SPM
Self-phase modulation. The nonlinear effect of a mode's phase modulation in response to its own intensity.

VCO
Voltage Controlled Oscillator. A device that produces A.C signals from D.C inputs.

VSWR
Voltage Standing Wave Ratio.

XPM
Cross-phase modulation. The nonlinear effect of a mode's phase modulation in response to the intensity of a secondary mode that is either orthogonal to it, or of a different wavelength.

Chapter 1

Project Overview

In recent years, ultrashort pulse phenomena has revolutionized optical frequency metrology [2], with interference of counter-propagating optical pulses at the very heart of ultra-sensitive phase measurements. Intracavity Phase Interferometry [10] has been demonstrated as the most sensitive phase detector, and applied to the detection of magnetic fields, inertial motion, displacements, and nonlinear index, just to name a few. So far, it has only been implemented with discrete components solid state lasers (i.e Ti:sapphire, Vanadate, and Optical Parametric Oscillators). All integrated fiber laser offers an attractive alternative, for being insensitive to air pollution, and able to operate with ultra-large cavities. There are however numerous challenges to overcome in implementing an all fiber IPI. A method has to be devised to control the crossing points of the two intracavity pulses, and prevent phase coupling between them (for instance by scattering) which would nullify the beat note to be measured (lock-in effect). Timing jitter issues are important, since the two pulse trains have to be interfered on a detector (i.e. the crossing points have to be the same at each round-trip). A first demonstration of IPI in an all fiber ring laser is presented, in which two pulses are circulated in opposite sense. This Chapter presents an overall idea of the entire project, with the following sections providing some background

information on its practical applications, previous work, and relevant aspects of the design.

1.1   Preliminary Work

The conception of the laser design was envisioned by Prof. Jean-Claude Diels[1], and part of it implemented by Thien Trang Dang, a former graduate student, at the Univ. of New Mexico. On her accounts, she was able to passively mode-lock the laser in one direction, obtaining pulses with round trip times of nearly 117ns and 100fs widths [35]. Figure 1.1 shows the setup used in the experiment, where bidirectional mode-locking of a fiber ring laser was attempted using a pair of amplitude modulators, the purpose of which will become clear in later Chapters. Sadly, bidirectional mode-locking was never fully stabilized, and that is precisely where the current project picks up.
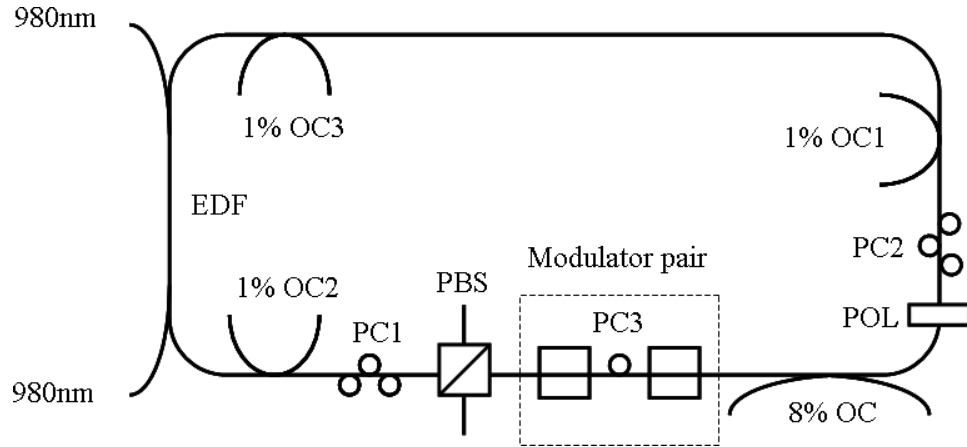
Figure 1.1: Schematics of fiber ring laser setup previously used to attempt bidirectional mode-locking.

---

[1]Physics and Astronomy Dept. at the Univ. of New Mexico.

1.2 Advantages of New Design

The design developed in this project offers the following advantages to the approach for bidirectional mode-locking of fiber ring lasers:

- **Generation of two independent pulses:** with two modulators firing at specific controlled times, two pulses can be generated completely independently, without the risk of frequency coupling between them (except at the location of their crossing points).

- **Active control of crossing point location:** using two modulators allows the location of the crossing points to be efficiently controlled. As will be later explained, a significant reduction of the dead band can be attained by choosing the pulses to cross at a point where the medium has the least amount of back-scattering.

- **Laser stabilization using self-regenerative system:** a regenerative system helps stabilize the laser by using the cavity's own round-trip time to synchronize the modulators, acting as a threshold gating controller through modulation of the system's loss (passive electronic control).

1.3 Applications to Metrology

The oldest application of ring lasers in metrology is inertial measurement — specifically rotation. The measurement is based on a phase shift introduced by rotation between two counter-rotating beams in a ring configuration; the so called "Sagnac effect". This phenomenon is named after Georges Sagnac [125, 126] who wrote the first publications about it in 1913. Figure 1.2 helps illustrate the principle.

In an absolute frame of reference (no acceleration), two counter-propagating optical waves will form a standing wave (Fig. 1.2a). As an observer moves counterclockwise about the frame, with an angular velocity Ω_{rot}, it perceives a "movement" of the standing wave's crests and troughs (fringes). This rate of change can be described in terms of a frequency change (also known as beat note):

$$\Delta\nu = \frac{v}{\lambda/2} = \frac{R\Omega_{rot}}{\lambda/2}, \tag{1.1}$$

where "v" is the tangential "linear" velocity of the observer, "λ" the wavelength of the optical wave, and "R" the radius of the ring laser.

(a) Absolute Frame   (b) Laboratory Frame
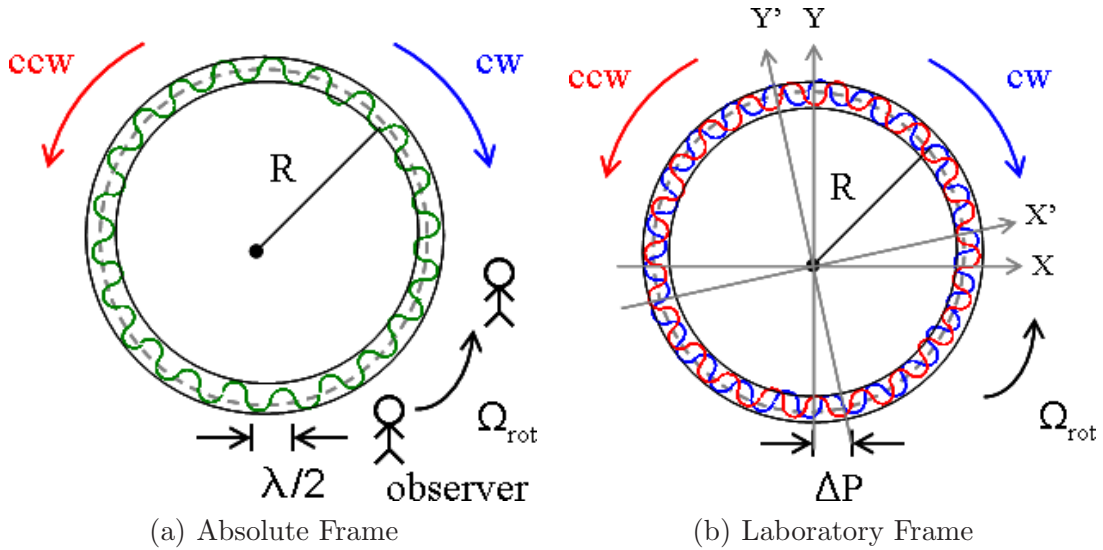
Figure 1.2: Sagnac Effect: description of the effect in two different inertial frames of reference: (a) an absolute frame, with no acceleration, where an observer rotates about it counter-clockwisely, and (b) the laboratory frame of reference where the ring laser itself rotates counter-clockwisely.

Similarly, one can think of this change in terms of the "Doppler Shift", i.e the change in fringe rate (frequency), as the observer looks forward (blue shift "ν_b") or backwards (red shift "ν_r") at the fringe pattern,

$$\Delta\nu = \nu_b - \nu_r = 2\frac{v}{c}\nu_{opt} = 2(\frac{\Omega R}{c})(\frac{c}{\lambda}) = \frac{R\Omega_{rot}}{\lambda/2}, \tag{1.2}$$

where "c" is the speed of light in vacuum, "ν_{opt}" is the optical frequency, and $\nu_b = \nu_{opt}(1 + v/c)$ and $\nu_r = \nu_{opt}(1 - v/c)$ are the "blue" and "red" shifts, respectively.

Another way of looking at it is at the laboratory frame, which is represented by the coordinates (X, Y) in Fig. 1.2b. As the laser rotates about an axis Z orthogonal to the plane of the laser, at an angular velocity "Ω_{rot}", the axis (X, Y) come into the position (X', Y'). In this laboratory frame, the apparent round trip time of the clockwise beam (red) is given by:

$$t_{cw} = \frac{2\pi R}{c - v} = \frac{2\pi R}{c - R\Omega_{rot}}. \tag{1.3}$$

As light travels in the direction of rotation of the frame, it takes longer for the clockwise beam (cw) to complete a round trip than the normal round trip time $t_{RT} = 2\pi R/c$. Similarly, the total transit round trip time of the counter-clockwise (ccw) beam, in the laboratory frame, is given by:

$$t_{ccw} = \frac{2\pi R}{c + v} = \frac{2\pi R}{c + R\Omega_{rot}}. \tag{1.4}$$

Because the frame is rotating in the direction opposite to the light, it takes less time for the cw beam to complete the round trip. The round trip time difference between the counter-propagating beams is, therefore:

$$\Delta t = t_{cw} - t_{ccw} = \frac{2\pi R}{c - v} - \frac{2\pi R}{c + v} = \frac{4A\Omega_{rot}}{c^2 - v^2} \simeq \frac{4A\Omega_{rot}}{c^2}, \tag{1.5}$$

where $A = \pi R^2$ is the area of the loop, and the last term is an approximation for the case of practical interest where $(R\Omega_{rot})^2 << c^2$. The associated optical path length difference between the counter-propagating pulses "ΔP" is

$$\Delta P = c\Delta t = \frac{4A\Omega_{rot}}{c}, \tag{1.6}$$

which leads to a phase difference $\Delta\varphi = k_0\Delta P$ between the counter-propagating beams, where $k_0 = 2\pi n_0/\lambda$ is an average wave vector in the cavity, assumed to have an average index "n_0".

In terms of frequency difference,

$$\Delta\nu = \frac{\Delta\varphi}{2\pi\tau_{RT}} = \frac{R\Omega_{rot}}{\lambda/2}, \tag{1.7}$$

which demonstrates that no matter how one looks at it, it will always lead to the same result (Eqs.(1.1, 1.2, and 1.7)).

1.3.1 Fiber Laser Gyroscope

The phase difference "$\Delta\varphi$" can be measured as a modulation of the intensity when the two counter-circulating beams are made to interfere on a detector. This is the measurement performed with the conventional Fiber Optical Gyroscope (FOG), which is a *passive* Sagnac interferometer (Fig. 1.4b). Considerable more sensitivity can be achieved in an *active* ring laser, where the phase shift per round trip $\Delta\varphi/\tau_{RT}$ results in a frequency difference:

$$\Delta\nu = \frac{\Delta\varphi}{2\pi\tau_{RT}} = \nu\frac{\Delta P}{P} = \frac{4A}{P\lambda}\Omega_{rot}. \tag{1.8}$$

The frequency difference "$\Delta\nu$" can be measured (as a beat note between the two outputs of the ring laser) with much more precision and accuracy than a phase difference (an intensity measurement). One might then wonder why the "FOG" has been developed, rather than an active laser gyroscope. The answer is that all gyroscope manufacturers have so far only considered *continuous wave* (CW) ring lasers, where crossing of the counter-propagating waves at a scattering interface[2], may nullify the beat note. When two counter-propagating optical signals cross at a scattering medium, a small reflected portion from each beam is imparted to the phase of the other, creating what is known as the "lock-in effect".

Figure 1.3a illustrates the effect. At the crossing surface, a small reflected percentage of the cw beam (blue) interacts with the ccw beam, and vice-versa. This

---

[2]In the case of a fiber, the scattering surface can be a fusion splice between two fibers.

interaction can be described by the set of coupled differential equations:

$$\frac{\partial E_{cw}}{\partial(t/\tau_{RT})} = -re^{i\epsilon}E_{ccw}, \tag{1.9a}$$

$$\frac{\partial E_{ccw}}{\partial(t/\tau_{RT})} = re^{i\epsilon}E_{cw}, \tag{1.9b}$$

where "r" represents the back-scattering coefficient, and "ϵ" a small phase factor.

(a) Lock-in Effect (b) Gyro Response
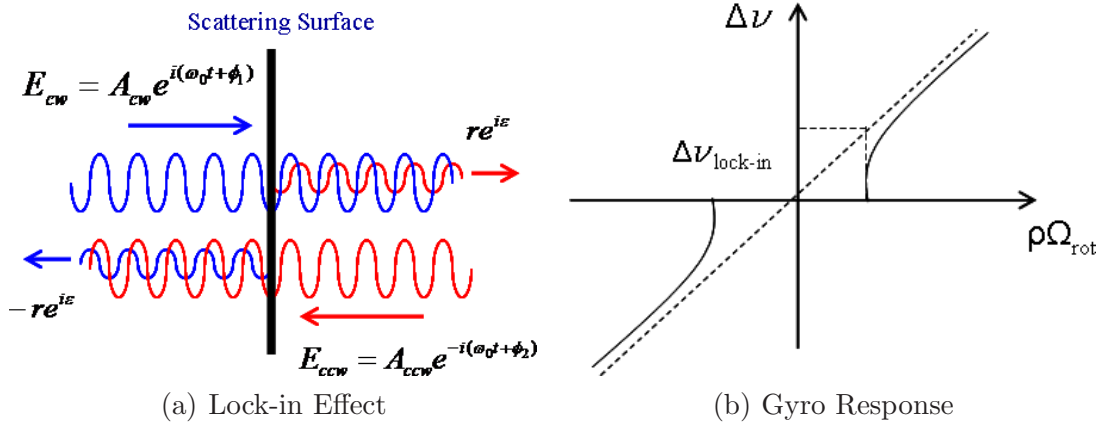
Figure 1.3: Illustration of frequency lock-in effect between counter-propagating optical waves: (a) wave interaction on a back-scattering surface, and (b) effects on the gyroscopic response of the system.

Solutions to these equations lead to a phase relation which, written in terms of a frequency difference, results in another equation describing the gyroscopic response of the system [40]:

$$\Delta\nu = \frac{\partial}{\partial t}(\frac{(\phi_2 - \phi_1)}{2\pi}) = \rho\Omega_{rot} - \frac{r}{2\pi\tau_{RT}}[\sin(\phi_2 - \phi_1 - \epsilon) + \sin(\phi_2 - \phi_1 + \epsilon)], \tag{1.10}$$

where $\rho = 4A/P\lambda$ is called the "geometric factor", as seen in Eq. (1.8).

In Eq. (1.10), the first term on the right hand side corresponds to the "ideal" linear gyroscopic response (the straight line in Fig. 1.3b). Because of lock-in effects, a correction - the second term on the right hand side of the equation - is added,

and the actual response looks like the asymptotic curve shown in Fig. 1.3b. This correction leads to a region of "no response" to rotation, also known as the "dead band". Solving Eq. (1.10) for $\Delta\nu = 0$ leads to a frequency difference value:

$$\Delta\nu_{lock-in} = \frac{r}{2\pi\tau_{RT}},\qquad\qquad(1.11)$$

which is often referred to as the "lock-in", or "dead band", frequency.

According to Eq. (1.8), the larger the dimension of the ring laser (ratio of A/P), the larger the beat note. But then also, the larger the lengths over which the counter-circulating beam scatter into each other, the larger the "lock-in effect". In the case of bidirectional CW laser, this effect is aggravated by the long interaction length between the counter-circulating beams. The same is not true for the case of mode-locked lasers, specially short ones, where the interaction is limited by the pulse widths. It has been demonstrated [143, 110] that, with mode-locked lasers, the dead band is only created by the back-scattering coefficient "r" *over the length of the pulses at their crossing point*, and therefore the dead band is no longer proportional to the perimeter of the ring laser. In addition to that, in ML lasers, the pulses can be made to cross outside the scattering medium.

As far as fiber ring lasers are concerned, one can appreciate its advantages over conventional ML lasers by looking at Eq. (1.7). With fiber lasers, it is easier to increase the sensitivity by simply increasing "R" (it is easy to create large loops with fibers). Furthermore, as indicated in Eq. (1.11), by increasing the loop size, and therefore the round-trip time, one can reduce the "$\Delta_{lock-in}$" as well. Table 1.1 shows a comparison of some typical dead band values for CW (commercially available) and ML fiber lasers, where the crossing point occurs in SMF (SiO_2) material. For a typical SMF, the value of the back-scattering coefficient is r=-2.76x10^{-63} per 1nsec pulse width. Using Eq. (1.11), and a round-trip time τ_{RT}=200nsec, the dead band values can be estimated for pulse widths of 100ps and 100fs, which are not uncommon

---

[3]See Appendix B for an explanation on how the value of "r" is determined.

in ML lasers. From these values, it is evident the advantage of using ML instead of CW lasers for gyroscopy.

	CW He-Ne Laser	ML Fiber Laser
DEAD BAND	10^3Hz	2.2Hz 1ns $2.2\text{x}10^{-1}$Hz 100ps $2.2\text{x}10^{-4}$Hz 100fs

Table 1.1: Comparison of dead band figures between a typical CW based gyroscope (He-Ne laser) and a mode-locked based gyroscope made with single mode fiber (SMF) material.

It is not the purpose of this dissertation to make an exhaustive report on the near infinite number of publications on laser gyroscopes. Such a review has been published by Chow *et al.* [28] and Chesnoy [25], on ring laser gyros, and Bergh *et al.* [14] and Jeong *et al.* [75], on fiber optic gyros. Other information are also available in more specific experimental reports [73, 83, 74, 121, 87, 69].

1.3.2   Magnetic Susceptibility Sensor

There is also another advantage in using short pulses: because they occupy different points in space at different times, they can be used to probe considerably more effects than just rotation. Pulses conserve their individuality during a round-trip. Hence, any effect that produces a "ΔP" in Eq. (1.8), such as linear and nonlinear index modification, acceleration, *etc* ... can be measured. For all sensor applications other than rotation sensing, Eq. (1.8) suggests that, the smaller the laser, the higher the sensitivity (since the beat note "$\Delta \nu$" is inversely proportional to the round-trip

time). There is however a notable exception, that of a magnetic susceptibility sensor, where large size offers an advantage.

A magnetic susceptibility sensor can be designed to use a beat note to measure a local magnetic field change by relating the change in frequency "$\Delta\nu$" to the change in magnetic susceptibility "$\Delta\mu$". The change in frequency is related to the change in magnetic susceptibility by $\Delta\nu/\nu = \Delta\mu/\mu$. In a certain application, a magnetic susceptibility sensor has been proposed as part of an effort for detection of ground water through ultra-sensitive magnetic measurements [38, 39]. The idea was to track changes in inductance of an LC circuit oscillator, due to local changes in magnetic susceptibility, from the change in the beat note produced from the counter-propagating modes of the optical oscillator. Figure 1.4a shows the schematics of the proposed experiment using phase measurements from a bidirectionally mode-locked fiber ring laser.

(a) Magnetic Sensor.   (b) Fiber Laser Gyroscope.
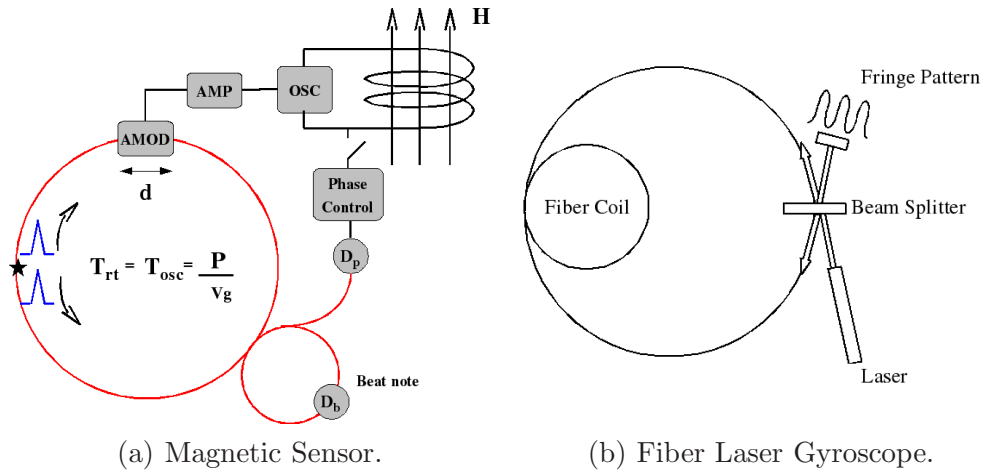
Figure 1.4: Two practical applications of ultrashort phase measurements to the field of metrology: (a) Magnetic susceptibility sensor (after Ref. [38]), and (b) Fiber laser gyroscope (after Ref. [28]).

Chapter 2

Theoretical Model

This chapter provides a theoretical background on pulse propagation in an optical fiber. It presents a comprehensive set of equations which are suitable to describe fiber optic propagation in a very generic way. It is divided in 4 sections. The first section introduces the wave equation in the context of the scalar Nonlinear Schrödinger Equation (NLSE), which helps understanding pulse propagation in a nonlinear dispersive medium, and presents a special class of solutions in the form of optical solitons. Section 2 broadens the scope of section 1 to the vector case, where the effects of Cross-Phase Modulation (XPM) on pulse propagation are described, in terms of the Coupled Nonlinear Schrödinger Equations (CNLSE). Consequently, this section also extends the discussion of soliton solutions to the case of vector solitons. In section 3, the effects of adding dopants to the host medium of a fiber are addressed, and how it modifies pulse propagation with the introduction of gain saturation, and gain dispersion in what is commonly known as the Ginzburg-Landau equation. It also discusses solutions to the propagation equation in the form of auto-solitons. Finally, the last section combines the results of the previous sections to produce a single set of generalized equations, which are the backbone of the numerical model/computer simulation of Chapter 4.

2.1   Nonlinear Wave Equation

In this section, the basic scalar Nonlinear Schrödinger Equation (NLSE), which is used to describe pulse propagation in a nonlinear dispersive medium, is derived. It begins with the derivation of the nonlinear wave equation and the effects of nonlinearity in the permittivity of the propagating medium. Later, it presents a description of an important class of solutions known as solitons. Unless otherwise specified, vector quantities will be described by bold-faced letters.

2.1.1   Nonlinear Schrödinger Equation (NLSE)

The starting point in any wave equation derivation are Maxwell's equations. From Faraday's law, the electric field vector $\mathbf{E}$ can be written in terms of the magnetic flux density $\mathbf{B}$,

$$\nabla \times \mathbf{E} = -\frac{\partial \mathbf{B}}{\partial t} = -\frac{\partial (\mu_o \mathbf{H} + \mathbf{M})}{\partial t}, \qquad (2.1)$$

where "μ_o" is the permeability of free space, $\mathbf{H}$ is the magnetic field vector, and $\mathbf{M}$, which is zero for fused silica (SiO_2) fibers, is the induced magnetic polarization vectors. Applying $\nabla \times$ on both sides of Eq. (2.1), and using the Ampere's law, which relates the magnetic field vector to the displacement vector $\mathbf{D}$,

$$\nabla \times \nabla \times \mathbf{E} = \nabla(\nabla.\mathbf{E}) - \nabla^2\mathbf{E} = -\mu_o \frac{\partial}{\partial t}(\nabla \times H) = -\mu_o \frac{\partial}{\partial t}[\mathbf{J}_f + \frac{\partial \mathbf{D}}{\partial t}], \qquad (2.2)$$

where the current density vector $\mathbf{J_f}$ is zero for SiO_2 fibers and, the electric displacement vector can be written as $\mathbf{D} = \epsilon_o \mathbf{E} + \mathbf{P}$, with $\mathbf{P}$ being the induced polarization vector, and "ϵ_o" the permittivity of free space. Equation. 2.2, then, takes the form,

$$\nabla(\nabla.\mathbf{E}) - \nabla^2\mathbf{E} = -\mu_o \frac{\partial^2}{\partial t^2}[\epsilon_o \mathbf{E} + \mathbf{P}] = -\mu_o\epsilon_o \frac{\partial^2}{\partial t^2}\mathbf{E} - \mu_o \frac{\partial^2}{\partial t^2}\mathbf{P}. \qquad (2.3)$$

Since there are no free charges in SiO_2 fiber (i.e $\nabla.\mathbf{D} = \rho_f = 0$), it can be shown that the term $\nabla(\nabla.\mathbf{E})$ in Eq. (2.3) is also zero. Making the substitution $\mu_o\epsilon_o = 1/c^2$,

where "c" is the speed of light in vacuum, Eq. (2.3) becomes,

$$(\nabla^2 - \frac{1}{c^2}\frac{\partial^2}{\partial t^2})\mathbf{E} = \mu_o\frac{\partial^2}{\partial t^2}\mathbf{P} = \mu_o\frac{\partial^2}{\partial t^2}(\mathbf{P}_L + \mathbf{P}_{NL}), \tag{2.4}$$

where vector fields $\mathbf{P_L}$, and $\mathbf{P_{NL}}$ are the linearly, and nonlinearly induced polarizations components, respectively.

The linear component $\mathbf{P_L}(\mathbf{r}, \mathbf{t})$ is related to $\mathbf{E}(\mathbf{r}, t)$ by the causal relation,

$$\mathbf{P}_L(\mathbf{r}, t) = \epsilon_o \int_{-\infty}^{\infty} \chi^{(1)}(t').\mathbf{E}(\mathbf{r}, t - t')dt', \tag{2.5}$$

where "$\chi^{(1)}$" is the first order susceptibility of the medium.

Likewise, $P_{NL}(\mathbf{r}, t)$ relates to $\mathbf{E}(\mathbf{r}, t)$ by the causal triple integral,

$$\mathbf{P}_{NL}(\mathbf{r}, t) = \epsilon_o \iiint_{-\infty}^{\infty} \chi^{(3)}(t_1, t_2, t_3) \vdots \mathbf{E}(\mathbf{r}, t - t_1)\mathbf{E}(\mathbf{r}, t - t_2)\mathbf{E}(\mathbf{r}, t - t_3)dt_1 dt_2 dt_3, \tag{2.6}$$

where "$\chi^{(3)}$" is the third order susceptibility of the medium, operator $\vdots$ denotes a tensor product, and $t_1 < t_2 < t_3$.

It is assumed for now that the fields maintain linear polarization along the $\hat{\mathbf{x}}$ axis, and that the Slowly Varying Envelope Approximation (SVEA) applies, i.e that the ratio of the pulse's spectral width "$\Delta\omega$" to its optical (light) frequency "ω_l" is such that $\Delta\omega/\omega_l << 1$. The electric field is written as:

$$\mathbf{E}(\mathbf{r}, t) = \hat{\mathbf{x}}\frac{1}{2}\{\mathcal{E}(\mathbf{r}, t)\exp\{i(\omega_l t - k_o z)\} + c.c\} = \hat{\mathbf{x}}\frac{1}{2}\{E(\mathbf{r}, t)\exp\{\omega_l t\} + c.c\}, \tag{2.7}$$

where $\mathbf{r} = x\hat{\mathbf{x}} + y\hat{\mathbf{y}} + z\hat{\mathbf{z}}$ is the position vector in Cartesian coordinates, $\mathcal{E}(r, t)$ is the field's amplitude envelope, E is the complex field envelope, "k_o" the propagation constant, and "c.c" stands for complex conjugate. Similarly, the linear polarization vector is written,

$$\mathbf{P}_L(\mathbf{r}, t) = \hat{\mathbf{x}}\frac{1}{2}\{\mathcal{P}_L(\mathbf{r}, t)\exp\{i(\omega_l t - k_o z)\} + c.c\} = \hat{\mathbf{x}}\frac{1}{2}\{P_L(\mathbf{r}, t)\exp\{\omega_l t\} + c.c\}. \tag{2.8}$$

If the nonlinear response is assumed to be instantaneous, an argument which is valid for pulse widths $\simeq 1\text{ps}$[1], the $\chi^{(3)}$ term in Eq. (2.6) can be written in terms of $\delta(t')$ functions. As a consequence, the triple integral collapses, and $\mathbf{P}_{NL}$ becomes,

$$\mathbf{P}_{NL} \simeq \epsilon_o \chi^{(3)} \colon \mathbf{E}(\mathbf{r},t)\mathbf{E}(\mathbf{r},t)\mathbf{E}(\mathbf{r},t). \tag{2.9}$$

Applying $\mathbf{E}(\mathbf{r},t)$, as written in Eq. (2.7), with $\mathbf{P}_{NL}(\mathbf{r},t)$ written as in Eq. (2.8), to Eq. (2.9), the resulting complex field envelope $P_{NL}(\mathbf{r},t)$ becomes:

$$P_{NL}(\mathbf{r},t) = \epsilon_o \epsilon_{nl} E(\mathbf{r},t) = \epsilon_o \frac{3}{4}\chi^{(3)}_{xxxx}|E(\mathbf{r},t)|^2 E(\mathbf{r},t), \tag{2.10}$$

where the third harmonic term is neglected in SiO_2, and a nonlinear contribution to the dielectric constant can be defined as $\epsilon_{nl} = \frac{3}{4}\chi^{(3)}_{xxxx}|E(\mathbf{r},t)|^2$.

In order to solve the nonlinear wave equation, it is convenient to work on the frequency domain, using the Fourier transform defined as,

$$\tilde{E}(\mathbf{r},\Omega) = \mathcal{F}\{E(\mathbf{r},t)\} = \int_{-\infty}^{\infty} E(\mathbf{r},t)\exp\{-i\Omega t\}dt, \tag{2.11}$$

where "Ω" represents the frequency variable. Henceforth, unless stated otherwise, the tilde sign denotes spectral representation.

Plugging Eqs. (2.5) and (2.10) into Eq. (2.4), Fourier transforming it, and considering, for now, $P_{NL}(\mathbf{r},t)$ as a small pertubation, Eq. (2.4) can be written, in scalar form, and after some simplification, as:

$$[\nabla^2 - \frac{(i\Omega)^2}{c^2}]\tilde{E}(\Omega_s) - \mu_o\epsilon_o(i\Omega)^2[\tilde{\chi}^{(1)}(\Omega)\tilde{E}(\Omega_s) + \epsilon_{nl}\tilde{E}(\Omega_s)] = 0, \tag{2.12}$$

where $\Omega_s = \Omega - \omega_l$ is the shifted-frequency variable, $\tilde{\chi}^{(1)}(\Omega)$ is the linear susceptibility in the frequency domain, and $\tilde{E}(\Omega_s)$ the Fourier transform of the amplitude field $E(\mathbf{r},t)$, as defined in Eq. (2.7). Re-arranging terms in Eq. (2.12), it becomes,

$$(\nabla^2 + \epsilon(\Omega)\frac{\Omega^2}{c^2})\tilde{E}(\mathbf{r},\Omega - \omega_l) = 0, \tag{2.13}$$

---

[1]In SiO_2 fibers, the electronic contribution to $\chi^{(3)}$ occurs at a 10fs time scale, and the Raman response at 60-70fs range.

where the permittivity $\epsilon(\Omega)$ is, therefore, given by:

$$\epsilon(\Omega) = 1 + \tilde{\chi}^{(1)}(\Omega) + \frac{3}{4}\chi^{(3)}_{xxxx}|E(\mathbf{r},t)|^2, \qquad (2.14)$$

or, as defined in terms of the refractive index,

$$\epsilon(\Omega) = (n(\Omega) + n_2|E|^2 + i\frac{\alpha(\Omega) + \alpha_2|E|^2}{2k_o})^2 = (n(\Omega) + \Delta n)^2. \qquad (2.15)$$

Here "$n(\Omega)$" and "n_2" are the linear and nonlinear index of refraction, and "$\alpha(\Omega)$" and "α_2" the linear and two photon absorption coefficients, respectively. Using Eqs. (2.14) and (2.15), they are found to be: $n(\Omega) = 1 + \frac{1}{2}\Re\{\tilde{\chi}^{(1)}(\Omega)\}$, $\alpha(\Omega) = \frac{\omega_l}{c}\Im\{\tilde{\chi}^{(1)}(\Omega)\}$, $n_2 = \frac{3}{8}\Re\{\chi^{(3)}_{xxxx}\}$, and $\alpha_2 = \frac{3\omega_l}{4c}\Im\{\chi^{(3)}_{xxxx}\}$, with $\Re$ and $\Im$ denoting real and imaginary parts, respectively. The two photon absorption coefficient α_2 is often neglected in fused silica fibers.

Generally, because of its geometry, it is convenient to write the wave equation (2.13) in cylindrical coordinates as,

$$(\frac{\partial^2}{\partial\rho^2} + \frac{1}{\rho}\frac{\partial}{\partial\rho} + \frac{1}{\rho^2}\frac{\partial^2}{\partial\phi^2} + \frac{\partial^2}{\partial z^2} + n^2 k_0^2)\tilde{\mathbf{E}} = 0, \qquad (2.16)$$

where a solution of the type $\tilde{E}_z = A(\Omega_s)F(\rho)\exp\{im\phi\}\exp\{-ik_o z\}$, chosen so that the $\tilde{E}_\rho$ and $\tilde{E}_\phi$ components can be derived from it ("m" being an integer), would lead to spatial eigen-modes of Bessel and modified Bessel functions.

In a different approach, a 2-D Gaussian function $F(x,y) = \exp\{-(x^2 + y^2)/w_o^2\}$ can be used as an approximation for the fundamental mode, where the fundamental radius "w_o" (beam radius at $1/e^2$ of the intensity) is related to the fiber's core radius "a" according to a chosen polynomial approximation model. For instance, in the "Myslinski Model" [107],

$$w_o = a(0.761 + \frac{1.237}{V^{1.5}} + \frac{1.429}{V^6}), \qquad (2.17)$$

where the normalized frequency is defined as $V = \frac{2\pi}{\lambda}a\text{NA} = \frac{2\pi}{\lambda}a\sqrt{(n_{co}^2 - n_{cl}^2)}$, with "NA" being the numerical aperture, and "n_{co}" and "n_{cl}" the index of refraction of

15

the core and cladding, respectively. For single mode fiber V is 2.405, which is the zeroth order radius of the Bessel function solution $F(\rho)$ of Eq. (2.16).

When a solution of the type $\tilde{E}(\mathbf{r}, \Omega_s) = F(x, y)\tilde{A}(z, \Omega_s)\exp\{-ik_o z\}$, in Cartesian coordinates, is plugged into the nonlinear wave equation (2.13), it leads, after much simplification, to a set of two equations:

$$[\nabla_t^2 + (\epsilon(\Omega)(\frac{\Omega}{c})^2 - \tilde{k}^2)]F(x, y) = 0, \tag{2.18a}$$

$$2ik_o\frac{\partial\tilde{A}(z, \Omega_s)}{\partial z} - [\tilde{k}^2 - k_o^2]\tilde{A}(z, \Omega_s) = 0. \tag{2.18b}$$

Here the second derivative $\partial^2\tilde{A}/\partial z^2$ is neglected under the SVEA assumption, and the "t" subscript in ∇_t^2 stands for "transverse" operation. Using the formalism of Eq. (2.15), and first-order perturbation theory [106], Eq. (2.18a) can be solved for $\tilde{k}$, giving:

$$\tilde{k}(\Omega) = k(\Omega) + \Delta k = k(\Omega) + \frac{k_o\iint_{-\infty}^{\infty}(n_2|E|^2 + i\frac{\alpha}{2k_o})|F(x', y')|^2 dx'dy'}{\iint_{-\infty}^{\infty}|F(x', y')|^2 dx'dy'}. \tag{2.19}$$

Since the main interest here is to study pulse evolution along a fiber in the z-direction, the primary concern is to find a solution to Eq. (2.18b), which can be written in the form,

$$\frac{\partial\tilde{A}}{\partial z} = -i\frac{(\tilde{k}^2(\Omega) - k_o^2)}{2k_o}\tilde{A} \simeq -i[\tilde{k}(\Omega) - k_o]\tilde{A}, \tag{2.20}$$

where $\tilde{k}^2(\Omega) - k_o^2 \simeq 2k_o(\tilde{k}(\Omega) - k_o)$, and, expanding the term $k(\Omega)$ of Eq. (2.20) in a Taylor Series about the light frequency ω_l,

$$k(\Omega) = k_o + k_1(\Omega - \omega_l) + \frac{1}{2}k_2(\Omega - \omega_l)^2 + ..., \tag{2.21}$$

with, $k_n = \frac{d^{(n)}}{d\Omega^n}k|_{\Omega=\omega_l}$, n integer. When $k(\Omega)$ and Δk are placed back into Eq. (2.20), and the equation is inverse Fourier transformed, using the definition,

$$E(\mathbf{r}, t) = \mathcal{F}\{\tilde{E}(\mathbf{r}, \Omega)\} = \frac{1}{2\pi}\int_{-\infty}^{\infty}\tilde{E}(\mathbf{r}, \Omega)\exp\{i\Omega t\}d\Omega. \tag{2.22}$$

All the terms containing $(\Omega - \omega_l)^n$, with $n = 1, 2, ..$, become $(-i\frac{\partial}{\partial t})^n$ in the time domain. The pulse evolution equation then becomes:

$$\frac{\partial}{\partial z}A(z,t) = -i[k_o + k_1\frac{-i\partial}{\partial t} + \frac{1}{2}k_2\frac{(-i)^2\partial^2}{\partial t^2} + ... + \Delta k - k_o]A(z,t), \qquad (2.23)$$

where Δk, as given in Eq. (2.19), can be reduced to the form,

$$\Delta k = k_o(n_2\frac{|A|^2}{A_{ef}} + i\frac{\alpha}{2k_o}) = \gamma|A|^2 + i\frac{\alpha}{2}. \qquad (2.24)$$

Here, the term $|A|^2$ has units of power (W) and the nonlinear coefficient $\gamma = n_2k_o/A_{ef}$ units of m^{-1}-W^{-1}. Using these units, the nonlinear index n_2 is given in m^2-W^{-1}. It can also be expressed in units of m^2-V^{-2}, in which case the field A must be expressed in units of V-m^{-1}. Unless otherwise specified, the units of field used throughout this text are W$^{\frac{1}{2}}$. The effective core area A_{ef} has units of m^2 and is formally defined as,

$$A_{ef} = \frac{(\iint_{-\infty}^{\infty}|F(x',y')|^2dx'dy')^4}{\iint_{-\infty}^{\infty}|F(x',y')|^4dx'dy'}. \qquad (2.25)$$

It can also be approximated to the area of the fundamental mode πw_o^2 using the mode field radius w_o of Eq. (2.17). Plugging Eq. (2.24) into Eq. (2.23), it becomes,

$$\frac{\partial A}{\partial z} + k_1\frac{\partial A}{\partial t} - \frac{i}{2}k_2\frac{\partial^2 A}{\partial t^2} - \frac{\alpha}{2}A = -i\gamma|A|^2A. \qquad (2.26)$$

The coefficients "k_1", and "k_2" in Eq. (2.26) represent the inverse group velocity and Group Velocity Dispersion (GVD) of the pulse, which are parameters usually expressed in units of m^{-1}-sec and ps^2-Km^{-1}, respectively. The coefficient "α" represents the gain ($\alpha > 0$), or loss ($\alpha < 0$), of the system, and is usually converted from units of dB-Km^{-1} to m^{-1} (for SiO$_2$, the intrinsic absorption is typically 0.2dB/Km at 1.5μm). The term on the right hand side of the equation represents the effect of Self-Phase Modulation (SPM) on the propagation of the pulse, and shall be discussed later, in the context of Cross-Phase Modulation (XPM). When the loss coefficient is

17

neglected in this equation, it becomes known as the Nonlinear Schrödinger Equation (NLSE). Next, an important class of solutions to Eq. (2.26), known as solitons, are considered.

2.1.2 Soliton Solutions

One interesting aspect of pulse propagation in optical fibers is their ability to sustain optical solitons. These are solutions to the NLSE which originate from a compensating effect between Self-Phase Modulation (SPM) and Group-Velocity Dispersion (GVD). This is particularly true for the scalar case of pulse propagation when it operates in the negative "anomalous" dispersion region. Neglecting loss, using the normalizing parameters $\xi = z/L_D$ and $U = A/\sqrt{P_o}$, and choosing a normalized retarded time frame, which moves at the pulse's group velocity $\tau = (t - k_1 z)/T_o$, Eq. (2.26) becomes, after simplification,

$$\frac{\partial U}{\partial \xi} - sgn\frac{i}{2}\frac{\partial^2 U}{\partial \tau^2} = -iN^2|U|^2 U, \qquad (2.27)$$

where U is normalized in terms of the peak power P_o of the input pulse, ξ in terms of the dispersion length $L_D = T_o^2/|k_2|$, T_o being the width of the input pulse, and the soliton order defined as $N = (L_D/L_N)^{\frac{1}{2}}$, with the nonlinear length defined as $L_{NL} = 1/\gamma P_o$. It is also assumed that, because the pulse propagates in the anomalous dispersion region (negative GVD), the sign of k_2 is negative, i.e $sgn = -1$.

Equation (2.27) can be further simplified if normalization to the soliton's order, i.e $u = NU$, takes place. After simplification, it takes the shape,

$$\frac{\partial u}{\partial \xi} + \frac{i}{2}\frac{\partial^2 u}{\partial \tau^2} = -i|u|^2 u. \qquad (2.28)$$

Exact solutions to Eq. (2.28) in the form of solitons can be obtained using the Inverse Scattering Method [60], which has been extensively applied to solve nonlinear

differential equations such as NLSE [165], the specifics of which is beyond the scope of this work. One particular case of interest is when $N = 1$ (fundamental soliton), which is given by:

$$u(\xi, \tau) = \text{sech}(\tau) \exp\{i\xi/2\}. \tag{2.29}$$

A pulse of this form, launched into a fiber (lossless and with a single propagating axis) will propagate indefinitely without distortion, provided that the condition $N = 1$ is satisfied. To account for the non-ideal case of a real optical fiber, the effects of birefringence, and, consequently XPM need to be included in the theoretical model. This will be the topic of next section.

2.2   Effects of Birefringence on Pulse Propagation

In real, non-ideal fibers, pulses do not propagate in a single axis, but, instead, the presence of birefringence breaks the degeneracy of the fundamental mode. It can considerably change the way in which a pulse evolves along the fiber [99, 144, 100, 102]. In this section, the analysis of pulse propagation is extended to the two-dimensional case of a vector field propagating in a non-ideal birefringent fiber. The field can be decomposed into two orthogonally polarized components, corresponding to the slow and fast axis of a fiber. Complimentary to the effect of SPM presented in the NLSE case, which accounts for the field acting on its own phase, the effects of the field acting on its orthogonally polarized counterpart is accounted as well, in the context of an optical phenomena known as Cross-Phase Modulation (XPM).

2.2.1   Coupled Nonlinear Schrödinger Equations (CNLSE)

Birefringence effects can be better understood in relation to a nonlinear effect known as Cross-Phase Modulation (XPM), which deals with the nonlinear interaction between two optical waves co-propagating inside a fiber. This interaction creates a coupling between the waves, and it can manifest itself with waves of different frequencies and same polarization, or with same frequency and different polarizations. As far as the primary interest of the numerical simulation is concerned, the discussion which follows concerns only XPM between orthogonally polarized waves.

It is convenient to start in the most general way, with a fiber displaying elliptical birefringence, and later reduce the equations to the particular case of interest, which is linearly birefringent fibers. For an elliptically birefringent fiber, the field vector can be described as,

$$\mathbf{E}(\mathbf{r}, t) = \frac{1}{2}\{(\hat{\mathbf{e}}_1 \mathcal{E}_x + \hat{\mathbf{e}}_2 \mathcal{E}_y) \exp\{i(\omega_l t - k_o z)\} + c.c\}, \tag{2.30}$$

where $\hat{\mathbf{e}}_1$ and $\hat{\mathbf{e}}_2$ represent a basis of orthonormal vectors defined as,

$$\hat{\mathbf{e}}_1 = \frac{\hat{\mathbf{x}} + ir\hat{\mathbf{y}}}{\sqrt{(1 + r^2)}}, \quad \text{and} \quad \hat{\mathbf{e}}_2 = \frac{r\hat{\mathbf{x}} - i\hat{\mathbf{y}}}{\sqrt{(1 + r^2)}},$$

and $r = \tan(\theta/2)$ represents the amount of ellipticity of the fiber, with "θ" being the ellipticity angle. Therefore, when $\theta = 0$, the fiber is linearly birefringent, and when $\theta = \pi/2$, circularly birefringent.

The polarization vector can also be expressed on the orthonormal basis as,

$$\mathbf{P}(\mathbf{r}, t) = \frac{1}{2}\{(\hat{\mathbf{e}}_1 \mathcal{P}_x + \hat{\mathbf{e}}_2 \mathcal{P}_y) \exp\{i(\omega_l t - k_o z)\} + c.c\}. \tag{2.31}$$

Plugging Eqs. (2.30) and (2.31) into Eq. (2.9), one follows a procedure similar to the one in Section 2.1.1. Here, instead of the single expansion of Eq.(2.21), one expands both $k_x(\Omega)$ and $k_y(\Omega)$. After much simplification, it leads to the evolution

equation for a vector pulse propagating inside an elliptically birefringent fiber,

$$\frac{\partial A_x}{\partial z} + i\frac{\Delta k_0}{2}A_x + k_{1x}\frac{\partial A_x}{\partial t} - \frac{i}{2}k_2\frac{\partial^2 A_x}{\partial t^2} - \frac{\alpha}{2}A_x = -i\gamma[(|A_x|^2 + B|A_y|^2)A_x +$$
$$CA_x^*A_y^2e^{-2i\Delta k_0 z}] - i\gamma D[(|A_y|^2 + 2|A_x|^2)A_y^2e^{-i\Delta kz} + CA_y^*A_x^2e^{i\Delta kz}], \qquad (2.32a)$$

$$\frac{\partial A_y}{\partial z} - i\frac{\Delta k_0}{2}A_y + k_{1y}\frac{\partial A_y}{\partial t} - \frac{i}{2}k_2\frac{\partial^2 A_y}{\partial t^2} + \frac{\alpha}{2}A_y = -i\gamma[(|A_y|^2 + B|A_x|^2)A_y +$$
$$CA_y^*A_x^2e^{+2i\Delta k_0 z}] - i\gamma D[(|A_x|^2 + 2|A_y|^2)A_x^2e^{i\Delta k_0 z} + CA_x^*A_y^2e^{-i\Delta kz}], \qquad (2.32b)$$

where A_x and A_y are the SVEA normalized amplitude fields of the slow and fast axes of the fiber, respectively, when $k_{1x} > k_{1y}$, $\Delta k_0 = (k_{0x} - k_{0y}) = (n_x - n_y)2\pi/\lambda_o$ is the wave-vector mismatch of the orthogonally polarized pulses of wavelength λ_o, and

$$B = \frac{2 + 2\sin^2(\theta)}{2 + \cos^2(\theta)}, \quad C = \frac{\cos^2(\theta)}{2 + \cos^2(\theta)}, \quad D = \frac{\sin(\theta)}{2\cos(\theta)}.$$

The left hand side of the equations (2.32a) and (2.32b) contains the lossy and dispersive, linear components, and the right hand side the nonlinear components. The coefficients "k_{1x}" and "k_{1y}" are the inverse group velocities in the x and y axes, respectively, and "k_2" the group velocity dispersion (GVD), which, for simplicity, is assumed equal for both axes. For linearly birefringent fibers, $\theta = 0$, $B = 2/3$, $C = 1/3$, and $D = 0$. Eqs. (2.32a) and (2.32b) then reduce to,

$$\frac{\partial A_x}{\partial z} + i\frac{\Delta k_0}{2}A_x + k_{1x}\frac{\partial A_x}{\partial t} - \frac{i}{2}k_2\frac{\partial^2 A_x}{\partial t^2} - \frac{\alpha}{2}A_x = -i\gamma[(|A_x|^2 + \frac{2}{3}|A_y|^2)A_x + \frac{1}{3}A_x^*A_y^2e^{-2i\Delta k_0 z}],$$
$$(2.33a)$$

$$\frac{\partial A_y}{\partial z} - i\frac{\Delta k_0}{2}A_y + k_{1y}\frac{\partial A_y}{\partial t} - \frac{i}{2}k_2\frac{\partial^2 A_y}{\partial t^2} - \frac{\alpha}{2}A_y = -i\gamma[(|A_y|^2 + \frac{2}{3}|A_x|^2)A_y + \frac{1}{3}A_y^*A_x^2e^{+2i\Delta k_0 z}].$$
$$(2.33b)$$

In the absence of loss, Eqs. (2.33a) and (2.33b) are sometimes referred to as the Coupled Nonlinear Schrödinger Equations (CNLSE). Because of Δk_0, the phase of

A_x and A_y varies rapidly with distance, which is very inconvenient for numerical simulations. Whenever one has a rapidly varying phase factor, one makes a change of variable to eliminate this variation. In this case, the transformation to a rotating frame $A_x = \mathcal{A}_x \exp\{-i\Delta k_0 z/2\}$ and $A_y = \mathcal{A}_y \exp\{i\Delta k_0 z/2\}$ eliminates phase factors associated with the linear birefringence in Eqs. (2.33a) and (2.33b). A special class of solutions to these equations, known as vector-soliton solutions, is presented next.

2.2.2 Vector-Soliton Solutions

As it happens in the scalar case, the CNLSE present a solution in the form of shape-preserving solitary waves. In this case, however, these solutions, known as vector-solitons [29], refer to a pulse that maintains not only its shape, but also its polarization state, as it propagates through the fiber. This holds true even if it propagates along one of the principal axes of the fiber (i.e the slow or the fast axes). Using normalization parameters $u = N\mathcal{A}_x/\sqrt{P_o}$, $v = N\mathcal{A}_y/\sqrt{P_o}$, $\xi = z/L_D$, as defined in Section 2.1.2 for the one dimensional case, and a retarded time frame $\tau = [t - (k_{1x} + k_{1y})/2]/T_o$, which, this time, uses the average of the inverse group velocities of each axis, Eqs (2.32a) and (2.32b) can be simplified into the form,

$$\frac{\partial u}{\partial \xi} + \Delta \bar{k}_1 \frac{\partial u}{\partial \tau} + \frac{i}{2}\frac{\partial^2 u}{\partial \tau^2} = -i(|u|^2 + B|v|^2)u, \tag{2.34a}$$

$$\frac{\partial v}{\partial \xi} - \Delta \bar{k}_1 \frac{\partial v}{\partial \tau} + \frac{i}{2}\frac{\partial^2 v}{\partial \tau^2} = -i(|v|^2 + B|u|^2)v, \tag{2.34b}$$

where a normalized inverse group-velocity mismatch term has been introduced as $\Delta \bar{k}_1 = T_o(k_{1x} - k_{1y})/(2|k_2|)$, and it has been assumed that the fiber is lossless and operates in the anomalous dispersion regime ($k_2 < 0$). It has also been assumed that the fiber is highly birefringent (i.e its beat length $L_B = 2\pi/[k_o(n_x - n_y)]$ is much smaller than the propagating length). Consequently, because the exponential of the last three terms in Eqs 2.32a and 2.32b oscillates very rapidly, their contribution on average is negligible, and those terms can be dropped altogether.

Equations (2.34a) and (2.34b) can be further simplified by introducing a new set of variables defined as $\tilde{u} = u \exp\{i(\Delta \overline{k}_1^2 \xi/2 - \Delta \overline{k}_1 \tau)\}$ and $\tilde{v} = v \exp\{i(\Delta \overline{k}_1^2 \xi/2 + \Delta \overline{k}_1 \tau)\}$. With this new set, the equations become independent of the group-velocity mismatch term,

$$\frac{\partial \tilde{u}}{\partial \xi} + \frac{i}{2}\frac{\partial^2 \tilde{u}}{\partial \tau^2} = -i(|\tilde{u}|^2 + B|\tilde{v}|^2)\tilde{u}, \tag{2.35a}$$

$$\frac{\partial \tilde{v}}{\partial \xi} + \frac{i}{2}\frac{\partial^2 \tilde{v}}{\partial \tau^2} = -i(|\tilde{v}|^2 + B|\tilde{u}|^2)\tilde{v}. \tag{2.35b}$$

A few important qualitative aspects arise from this new set of equations. For instance, when $B = 0$, there is no XPM between the pulses, and the decoupling of the equations lead to a set of two independent soliton solutions, each as described in Section 2.1.2. The only case where these equations can be solved using the Inverse Scattering method is when $B = 1$. When that happens, it leads to solutions of the type [166],

$$\tilde{u}(\xi, \tau) = \cos(\theta_p)\text{sech}(\tau)\exp\{i\xi/2\}, \tag{2.36a}$$

$$\tilde{v}(\xi, \tau) = \sin(\theta_p)\text{sech}(\tau)\exp\{i\xi/2\}, \tag{2.36b}$$

where they correspond to a vector soliton of order $N = 1$, much like as in the scalar case, with "θ_p" being its angle of polarization. For the case when $B \neq 1$, solutions to Eqs. 2.35a and 2.35b are not categorized as solitons in a mathematical way, since they can not be directly solved with the Inverse Scattering method. However, such solutions do exist, and preserve their shape. They are usually referred as "Solitary Waves" solutions, and have been extensively studied. For instance, in the case when $\theta_p = 45^o$ (solitons with the same amplitude), these solutions are given by [145],

$$\tilde{u} = \tilde{v} = \eta\text{sech}[(1 + B)^{\frac{1}{2}}\eta\tau]\exp\{i(1 + B)\eta^2\xi/2\}, \tag{2.37}$$

where η is the amplitude of the solitary wave. In comparison to the scalar solution, this solution is narrower by a factor of $(1 + B)^{\frac{1}{2}}$, or 1.29 for linearly birefringent fibers ($B = 2/3$).

Another type of solution, which is due to the cross-phase interaction between two waves of the same polarization states and different wavelengths, is the so called twin-pulse soliton. These types of soliton have been studied in the context of passive mode-locking of fiber lasers. Observation of passive harmonic mode-locking of twin-pulse solitons in an erbium-doped fiber ring laser has been reported, in a 2004 experiment [167]. Other regimes of operation of solitons, such as normal, bound, and noise-like have also been reported experimentally in passive mode-locked fiber ring lasers [65]. It is not, however, of any interest here to study these solutions as they are not directly related to the effects of NPR, which is the main focus of the simulation. Next, the effects of gain saturation and gain dispersion on pulse propagation in an optical fiber are described.

2.3 Ultrashort Pulse Amplification

So far, the discussion has been limited to pulse propagation in a nonlinear, dispersive, birefringent medium, without any mention of gain. To create an equation so general that can fully describe pulse propagation even in the presence of gain, the effects of dopant ions, such as Er^{+3}, in the host medium, must be accounted for as well. That is the case, for instance, of a pulse propagating in an Erbium-Doped Fiber (EDF). In this case, an extra polarization term $\mathbf{P}_d$, due to the presence of dopants, must be included in the wave equation (2.4), i.e,

$$(\nabla^2 - \frac{1}{c^2}\frac{\partial^2}{\partial^2 t})\mathbf{E} = \mu_o \frac{\partial^2}{\partial^2 t}(\mathbf{P}_L + \mathbf{P}_{NL} + \mathbf{P}_d), \tag{2.38}$$

which can be written in the frequency domain, similarly to Eq. (2.13), with the permittivity $\epsilon(\Omega)$ being replaced by $\epsilon_d(\Omega)$, which accounts for the presence of the dopants,

$$\epsilon_d(\Omega) = 1 + \tilde{\chi}^{(1)}(\Omega) + \frac{3}{4}\chi^{(3)}_{xxxx}|E(\mathbf{r}, t)|^2 + \tilde{\chi}_d(\Omega). \tag{2.39}$$

Here, "$\tilde{\chi}_d(\Omega)$" is the contribution from the dopants to the susceptibility. Using Eq. (2.15), the permittivity can be written in terms of the index of refraction. After much simplification, the propagation constant can be found as,

$$k_d(\Omega) = \sqrt{\epsilon_d(\Omega)}\frac{\Omega}{c} = [n(\Omega) + n_2|E|^2 + i\frac{\alpha'}{2}(\frac{c}{\Omega}) + \frac{1}{2}\tilde{\chi}_d(\Omega)]\frac{\Omega}{c}, \qquad (2.40)$$

where $\alpha' = \alpha + \alpha_2|E|^2$, and, unlike what occurs in pure SiO_2 fiber, the effects of two-photon absorption may become relevant in highly nonlinear fibers[2]. Following a procedure similar to the one described from Eqs. (2.13) to (2.20), the scalar propagation equation describing pulse evolution in a nonlinear, dispersive, medium, in the presence of dopants, takes the form,

$$\frac{\partial\tilde{A}}{\partial z} = -i\frac{[k_d^2(\Omega) - k_o^2]}{2k_o}\tilde{A} \simeq -i[k_d(\Omega) - k_o]\tilde{A} = -i[k(\Omega) + \Delta k_d - k_o]\tilde{A}, \qquad (2.41)$$

where, once again, an approximation was made with $k_d^2(\Omega) - k_o^2 \simeq 2k_o(k_d(\Omega) - k_o)$, $k(\Omega)$ given by Eq. (2.21), and $\Delta k_d = \Delta k + (1/2)\tilde{\chi}_d\Omega/c$, with Δk defined as in Eq. (2.24), except that, in the present case, α is being replaced by α'. As it will be shown in the next section, the contribution of dopants to the susceptibility $\tilde{\chi}_d$ not only depends on frequency Ω, but also on the spatial coordinates. It can be derived from the Bloch equations, used extensively to study coherent interaction between optical waves and their propagating medium, within a two-level system approximation.

2.3.1 The Maxwell-Bloch Equations

In order to study pulse propagation in the presence of Er^{+3} ions in a $Si0_2$ host, the Bloch equations can be used to describe the coherence response from the doped propagating medium to an input pulse, within a two-level system approximation ([41]

---

[2]Such are the cases for chalcogenide glass [11] and lead silicate [112] optical fibers

and [131]). They are, in conjunction with the equation describing pulse evolution along the fiber, given by the set of equations,

$$i\frac{\partial P_d}{\partial t} = -i\frac{P_d}{T_2} - (\omega_a - \omega_l)P_d - \frac{\mu^2}{\hbar}EW, \tag{2.42a}$$

$$\frac{\partial W}{\partial t} = -\frac{i}{2\hbar}\{EP_d^* - E^*P_d\} - \frac{W - W_o}{T_1}, \tag{2.42b}$$

where "ω_l" and "ω_a" are the optical and atomic resonance frequencies, "μ" is the dipole moment, and "T_1" and "T_2" the relaxation time of the population inversion "W" and polarization (dipole) of the two-level system, respectively. The population inversion is defined as $W = N_o(\rho_{22} - \rho_{11})$, with "$N_o$" being the doping density of the two-level system, "ρ_{22}" and "ρ_{11}" the diagonal elements of its density matrix, and "W_o" the equilibrium inversion.

For the relatively long pulse being considered here, one solves Eqs. (2.42a) and (2.42b) for P_d to get Eq. (2.43). A crude shortcut is made by assuming this solution to be valid for each frequency component [26],

$$\tilde{\mathbf{P}}_d(\mathbf{r}, \Omega_s) = \epsilon_o\tilde{\chi}_d(\mathbf{r}, \Omega)\tilde{\mathbf{E}}(\mathbf{r}, \Omega_s) = \epsilon_o\frac{\sigma_s W(\mathbf{r})(n_o c/\omega_l)}{(\Omega - \omega_a)T_2 - i}\tilde{\mathbf{E}}(\mathbf{r}, \Omega_s), \tag{2.43}$$

where the optical input signal transition cross-section has been defined as $\sigma_s = \mu^2\omega_l T_2/(\epsilon_o\hbar n_o c)$, and the susceptibility can then be given by,

$$\tilde{\chi}_d(\mathbf{r}, \Omega) = \frac{\sigma_s W(\mathbf{r})(n_o c/\omega_l)}{(\Omega - \omega_a)T_2 - i} = \frac{g_p n_o c}{\omega_l}\frac{(\Omega - \omega_a)T_2 + i}{1 + (\Omega - \omega_a)^2 T_2^2}. \tag{2.44}$$

Here, the peak gain has been approximated as $g_p \simeq \sigma_s W(\mathbf{r})$. Because of $\tilde{\chi}_d$ dependence on Ω, the term Δk_d in Eq. (2.41) is also Ω dependent,

$$\Delta k_d(\Omega) = \Delta k + \frac{1}{2}(\frac{\omega_l}{n_o c})\tilde{\chi}_d(\Omega) = \gamma|A|^2 + \frac{i}{2}(\alpha + \frac{\alpha_2|A|^2}{A_{ef}}) + \frac{g_p}{2}\frac{(\Omega - \omega_a)T_2 + i}{1 + (\Omega - \omega_a)^2 T_2^2}, \tag{2.45}$$

where Δk has been written in terms of Eq. (2.24). The second term of Eq. (2.45) can be then expanded in a Taylor Series about the light frequency ω_l,

$$\Delta k_d(\Omega) = \gamma|A|^2 + \frac{i}{2}(\alpha + \frac{\alpha_2|A|^2}{A_{ef}}) + \frac{g_p}{2}[\frac{\delta + i}{1 + \delta^2} + \frac{1 - \delta^2 - 2i\delta}{(1 + \delta^2)^2}(\Omega - \omega_l)T_2 +$$
$$\frac{\delta(\delta^2 - 3) - i(1 - 3\delta^2)}{(1 + \delta^2)^3}(\Omega - \omega_l)^2 T_2^2 + ...], \tag{2.46}$$

where a detuning parameter has been defined as $\delta = (\omega_l - \omega_a)T_2$. Substituting Δk_d from Eq. (2.46) into Eq. (2.41), with $k(\Omega)$ expanded as in Eq. (2.21), and re-arranging terms to combine $(\Omega - \omega_l)$ factors together,

$$\frac{\partial \tilde{A}}{\partial z} = -i\{k_1^{ef}(\Omega - \omega_l) + \frac{1}{2}k_2^{ef}(\Omega - \omega_l)^2 + ... + \gamma|A|^2 + \frac{i}{2}(\alpha + \frac{\alpha_2|A|^2}{A_{ef}}) +$$
$$+ \frac{g_p}{2}(\frac{\delta + i}{1 + \delta^2})]\}\tilde{A}. \tag{2.47}$$

Here, an effective first and second order propagation parameters have been introduced, where $k_1^{ef} = k_1 + (g_p/2)[(1-\delta^2-2i\delta)/(1+\delta^2)^2]T_2$, and $k_2^{ef} = k_2+(g_p/2)\{[\delta(\delta^2-3)-i(1-3\delta^2)]/(1+\delta^2)^3\}T_2^2$. The gain related terms of these coefficients are associated with an effect of dopants known as "gain dispersion".

Inverse Fourier transforming Eq. (2.47), where, once again, all factors $(\Omega - \omega_l)^n$, n integer, become $-i\partial^n/\partial t^n$, and maintaining only the first and second order terms, leads to a time domain evolution equation given by,

$$\frac{\partial A}{\partial z} + k_1^{ef}\frac{\partial A}{\partial t} - \frac{i}{2}k_2^{ef}\frac{\partial^2 A}{\partial t^2} = -i\gamma|A|^2A - \frac{i}{2}[g_p(\frac{\delta + i}{1 + \delta^2}) + i(\alpha + \alpha_2|A|^2)]A. \tag{2.48}$$

Equation (2.48), together with Eqs. (2.42a) and (2.42b) form what is known as the Maxwell-Bloch equations, and they must be solved simultaneously in order to characterize pulse propagation in a two-level approximated doped medium. It is also in the form of an equation known as the Ginzburg-Landau equation, which has been extensivelly studied in the context of fluid mechanics, and is the topic of next section.

2.3.2 The Ginzburg-Landau Equation

A few normalization can be made to Eq. (2.48), using parameters $U = A/\sqrt{P_o}$, $\xi = z/L_D$, a retarded time frame defined as $\tau = (t - k_1^{ef}z)/To$, and the soliton order

$N = (L_D/L_{NL})^{\frac{1}{2}}$, resulting in the equation,

$$\frac{\partial U}{\partial \xi} - \frac{i}{2}(sgn + d)\frac{\partial^2 U}{\partial \tau^2} = -iN^2|U|^2 U - \frac{i}{2}(\eta + i\eta_2|U|^2)U. \tag{2.49}$$

Here, the term *sgn* denotes the sign of k_2 (i.e +1 for normal dispersion regime and -1 for anomalous), and the coefficients $\eta = \{g_p[(\delta + i)/(1 + \delta^2)] + i\alpha\}L_D$, and $d = g_p\{[\delta(\delta^2 - 3) - i(1 - 3\delta^2)]/(1 + \delta^2)^3\}T_2^2/(2|k_2|)$ are related to the gain and dispersion gain, respectively. The term $\eta_2 = \alpha_2 P_o L_D$ is responsible for the effects of two-photon absorption. Because d is related to T_2, it is associated to the bandwidth of the amplifier.

In Eq. (2.44), the peak gain is described as $g_p \simeq \sigma_s W$. In reality, it should be averaged over the entire spatial profile of the fundamental mode $F(x, y)$ as,

$$g_p(z, t) = \frac{\sigma_s \iint_{-\infty}^{\infty} W(\mathbf{r}, t)|F(x', y')|^2 dx' dy'}{\iint_{-\infty}^{\infty} |F(x', y')|^2 dx' dy'}. \tag{2.50}$$

In practice, however, since doping is usually limited to a small area of the fiber core, where the doping density and input signal intensity distribution can be assumed nearly uniform, the population inversion can be assumed constant on this area, and zero outside. In that case, the peak gain in Eq. (2.50) can be approximated by $g_p \simeq \sigma_s \Gamma W(\mathbf{r}, t)$, where gamma is known as the confinement (or overlap) factor, and represents the fraction of the pulse energy which is confined to the doped area. Using the Gaussian approximation to the fundamental mode (Section 2.1.1), the confinement factor can be written as $\Gamma = 1 - \exp\{-b^2/2w_o^2\}$, where b is the erbium dopant radius, and w_o is the mode field diameter (see Eq. (2.17)). When solving the Maxwell-Bloch equations, it is often desirable to express Eq. (2.42b) in terms of the peak gain. To obtain a rate equation for g_p, equation $g_p = \sigma_s \Gamma W$ must be combined with Eq. (2.42b) to give,

$$\frac{\partial g_p}{\partial t} = \frac{g_o - g_p}{T_1} - (\frac{2\sigma_s}{\hbar\omega_l})g_p I, \tag{2.51}$$

where $g_o = \sigma_s W_o$ is the small signal gain coefficient, and $I = \frac{1}{2}\epsilon_o c n_o |E|^2$ is the intensity of the optical wave, with $n_o = n(\omega_l)$ being the index of refraction at the optical frequency. In deriving Eq. (2.51), the first term in the right hand side of Eq. (2.42b) was solved using Eqs. (2.44) and $P = \epsilon_o \tilde{\chi}_d(\Omega) E$, such that, $-i\{EP_d^* - E^* P_d\}/2\hbar = \Im\{EP_d^*\}/\hbar = \epsilon_o |E|^2 \Im\{\tilde{\chi}_d(\Omega)\}/\hbar = -\epsilon_o n_o c |E|^2 g_p/\hbar\omega_l$, at resonance. It has also been assumed a homogeneously broadened gain profile.

Equation (2.51) can be solved considering that, for practical purposes, the width of the input pulse is much smaller than the population relaxation time, i.e $T_o \ll T_1$, which for an Erbium doped fiber is on the order of 1-10msec. Consequently, first term on the right hand side of Eq. (2.51) can be neglected, and the equation can be easily integrated as,

$$g_p = g_o \exp\{-\frac{1}{E_s}\int_{-\infty}^t |A(z,t')|^2 dt'\}, \tag{2.52}$$

where "E_s" represents the saturation energy, and is defined as $E_s = \hbar\omega_l A_s/2\sigma_s$, with "$A_s$" being the mode area. In the saturated gain regime, the peak gain becomes time dependent. In terms of normalized parameters, and for the case where $\alpha = \alpha_2 = 0$, and there is no detuning ($\delta = 0$), $\eta = \eta_o \exp\{-s\int_{-\infty}^\tau |U(\xi,\tau')|^2 d\tau'\}$, where the saturation parameter is defined as $s = P_o T_o/E_s$, and the small signal gain parameter $\eta_o = ig_o L_D$. Similarly, the gain dispersion parameter becomes $d = d_o \exp\{-s\int_{-\infty}^\tau |U(\xi,\tau')|^2 d\tau'\}$, with $d_o = -ig_o T_2^2/(2|k_2|)$. Equation (2.49) then becomes, for the case of anomalous dispersion ($k_2 < 0$),

$$\frac{\partial U}{\partial \xi} + \frac{i}{2}(1-d)\frac{\partial^2 U}{\partial \tau^2} + iN^2|U|^2 U = -\frac{i}{2}\eta U. \tag{2.53}$$

In the absence of gain saturation, $s \ll 1$, $\eta \to \eta_o$, $d \to d_o$. Because the saturation energy is usually large in doped fibers ($E_s \simeq 1\mu J$), it is likely that gain saturation be negligible in an amplifier. However, because the main interest here is with mode-locked fiber lasers, successive passes of a pulse through the gain medium is likely to saturated the gain.

2.3.3 Auto-Soliton Solutions

Because the Ginzburg-Landau equation is non integrable by the inverse scattering method, solitons are not considered a solution in a strictly mathematical sense. The equation does have, however, shape-preserving solitary-wave solutions. These solutions are usually known as "amplifier", or "auto-" solitons [5, 66], where the name comes from the fact that any input pulse, irrespective of their width and peak power, will evolve toward a unique soliton, which is supported by the amplifier.

Writing Eq. (2.49), with a new normalization parameter $u = NU$,

$$\frac{\partial u}{\partial \xi} + \frac{i}{2}(1 - d_o)\frac{\partial^2 u}{\partial \tau^2} + i(1 + \frac{i}{2}\eta_2)|u|^2 u = -\frac{i}{2}\eta_o u. \tag{2.54}$$

A solution of Eq. (2.54) has the form [122],

$$u(\xi, \tau) = N_s[\mathrm{sech}(p\tau)]^{1+iq}\exp\{-\frac{i}{2}p^2[sgn(1 - q^2) - 2qd_o]\xi\}, \tag{2.55}$$

where the new parameters,

$$N_s^2 = \frac{1}{2}p^2[sgn(q^2 - 2) + 3qd_o], \quad p^2 = -\eta_o[d_o(1 - q^2) + 2(sgn)q]^{-1},$$

and "q", a solution to the quadratic equation,

$$(d_o - \eta_2 sgn/2)q^2 - 3(sgn + \eta_2 d_o/2)q + (\eta_2 - 2d_o) = 0,$$

are determined by substituting Eq. (2.55) into Eq. (2.54).

Equation (2.55) reduces to a normal soliton solution when $sgn = -1$, and $d_o = \eta_o = \eta_2 = 0$. Standard soliton solution supports a family of fundamental solitons such that $N_s = p$. In the case of the Ginzburg-Landau equation, "p" and "N_s" are fixed in terms of "η_o" and "d_o".

It has been shown that solitons can maintain a high degree of polarization over an ultra-long distance transmission system consisting of birefringent, dispersion-shifted

fiber segments and erbium amplifiers [47]. Numerical studies of the initial value problem for soliton pulse propagation have reviewed that chirped solitons are only stable in the normal-dispersion regime, which is the case for erbium-doped fibers [6].

2.4   The Master Propagation Equations

So far, effects of birefringence on pulse propagation have been studied through the CNLSE (Eqs. (2.32a) and (2.32b)), and the vector soliton solutions (Eqs. (2.36a) and (2.36b)). It has been also investigated the effects of dopants introduced in SiO_2 hosts, on the context of pulse amplification, particularly in the case of gain saturation (Eq. (2.49)), and solutions to the Ginzburg-Landau equation, in the form of auto-solitons. It is now time to turn the attention on the combination of these two effects, and how they play a rule on the propagation of a pulse, which can be described by a general set of equations defined here as the "Master Propagation Equations". These equations, are generalized in such a form that it may be used with all fiber types in the numerical simulation. Here, starting with Eqs. (2.32a) and (2.32b), assuming a linear birefringent medium ($\theta = 0$), and using a variable transformation, where $A_x = \mathcal{A}_x \exp\{-i\Delta k_o z/2\}$ and $A_y = \mathcal{A}_y \exp\{+i\Delta k_o z/2\}$ are expressed in a rotating frame,

$$\frac{\partial \mathcal{A}_x}{\partial z} + k_{1x}\frac{\partial \mathcal{A}_x}{\partial t} - \frac{i}{2}k_2\frac{\partial^2 \mathcal{A}_x}{\partial t^2} - \frac{\alpha}{2}\mathcal{A}_x = -i\gamma[(|\mathcal{A}_x|^2 + \frac{2}{3}|A_y|^2)\mathcal{A}_x + \frac{1}{3}\mathcal{A}_x^{*}A_y^{2}], \quad (2.56a)$$

$$\frac{\partial A_y}{\partial z} + k_{1y}\frac{\partial A_y}{\partial t} - \frac{i}{2}k_2\frac{\partial^2 A_y}{\partial t^2} - \frac{\alpha}{2}A_y = -i\gamma[(|A_y|^2 + \frac{2}{3}|\mathcal{A}_x|^2)A_y + \frac{1}{3}A_y^{*}\mathcal{A}_x^{2}]. \quad (2.56b)$$

Next, the effects of gain saturation, gain dispersion, and detuning are included:

$$\frac{\partial \mathcal{A}_x}{\partial z} + k_{1x}^{ef}\frac{\partial \mathcal{A}_x}{\partial t} - \frac{i}{2}k_2^{ef}\frac{\partial^2 \mathcal{A}_x}{\partial t^2} = -i\gamma[(|\mathcal{A}_x|^2 + \frac{2}{3}|A_y|^2)\mathcal{A}_x + \frac{1}{3}\mathcal{A}_x^{*}A_y^{2}] +$$
$$-\frac{i}{2}[g_p(\frac{\delta + i}{1 + \delta^2}) + i\alpha]\mathcal{A}_x, \quad (2.57)$$

$$\frac{\partial A_y}{\partial z} + k_{1y}^{ef}\frac{\partial A_y}{\partial t} - \frac{i}{2}k_2^{ef}\frac{\partial^2 A_y}{\partial t^2} = -i\gamma[(|A_y|^2 + \frac{2}{3}|\mathcal{A}_x|^2)A_y + \frac{1}{3}A_y{}^*\mathcal{A}_x{}^2] +$$
$$-\frac{i}{2}[g_p(\frac{\delta+i}{1+\delta^2}) + i\alpha]A_y, \tag{2.58}$$

where, again, the effective first and second orders propagation parameters are given by $k_{1x,y}^{ef} = k_{1x,y} + (g_p/2)\{[1-\delta^2-2i\delta]/(1+\delta^2)^2\}T_2$, and $k_2^{ef} = k_2 + (g_p/2)\{[\delta(\delta^2 - 3) - i(1-3\delta^2)]/(1+\delta^2)^3\}T_2^2$, respectively. By making a change in variable $\xi = z/L_D$, introducing a time moving frame $\tau = \{t - [(k_{1x}^{ef} + k_{1y}^{ef})/2]z\}/T_o$, and normalizing the fields as $u = N\mathcal{A}_x/\sqrt{P_o}$ and $v = N\mathcal{A}_y/\sqrt{P_o}$, the master equations become, after simplification,

$$\frac{\partial u}{\partial \xi} + \kappa_1\frac{\partial u}{\partial \tau} - \frac{i}{2}\frac{k_2^{ef}}{|k_2|}\frac{\partial^2 u}{\partial \tau^2} = -i[(|u|^2 + \frac{2}{3}|v|^2)u + \frac{1}{3}u^*v^2] - \frac{i}{2}[g_p(\frac{\delta+i}{1+\delta^2}) + i\alpha]\frac{T_o^2}{|k_2|}u, \tag{2.59a}$$

$$\frac{\partial v}{\partial \xi} - \kappa_1\frac{\partial v}{\partial \tau} - \frac{i}{2}\frac{k_2^{ef}}{|k_2|}\frac{\partial^2 v}{\partial \tau^2} = -i[(|v|^2 + \frac{2}{3}|u|^2)v + \frac{1}{3}v^*u^2] - \frac{i}{2}[g_p(\frac{\delta+i}{1+\delta^2}) + i\alpha]\frac{T_o^2}{2|k_2|}v, \tag{2.59b}$$

where, a normalized inverse group-velocity mismatch term, defined as $\kappa_1 = T_o(k_{1x} - k_{1y})/(2|k_2|)$, has been added. Using the notation formalism $k_2^{ef}/|k_2| = sgn + d$, where sgn, as previously defined, represents the sign of k_2, the gain-dispersion parameter $d = (g_p/2)\{[\delta(\delta^2 - 3) - i(1-3\delta^2)]/(1+\delta^2)^3\}(T_2^2/|k_2|)$, and writing $\eta = -i\{g_p[(\delta + i)/(1+\delta^2)] + i\alpha\}[T_o^2/(2|k_2|)]$, the master equations are reduced to the simple form,

$$\frac{\partial u}{\partial \xi} + \kappa_1\frac{\partial u}{\partial \tau} - \frac{i}{2}(sgn + d)\frac{\partial^2 u}{\partial \tau^2} = -i[(|u|^2 + \frac{2}{3}|v|^2)u + \frac{1}{3}u^*v^2] + \eta u, \tag{2.60a}$$

$$\frac{\partial v}{\partial \xi} - \kappa_1\frac{\partial v}{\partial \tau} - \frac{i}{2}(sgn + d)\frac{\partial^2 v}{\partial \tau^2} = -i[(|v|^2 + \frac{2}{3}|u|^2)v + \frac{1}{3}v^*u^2] + \eta v. \tag{2.60b}$$

Numerical studies of the combined effects of cross-phase modulation and doping, along with other higher nonlinear order effects, have been reported in the past [157].

Chapter 3

Mode-locking Mechanism

Mode-locked fiber lasers have been the subject of much theoretical studies in both a passive [133] and active [119] sense. In this chapter, a general description of the bidirectional mode-locking structure of the fiber ring laser is presented. It is a hybridization of a passive mechanism with an active element that generates independent - frequency unlocked- pulses, stabilizes them, and controls their crossing-points. The first half of the chapter describes the passive system, and the last half, the active control scheme.

3.1   The Passive Mechanism

The passive mechanism corresponds to those aspects of lasing which allow the dynamics of the system to naturally produce pulses that are able to self-sustain without an active controlling element to force oscillation. They are essentially composed of a gain medium, which creates threshold conditions for CW lasing, and a Fast Saturable Absorber (FSA), which generates and compresses the pulses. The gain medium, in the present case, is provided by a section of Erbium-Doped Fiber (EDF), which is a

distributed gain medium with high saturation energy E_s (typically on the order of μJs). Appendix A.2 provides a more detailed description of optical amplifiers based on rare earth doped fibers.

(a) 10μs/div scale   (b) 50ns/div scale
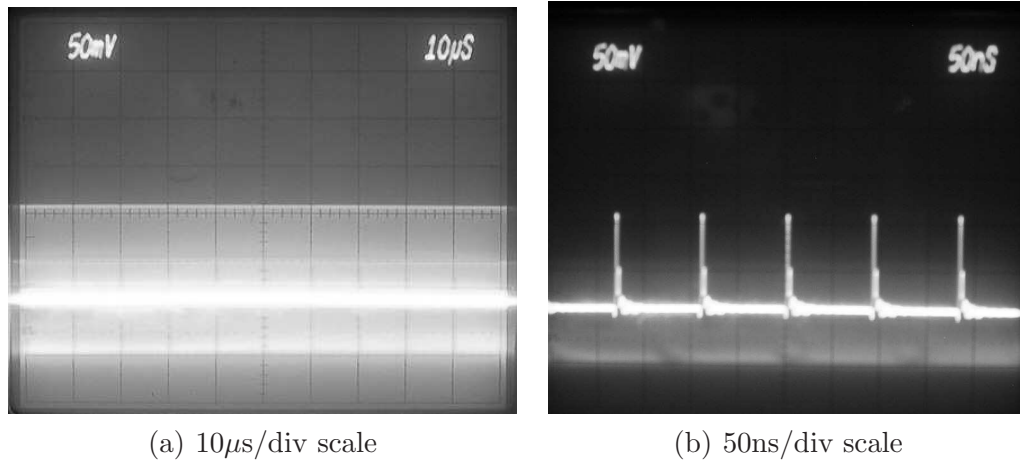
Figure 3.1: Unidirectional passive mode-locking using carbon-nanotube as saturable absorber in (a)10μsec/div and (b)50ns/div time scales.

To create pulses from CW lasing, a FSA must be inserted on the laser. There has been many reports of fiber laser mode-locking using several types of FSAs. From pulse formation using nonlinear optical loop mirrrors [42, 53, 70, 154, 151, 128, 45] and Sagnac interferometers [85, 30], to mode-locking using semiconductor saturable absorbers [94, 78, 105, 64, 132], pulses as narrow as 42fs have been achieved in passively mode-locked fiber laser systems [117]. During the project, an FSA based on a carbon nanotube structure was initially considered. Although this type of FSA has been successfully used for mode-locking in recent experiments involving fiber lasers [129, 155], it presented a fundamental problem in the case of bidirectional mode-locking. Because crossing of the pulses happens at the absorber, the dead-band is considerably enlarged. Therefore, even though bidirectionality may be attained [80], its limitation on beat note detection will make the system not a good

choice for sensor applications. Nonetheless, an experiment using a simple ring laser showed stable generation of high harmonic mode-locked lasing (Fig. 3.1), rendering promising future applications of carbon nanotubes in unidirectional mode-locking.

The choice of FSA for the laser in this project involves the use of Nonlinear Polarization Rotation (NPR). Several theoretical models of erbium-doped fiber lasers passively mode-locked by NPR have been studied in the past [127], and experimental use of NPR to produce mode-locked pulses demonstrated several times [96, 138, 116]. Appendix A.4 further details the NPR mechanism, and Figure 3.2 illustrates the principle of its use as a FSA.
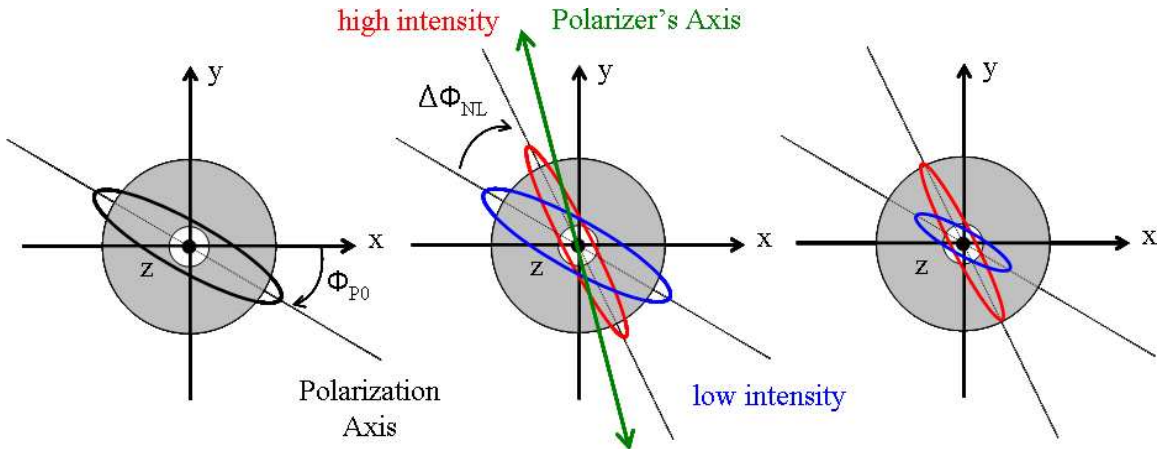
Figure 3.2: Polarization evolution of the low (blue) and high (red) intensity components of a pulse propagating along a section of SMF in an NPR based FSA.

An optical pulse propagating along a section of SMF, with an elliptical input polarization state, at an angle "Φ_{po}" relative to the slow axis (X) of the fiber (left), experiences an intensity dependent rotation of its polarization, so that, at the end of the fiber, the axis of its high intensity component (red) is rotated an angle "$\Delta\Phi_{NL}$" relative to its low intensity (blue) component (middle). As the polarization of the high intensity component is closely aligned to the axis of a linear polarizer placed at the end of the fiber section, it will experience less attenuation than the lower intensity

component (right). The higher attenuation on the tails of the pulse narrows its width, emulating an FSA effect. In practice, the polarization state of the high intensity portion of the pulse is adjusted to the axis of the polarizer using a Polarization Controller (PC) which acts as a polarization transformation element. Figure 3.3 shows how the NPR based FSA is used on the present cavity to produce passive bidirectional mode-locking.
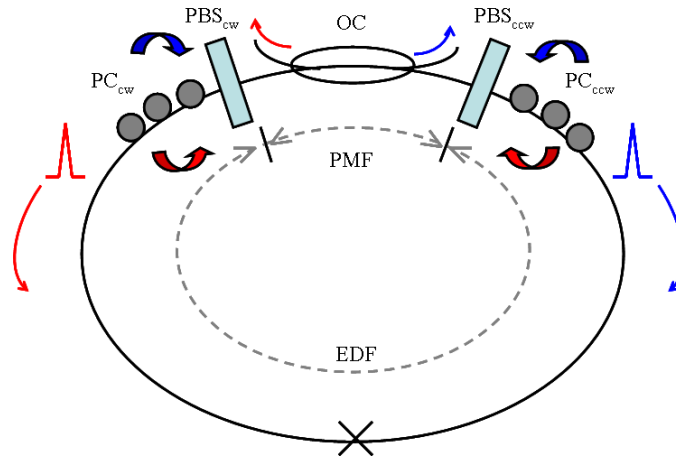
Figure 3.3: Schematics of the basic passive bidirectional mode-locking mechanism.

Initially, a pulse traveling clockwise (blue pulse on the upper right) experiences nonlinear polarization rotation along the section of EDF. As it reaches PC_{cw}, the polarization of the high intensity component is rotated to match the slow axis of a Polarization Beam Splitter (PBS_{cw}), which acts as a linear polarizer placed right behind it. The non-rejecting axis of PBS_{cw} is aligned to the slow axis of a section of Polarization Maintaining Fiber (PMF). During propagation in the PMF section, the pulse travels linearly polarized and may be monitored using an Optical Coupler (OC). After passing PBS_{ccw}, the signal undergoes virtually no attenuation, since it is also aligned to the slow axis of the fiber. At the output of PBS_{ccw}, a second polarization controller PC_{ccw} performs an inverse polarization transformation on the pulse, and the process repeats itself. Because the pulse comes out linearly polarized after PBS_{ccw}

the ellipticity necessary for NPR to occur is given by a phase delay between the orthogonally polarized components of the pulse, introduced either by PBS$_{ccw}$ or the linear birefringence of the EDF itself. At each round trip, the narrowing of the pulse due to the FSA is compensated by a broadening due to an overall net chromatic dispersion (GVD) of the ring laser. After several round trips the two processes are balanced, the pulse energy stabilized, and, at that point, the laser is said to have reached passive mode-locking. In addition to producing NPR on the pulse's polarization state, the EDF also provides the gain of the system which is balanced by its net loss per round trip. In the case of the ccw pulse, the process occurs in a similar manner, only in this case, at the opposite direction, with inverse rotation of polarization angles.

Figure 3.4 shows the four stages of the FSA acting on a pulse, and its corresponding effects on the polarization states at its lower (tails), fwhm (middle section), and high intensity (upper level) components. Note the nonlinear change in polarization between high and low intensity components after propagating along the EDF (upper right figure), and the shortening of the pulse as it passes the absorber (lower right), with its linear polarization states across the entire pulse.

3.2 The Active Mechanism

In a completely active mode-locked laser, the cavity repetition rate is solely determined by the clock and response time of the active component, and it has been used in the past to generate pulses in erbium doped fiber lasers [123, 20]. In the active-passive hybrid case, mode-locking is attained with an active element helping the passive system start off, as it normally would not in a completely passive way. That is mostly the case for bidirectional mode-locked fiber lasers, although passive generation has been reported under special circumstances [84, 80]. The problem

(a) Initial pulse.

(b) Nonlinear rotation.

(c) Linear rotation.

(d) Absorption.
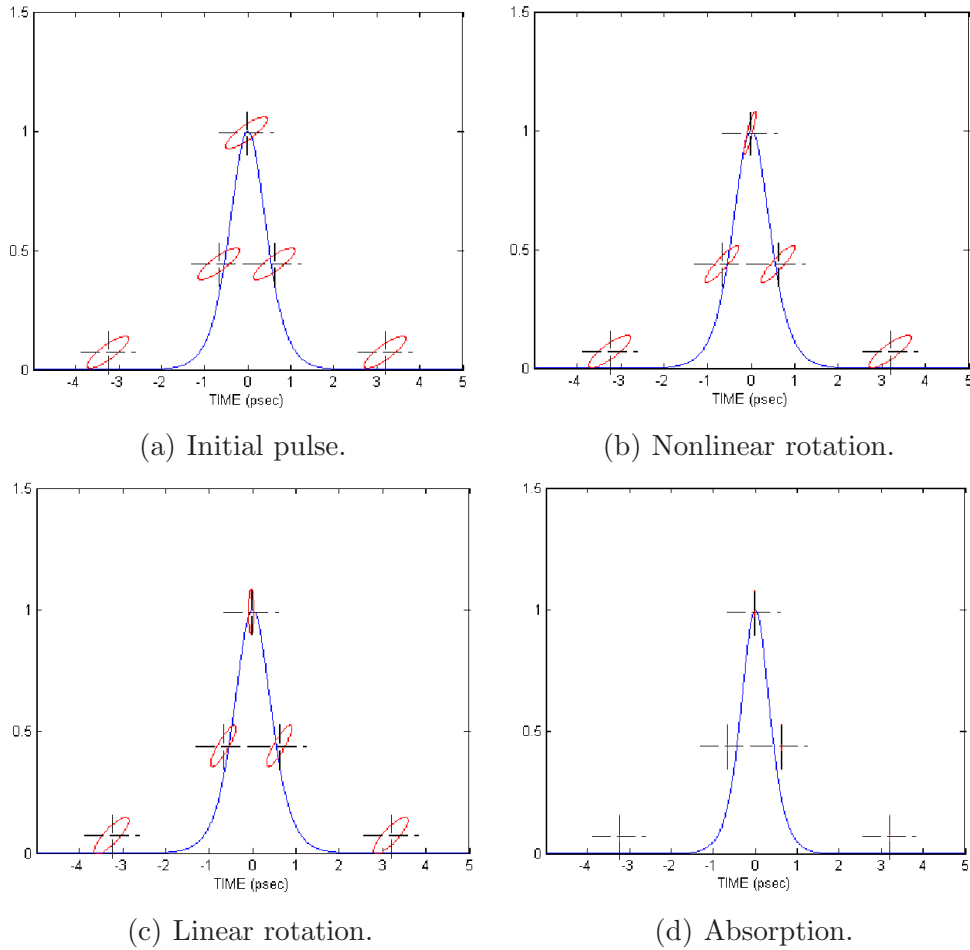
Figure 3.4: Pulse polarization evolution on several stages of the FSA.

usually relates to the fact that acquiring high levels of energy to self-sustain mode-locking is not easily achievable from mere passive phenomena such as generation from single photon events, which are usually associated with self-starting passive systems [96, 97, 138, 24]. In most cases, even for unidirectional mode-locking, the presence of an isolator is required to block unwanted energy loss in counter-propagating direction.

In the bidirectional case, the problem may be overcome with the use of a "thresh-

old gating" control mechanism which lowers the loss of the laser ("opens the gate") at a given time, allowing a pulse to start, while keeping it high ("closed gate") at any other time. That way, an "open/close" sequence can be created to allow a pulse to propagate in a given direction, at a given time, blocking any unwanted counter-propagating pulses, and, at another chosen time, in a similar way, start a counter-propagating pulse, blocking unwanted light in the opposite direction. This section describes the synchronization/sequencing mechanism to produce such sequences, while actual implementation of such mechanism are described in later chapters.
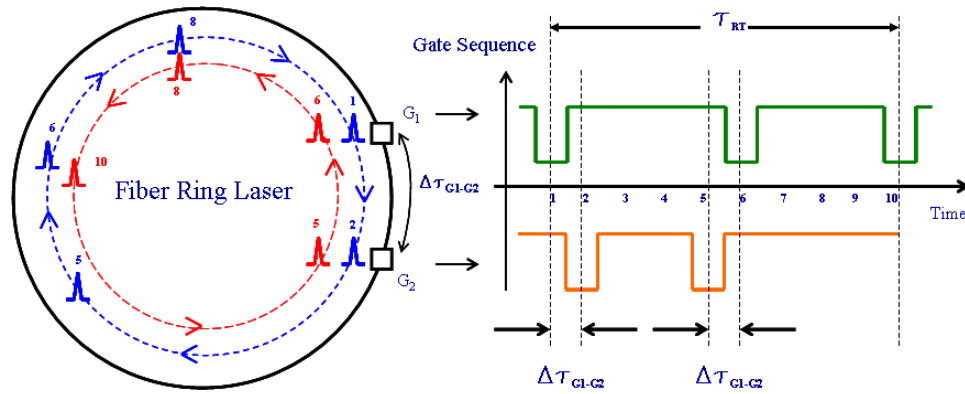
Figure 3.5: Synchronization schemes to open and closing of gates G_1 and G_2, relative to the round-trip travel time of the bidirectional counter-propagating pulses.

3.2.1   Synchronization of Counter-Propagating Modes

To create two independent pulses – i.e pulses that have no phase coupling – a pair of gates must be used so that whenever one "fires" (opens) at a given time, the second will fire a travel time later to allow the pulse to pass through. Figure. 3.5 shows how synchronization of two gates can be achieved in order to produce bidirectional oscillation. It shows a ring laser represented by a circle with two gates positioned such that the time it takes for a pulse to travel from one to the other is "$\Delta\tau_{G1-G2}$".

The waveforms at the right represent the open/close gate sequences for "G_1" (green) and "G_2" (orange) as a function of arbitrary time intervals. At T=1, G_1 opens for a pulse to propagate in the cw direction. A time "$\Delta\tau_{G1-G2}$" later, G_2 must open to allow the cw pulse to propagate through. At the same time, the opening of G_2 may allow light to propagate back in the direction of G_1, which will remain closed a time $\Delta\tau_{G1-G2}$. The surviving pulse will continue traveling in the cw direction when, at time T=5, G_2 opens to start a pulse in the ccw direction. Again, $\Delta\tau_{G1-G2}$ later, G_1 opens to allow the ccw pulse to go through, and another $\Delta\tau_{G1-G2}$ later, G_2 closes to extinguish any unwanted coming in the opposite direction. The pulses cross at T=8, a time which is fixed upon the firing of G_2 for the ccw pulse. Finally, at T=10, which corresponds to an entire round trip travel time τ_{rt} relative to T=1, G_1 opens again to allow the cw pulse to continue propagating, and the entire process repeats again.
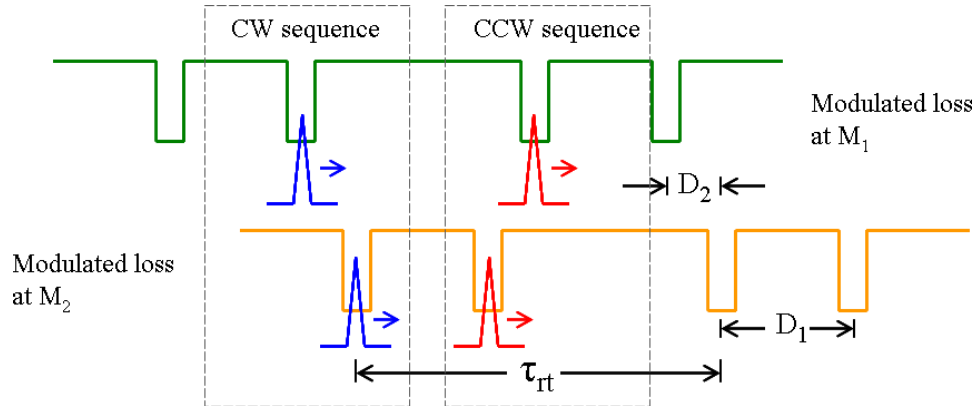
Figure 3.6: Sequence waveforms of gates G_1 and G_2 for bidirectional mode-locking operation.

3.2.2 Sequence Waveforms for G_1 and G_2

The open/close sequence of gates G_1 and G_2, required to produce bidirectional mode-locking, can be summarized by the waveforms shown in Fig. 3.6. An opening/closing of G_1 followed by an opening/closing of G_2 defines a cw sequence, whereas an opening/closing of G_2 followed by an opening/closing of G_1 defines a ccw sequence. This process must be repeated every round trip time for the laser to sustain bidirectional mode-locking. When properly implemented, these waveforms offer two advantages over passive bidirectional mode-locking: (1) not only the two pulses can be formed independently, but also, by controlling the timing that the second gate opens, one is essentially controlling the crossing-points of the counter-propagating pulses. This enables the choice of a crossing point away from a scattering interface, such as a splice intersection. In Chapter 5, a description of how to create these waveforms using a signal from the laser itself is presented.

Chapter 4

Numerical Model and Computer Simulation

In this chapter, the numerical model and computer simulation of the passive system introduced in Section 3.1 is presented. First, the logic of the program and numerical representation of the laser's elements, i.e the propagators and transformation matrices, are described. Then, the results of the computation are shown, and the significance of the findings discussed.

4.1 Numerical model of mode-locking mechanism

When envisioning a practical experimental setup for the laser shown in Fig. 3.3, it is most beneficial to gain an understanding of the circumstances in which it can sustain counter-propagating mode-lock pulsing. In other words, one needs to understand the interplay between gain saturation, NPR, absorption and other effects of fiber propagation, as well as the conditions at which the oscillation stabilizes after evolving several round trips. The next sections describes the logic of the computer program

made to address this issue.
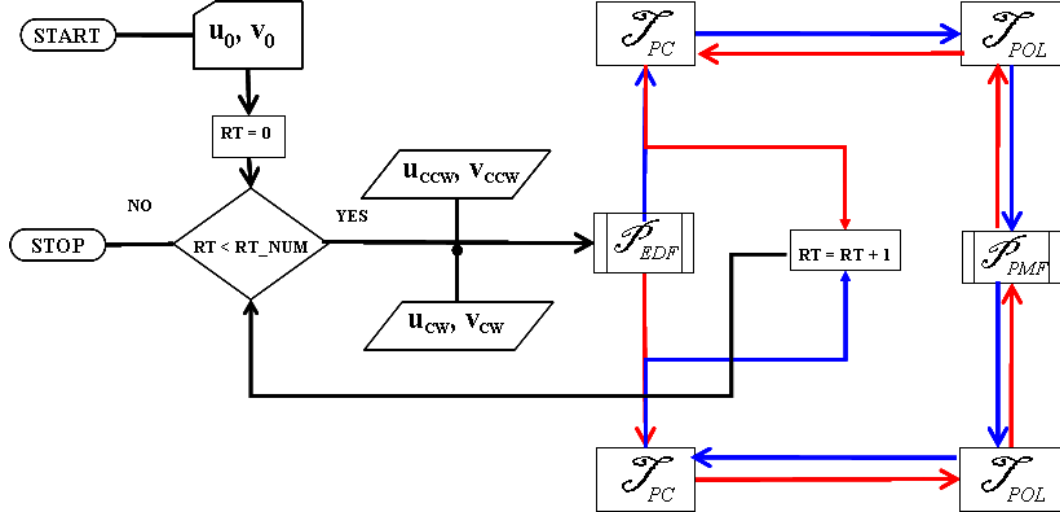
Figure 4.1: Flow chart diagram of the computer simulation.

4.1.1 Logic of program

The logic of the program is very simple, and is best understood from the flowchart diagram of Fig. 4.1. The program simulates bidirectional mode-locking using an algorithm composed uniquely of propagators, corresponding to sections of fibers, and matrices representing passive elements of the laser (i.e polarization transformations and polarizers). Blue lines indicate clockwise direction, and red counter-clockwise. The whole process is carried out in Johnson matrix formalism. The linearly polarized input field vector is assumed a hyperbolic secant function of the form:

$$\mathbf{X}_o(\xi, \tau) = \begin{pmatrix} u_0(\xi, \tau) \\ v_0(\xi, \tau) \end{pmatrix} = A\mathrm{sech}(\frac{\tau}{T_o}) \begin{pmatrix} \cos(\theta_o) \\ \sin(\theta_o)\exp\{-i\phi_o\} \end{pmatrix}, \tag{4.1}$$

where the "T_o" is the initial pulse width, "A" is the normalized amplitude, "θ_o" the angle of polarization relative to the slow axis "u", and "ϕ_o" a small initial phase delay between the orthogonally polarized fields.

A round trip counter "RT" starts the program. If the total number of round trips has not been reached, the solution enters the program and the pulses, cw and ccw, propagate along a section of EDF. Each time a pulse passes the erbium fiber, the small signal gain "g_o" is saturated. Within the two-level system approximation made here, this corresponds to a depletion on the population of the second level as the pulse travels along a section of the fiber. It also means that, as the pulse propagates inside the erbium, the gain is a function of time. The net saturated gain coefficient, assuming no detuning ($\delta = 0$), is given by:

$$\eta(\tau) = \frac{L_{Dedf}}{2}(g_o \exp\{-\frac{P_o T_o}{E_s} \int_{-\infty}^{+\tau} I(\xi, \tau')d\tau'\} + \alpha), \tag{4.2}$$

where, "P_o" and "T_o" are the pulse's peak power and width, respectively, "$I(\xi, \tau)$" its normalized intensity, "L_{Dedf}" the dispersion length of the EDF, "E_s" its saturation energy, and "α" its loss, which is negative, as defined in Chapter 2.

The gain is also a function of space, as it starts to locally recover immediately after a pulse crosses a section of fiber. The recovery is given by the equation:

$$go_{in} = go + (go_{in} - go)\exp\{-\tau_{RT}/T_p\}, \tag{4.3}$$

where "go_{in}" is the small signal gain after a period of recovery determined by the round-trip time "τ_{RT}", and a recovery time parameter "T_p" [41].

At the end of the EDF section, the counter-circulating pulses encounter a polarization controller, represented by a polarization transformation matrix [162, 21, 22]:

$$\mathcal{T}_{\mathbf{pc}} = \begin{pmatrix} \cos\Theta & -\sin\Theta \\ \sin\Theta & \cos\Theta \end{pmatrix} \begin{pmatrix} e^{-i\Phi/2} & 0 \\ 0 & e^{i\Phi/2} \end{pmatrix} \begin{pmatrix} \cos\Theta & \sin\Theta \\ -\sin\Theta & \cos\Theta \end{pmatrix}. \tag{4.4}$$

The polarization transformation matrix has the dual role of converting the pulse's peak polarization state to linearly polarized, and aligning its angle to match the angle of the polarizer's axis (which is along the slow axis of the PMF). The peak

polarization angle, or "tilt" angle "τ_p", is determined by the magnitude and phase of the field components at the peak point, "u_p", "v_p", using the relations [12]:

$$\sin(2\epsilon_p) = \sin(2\gamma_p)\sin(2\delta_p), \tag{4.5}$$

$$\tan(2\tau_p) = \tan(2\gamma_p)\cos(\delta_p), \tag{4.6}$$

where $\gamma_p = tan^{-1}(v_p/u_p)$, and $\delta_p = \phi_v - \phi_u$ is the phase difference between the u_p and v_p components, and "ϵ_p" a parameter related to the eccentricity of the ellipsis.

The value of "Φ" in Eq. (4.4) is fixed at the beginning of the program, and, together with the value of "Θ", as mentioned, set to linearize the polarization of the peak component, and rotate it to match the axis of the polarizer. Analytically, this operation corresponds to solving the equation:

$$\mathcal{T}_{\mathbf{pc}}\begin{pmatrix} |u_p| \\ |v_p|\exp\{-i\phi_p\} \end{pmatrix} = (|\mathbf{u_p}|^2 + |\mathbf{v_p}|^2)^{\frac{1}{2}}\begin{pmatrix} \cos\theta \\ \sin\theta, \end{pmatrix}\exp\{-\mathbf{i}\phi\}, \tag{4.7}$$

for Θ and Φ by setting the output matrix to represent the peak fields u_p and v_p as linearly polarized light with azimuth angle "θ" and common phase "ϕ". Solution to Eq. (4.7) leads to the relations:

$$\tan(2\Theta) = \frac{|u_p|^2\tan^2\theta - |v_p|^2}{\tan\theta(|u_p|^2 + |v_p|^2) - |u_p||v_p|\cos\phi_p(1 + \tan^2\theta)}, \tag{4.8}$$

$$\tan(\frac{\Phi}{2}) = \frac{|v_p|\cos\phi_p - |u_p|\tan\theta}{|v_p|\sin\phi_p[\tan\theta\sin(2\Theta) + cos(2\Theta)]}, \tag{4.9}$$

where, in this particular case, θ and ϕ are set to zero to produce linearly polarized light matched to the axis of the polarizer.

After the polarization transformation, the pulse must pass the absorbing element, i.e a linear polarizer, which is represented by the matrix:

$$\mathcal{T}_{\mathbf{POL}} = \begin{pmatrix} \cos^2(\theta_{pol}) & \cos(\theta_{pol})\sin(\theta_{pol}) \\ \cos(\theta_{pol})\sin(\theta_{pol}) & \sin^2(\theta_{pol}), \end{pmatrix}, \tag{4.10}$$

where, as mentioned earlier, the angle of the polarizer relative to the slow axis is assumed 0. Next, the pulse propagates through a section of PMF, which is simulated by a highly birefringent SMF, intended to emulate a polarization maintaining effect. At the end of the section, it passes through another polarizer, again with its axis aligned to the slow axis of the fiber, and, finally, a second PC performs an inverse polarization transformation with respect to the first PC. In this operation, Θ is replaced by its inverse, and the Φ exponential terms of Eq. (4.4) by their conjugate. The idea is that the inverse transformation works as a forward transformation for the counter-propagating pulse, since its slow axis is reversed relative to the direction in the forward-propagating case (Fig. 4.2). At this point, the program checks the number of round trips, and if the maximum is reached, it halts and outputs the evolved pulse, otherwise, it repeats the process again.
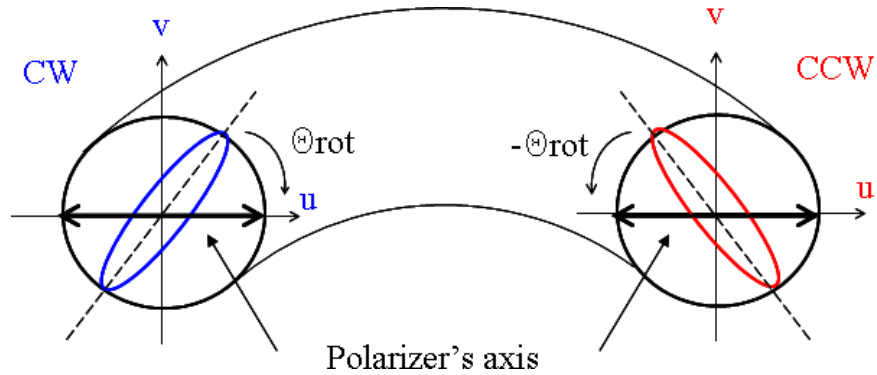
Figure 4.2: Cw and ccw axes location relative to the polarizer's axis and SMF slow axis.

As mentioned earlier, the program essentially consists of two basic elements: fiber propagators, and matrices. Before describing the propagators, it is useful to introduce a brief explanation of the method used for propagation known as the Split-Step Fourier Method (SSFM), which is the topic of next section.

4.1.2   The Split-Step Fourier Method

The Split-Step Fourier Method [56, 57] solves the NLSE equation by breaking it down into two separate operators: a nonlinear "$\hat{N}$", which is solved in the time domain, and a dispersion "linear" operator "$\hat{D}$", which is solved in the frequency domain. The NLSE equation is written in the form:

$$\frac{\partial A}{\partial z}(\xi + h, \tau) = (\hat{N} + \hat{D})A(\xi, \tau), \tag{4.11}$$

where "A" here represents an arbitrary field such as "u" or "v".

The method makes an approximation which considers the linear and nonlinear operators to commute in a localized small length "h" of fiber. Solutions to Eq. (4.11) are, therefore, written as:

$$A(\xi + h, \tau) = \exp\{h(\hat{N} + \hat{D})\}A(\xi, \tau) \approx \exp\{h\hat{N}\}\exp\{h\hat{D}\}A(\xi, \tau). \tag{4.12}$$

In doing the above approximation, one considers negligible the error originated from the fact that the operators $\hat{N}$ and $\hat{D}$ do not commute[1]. In the actual algorithm, the SSFM is written in its symmetrical form [58]:

$$A(\xi + h, \tau) = \mathcal{FT}^{-1}\{e^{\frac{h}{2}D(\Omega)}\mathcal{FT}\{e^{\int_{\xi}^{\xi+h}\hat{N}(\xi')d\xi'}\mathcal{FT}^{-1}\{e^{\frac{h}{2}\hat{D}(\Omega)}\tilde{A}(\xi, \Omega)\}\}\}, \tag{4.13}$$

where, $\tilde{A}$ denotes representation of A in the frequency domain.

Although many algorithms for pulse propagation are written using "finite differences method", SSFM remains a good choice to solving the NLSE when modeling high-speed pulse propagation in optical fibers [136, 104].

---

[1]In reality, the exponential term on the right side of the equation is of the form $\exp(h\hat{D})\exp(h\hat{N}) = \exp(h\hat{D} + h\hat{N} + \frac{1}{2}(h)^2[\hat{D}, \hat{N}] + ...)$, from where, one estimates the error to be on the order of $(h)^2$.

4.1.3 Fiber Propagator

Numerical modeling of a pulse propagation along a fiber requires finding the solution to a initial value problem, using a propagator. In the present case, an initial solution to the Nonlinear Schrödinger equation was assumed in the form of a vector soliton, given by Eq. (4.1), and propagated along a fiber using the SSFM. In order to use SSFM, Eqs. (2.60a) and (2.60b) are written in a form, similar to Eq. (4.12). In doing so, the dispersion operators for u and v can be defined in the frequency domain as,

$$\hat{D}_u(\Omega) = \eta - i\kappa_1\Omega - \frac{i}{2}(sgn + d)\Omega^2 = \eta - i\kappa_1\Omega - \frac{i}{2}\kappa_2\Omega^2, \tag{4.14}$$

and

$$\hat{D}_v(\Omega) = \eta + i\kappa_1\Omega - \frac{i}{2}(sgn + d)\Omega^2 = \eta + i\kappa_1\Omega - \frac{i}{2}\kappa_2\Omega^2, \tag{4.15}$$

and, the nonlinear operators defined as,

$$\hat{N}_u = -i[(|u|^2 + \frac{2}{3}|v|^2)u + \frac{1}{3}v^2 e^{-i2\phi_u}], \tag{4.16}$$

and

$$\hat{N}_v = -i[(|v|^2 + \frac{2}{3}|u|^2)v + \frac{1}{3}u^2 e^{-i2\phi_v}]. \tag{4.17}$$

The dispersion operator describes the effects of group-velocity mismatch (κ_1), group-velocity dispersion (sgn), dispersion gain (d), and saturated net gain (η). The nonlinear operator describes the effects of self-phase modulation, cross-phase modulation, and four wave mixing (coherence coupling). In matrix form, the operators are written as:

$$\tilde{\mathcal{D}}(\Omega) = \begin{pmatrix} \exp\{\frac{h}{2}\hat{D}_u(\Omega)\} & 0 \\ 0 & \exp\{\frac{h}{2}\hat{D}_v(\Omega)\} \end{pmatrix}, \tag{4.18}$$

and

$$\mathcal{N} = \begin{pmatrix} \exp\{\frac{h}{2}(\hat{N}_{u0}) + \hat{N}_{uh})\} & 0 \\ 0 & \exp\{\frac{h}{2}(\hat{N}_{v0} + \hat{N}_{vh})\} \end{pmatrix}, \tag{4.19}$$

where the sum on the exponent terms of the matrix $\mathcal{N}$ corresponds to the numerical integration in Eq. (4.13) over the interval ξ to $\xi+h$, carried out using the trapezoidal rule. Propagating through a section of fiber then becomes a product of matrices interleaved by forward/backward Fourier transformations:

$$\mathbf{x}(\xi + h, \tau) = \mathcal{FT}^{-1}\{\tilde{\mathcal{D}}(\Omega_j).\mathcal{FT}\}\mathcal{N}\mathcal{FT}^{-1}\{\tilde{\mathcal{D}}(\Omega_j).\mathcal{FT}\}\mathbf{x}(\xi, \tau). \qquad (4.20)$$
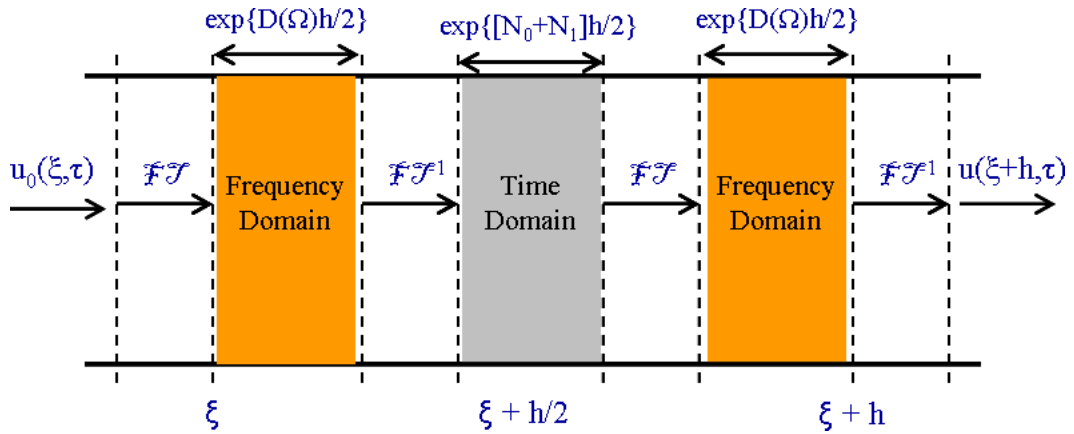
Figure 4.3: Schematics of the Split-Step Fourier Method.

Figure 4.3 illustrates how the SSFM works on an input pulse $u_0(\xi, \tau)$. Initially, the pulse is Fourier transformed and propagated along half the distance "h" in the spectral domain using the dispersion operator. The nonlinear operator term is, then, integrated in space from ξ to $\xi + h$, initially using the values of u and v at midpoint in place of their values at the end of the interval[2]. The pulse is inverse Fourier transformed prior to applying the nonlinear term which acts as if propagating it though the entire space interval in the time domain. The pulse is, then, once more Fourier transformed, and once more propagated another "h/2" distance in frequency domain using the dispersion operator. Finally, it is inverse Fourier transformed once again into the output pulse $u(\xi + h, \tau)$.

---

[2]This integration is later corrected iteratively after the values of u, and v are determined at $\xi + h$.

4.2   Computer Simulation and Numerical Results

The system was simulated in Matlab 7 with a propagator, written in C language, compiled as a MEX file which is easily accessible from the main program as a Matlab function. The propagator can be adapted to simulate pulse propagation in both EDF and PMF, depending on how the parameters are entered in the sub-routine. In the case of propagation in EDF, a net saturated gain is updated at each spatial step of fiber corresponding to a fraction of its total length, with the integration, which regulates the saturation, performed at each time step. Also, at each spatial step, a bandwidth limiting filter, resulting from "gain-dispersion effects", is applied to the pulse in frequency domain. Figure 4.4 illustrates this process.
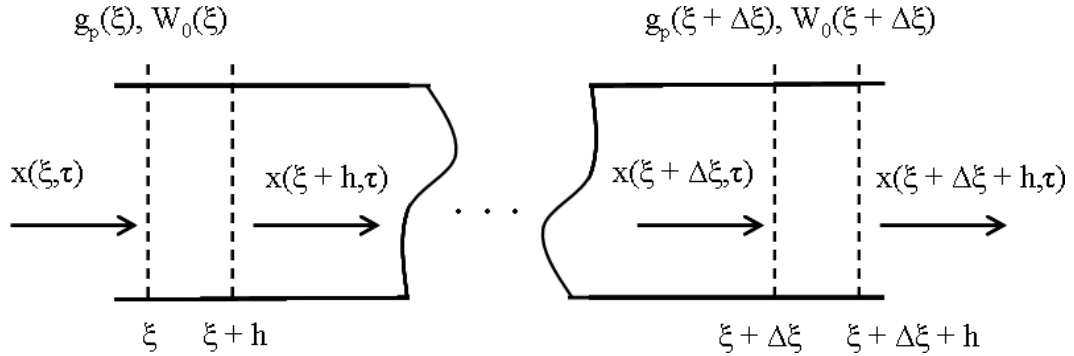
Figure 4.4: Schematics of numerical model for pulse propagation along EDFs.

The dispersion distance $L_{Dedf} = T_o^2/|\text{GVD}_{edf}|$, as previously defined, is kept constant throughout the program, with $\text{GVD}_{edf} = 20\text{ps}^2/\text{Km}$ being the group-velocity dispersion of the EDF, and To the initial pulse width. The initial small signal gain $g_o = 0.076\text{m}^{-1}$, and the loss $\alpha = \text{-}4.6\text{x}10^{-5}\text{m}^{-1}$. The saturation energy $E_s = 4\mu\text{J}$, and $I(\xi, \tau)$, which is the normalized pulse intensity at a propagating distance ξ, was integrated, at each time interval of the pulse, according to Eq. (4.2), to access the saturation correction to the small signal gain. The input peak power P_o, given in Watts, was kept constant throughout the simulation. The normalized birefringence

term, given by

$$\kappa_o = k_o B_{edf} \frac{L_{Dedf}}{2} = k_o(n_x - n_y)\frac{L_{Dedf}}{2}, \tag{4.21}$$

was calculated using a degree of modal birefringence $B_{edf} = 6\text{x}10^{-7}$. The normalized inverse-group-velocity term was approximated as

$$\kappa_1 \simeq PMD\frac{T_o}{|\text{GVD}|}, \tag{4.22}$$

with a polarization mode dispersion PMD = 0.002ps/m. Finally, the GVD-gain dispersion term, again assuming no detuning effects,

$$\kappa_2 = (sgn + d) = 1 - i\frac{T_2^2}{2|\text{GVD}|}g_o \exp\{-\frac{P_o T_o}{E_s}\int_{-\infty}^{+\tau} I(\xi, \tau')d\tau'\}, \tag{4.23}$$

was calculated using a dipole-moment relaxation $T_2 = 0.1$ps, and a positive GVD sign, i.e sgn=+1. Figure 4.5 shows the evolution of a pulse with 100ps width and 60W peak power along a 50m long section of EDF with a high saturation energy level.
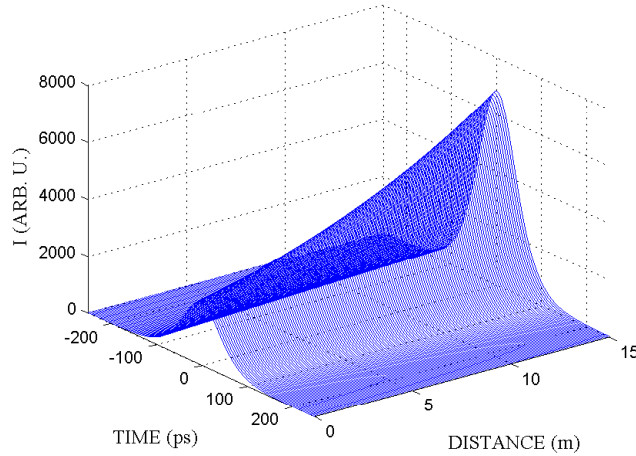
Figure 4.5: Evolution of a 100ps wide, 60W peak power pulse launched in a 15m long section of high saturation energy EDF.

For the case of the PMF propagator, the parameters are defined very much like the EDF's, except that, in this case, the gain term is neglected in Eqs. (4.2), i.e

$\eta = \alpha L_{Dpmf}/2$, with the intrinsic loss coefficient α=-4.6x10^{-5}m^{-1}, and the dispersion length L_{Dpmf}, calculated using a GVD$_{pmf}$=-20ps^2/Km. Again, as in the case of the EDF, L_{Dpmf} is kept constant throughout the computation. The coefficients κ_0, κ_1, and κ_2 are calculated in a similar way, as for the case of the EDF. In this case, however, sgn=-1, with d=0.
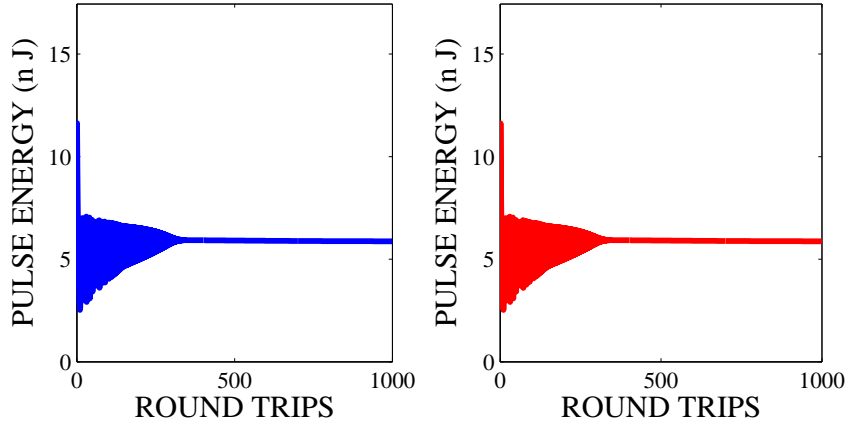
Figure 4.6: Pulse energy as a function of round-trip time for the cw (blue) and ccw (red) pulses.

The pulse has a wavelength λ_o=1.5μm, and is normalized to the soliton order N. At each point where the pulse leaves a propagator, it gets converted to field quantities, in W$^{\frac{1}{2}}$ units, and re-normalized to the specific fiber length units (L_D, L_N) every time it enters a propagator. The nonlinear length L_N is kept constant for each fiber type, calculated using nonlinear coefficient values γ_{edf}=0.004m^{-1}W^{-1}, and γ_{pmf}=0.0015m^{-1}W^{-1} for the EDF and PMF, respectively.

4.2.1   Threshold Mode-locking

The simulation was run with a lumped linear loss of $\simeq 20\%$ and peak power threshold values P_o=60W for both cw and ccw pulses. Figure 4.6 shows the pulse energy shape

results for a simulation of over 1000 round trips. The blue line on the left side graph represents the energy per pulse for the cw light, and the red line, on the right side graph, for the ccw. It is observed that, for both pulses, mode-locking was able stabilize and sustain after $\simeq 300$ round trips with a steady-state energy level of 6nJ/pulse, and an average power of 600mW for each pulse. The recovered small signal gain is also monitored in the simulation, at the input to the EDF (Fig.4.7). As the round trips pass, and mode-locking stabilizes, so does go_{in}, in steady-state, to nearly 0.05m^{-1} for both cw an ccw pulses.
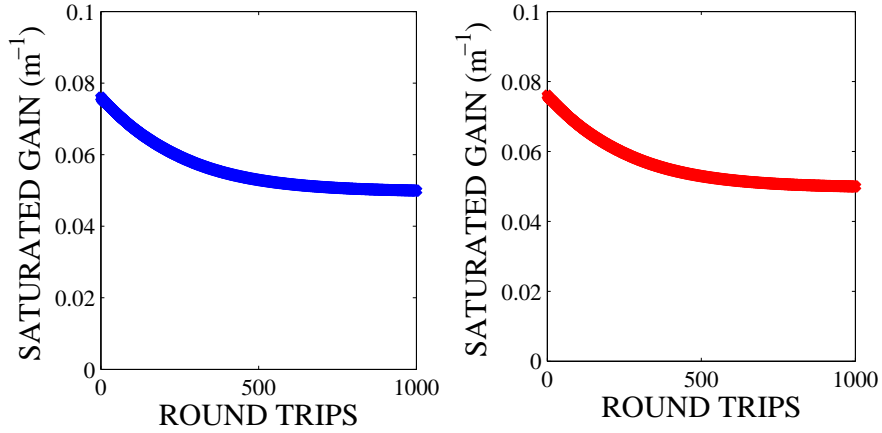
Figure 4.7: Small signal gain at the input of the EDF as a function of round-trips.

Another parameter of interest is the pulse width, which undergoes a significant reduction from an initial 100ps to nearly 8ps for each pulse (Fig. 4.8). In this simulation, the pulse width is determined by the "root-mean-square" (rms) value, rather than the fwhm value. The rms value T_{rms} is calculated from the equation:

$$T_{rms} = (<t^2> - <t>^2)^{\frac{1}{2}}, \tag{4.24}$$

where the brackets denote expected values. For a field distribution A(t), $<t^n>$ is defined as:

$$<t^n> = \frac{\int_{-\infty}^{+\infty} t'^n |A(t')|^2 dt'}{\int_{-\infty}^{+\infty} |A(t')|^2 dt'}, \tag{4.25}$$

where the denominator is known as the "center of gravity" (c.o.g) of the distribution and it measures how much the pulse moves about the time center $\tau=0$.
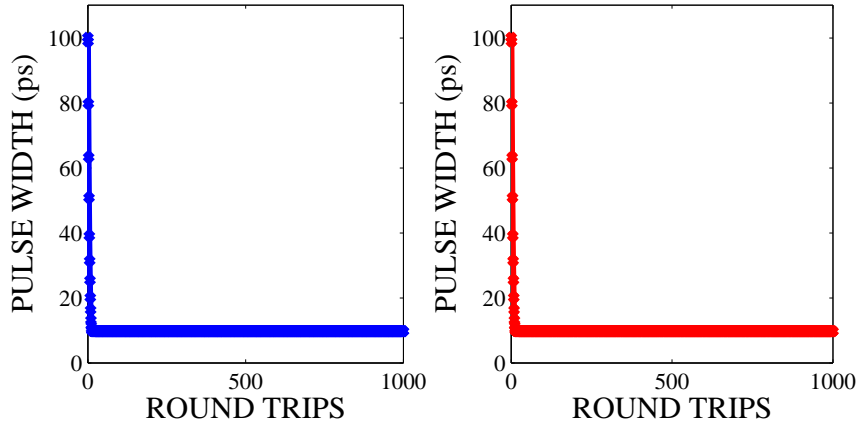
Figure 4.8: Pulse width as a function of round-trip time for a simulation at threshold value for the cw/ccw pulses.
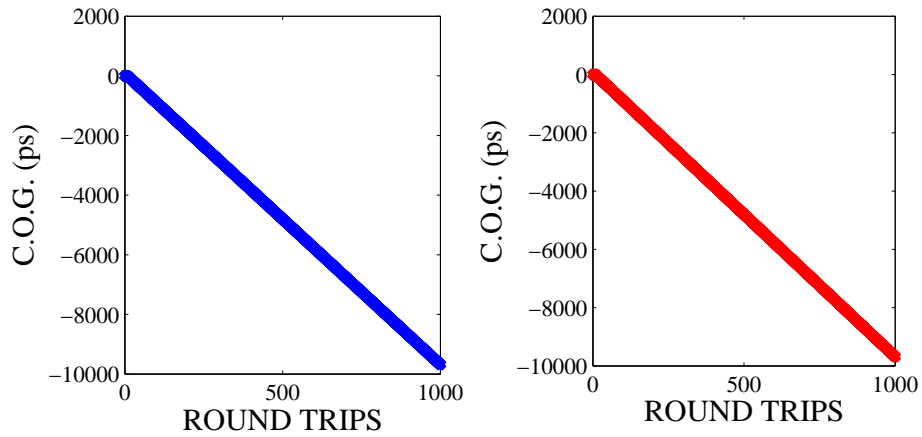
Figure 4.9: Evolution of center of gravity for each pulse as a function of round-trip.

The accumulated c.o.gs, as seen in Fig. 4.9, change linearly with round-trip time. Each slope represents the average group-velocity of each pulse, which is constant and

equal, meaning that, at each round-trip, they travel with the same constant velocity, and, thus, cross at precisely the same location.
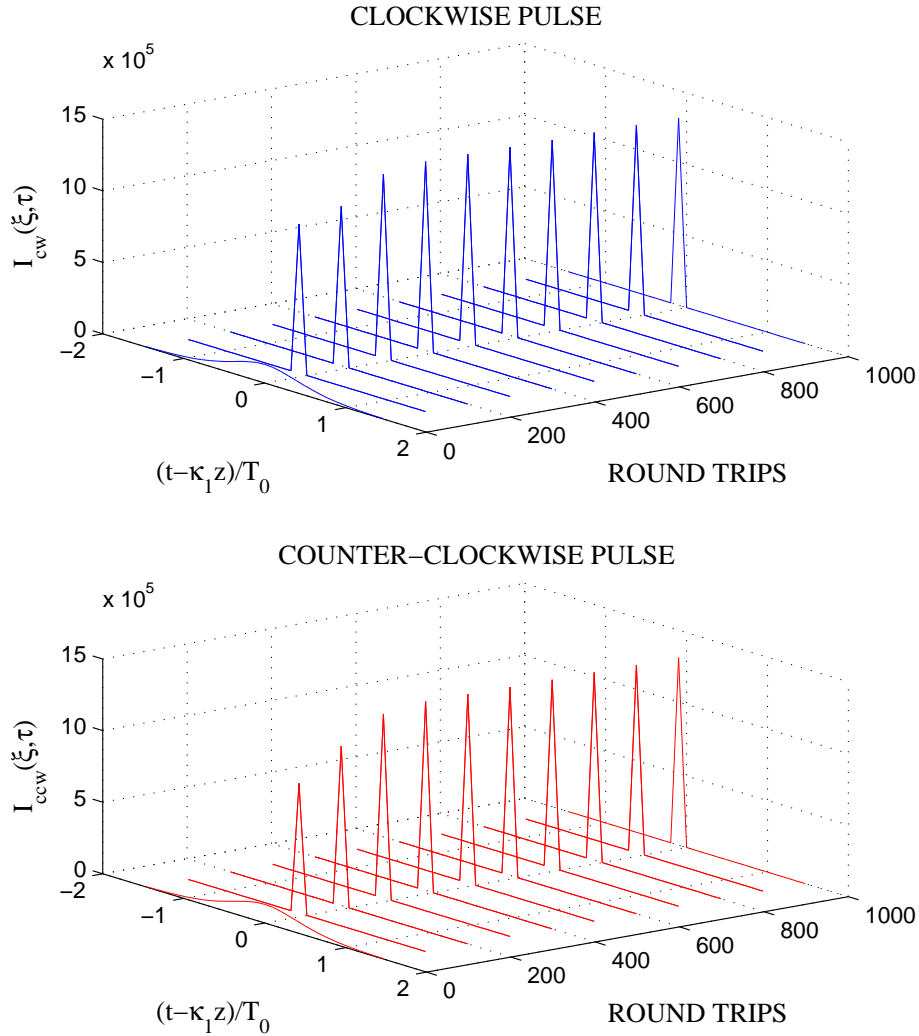
Figure 4.10: Pulse shape evolution after several round-trips for the cw (blue) and ccw (red) pulses at every 100 round-trips.

Finally, the change in pulse shape is shown in the mode-locked pulse pattern of Fig. 4.10. It is seen that after 300 round-trips the shape of the pulse stabilizes.

4.2.2   Input Power Sensitivity and Polarization Noise

In order to get a better assessment of mode-locking performance on a real situation, a change in the initial input power condition, and polarization instabilities were introduced to the system. The first one is aimed at understanding the effects of unequal cw/ccw input power on the mode-locking stability, and the later at studying the effects on mode-locking created by random drifts on the polarization state of one of the pulses. To create the first effect, a simulation was run using one pulse at threshold input peak power, and the other at a higher power.
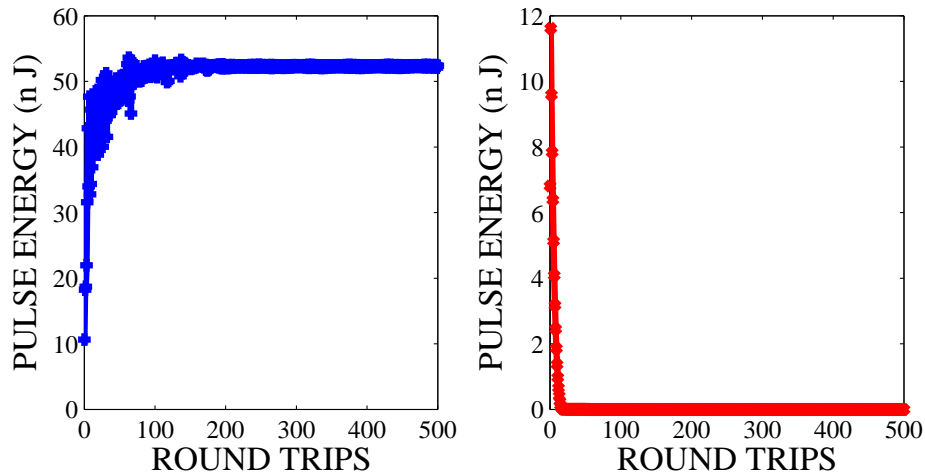
Figure 4.11: Pulse energy values for the simulation results using a cw pulse (blue) with an initial peak power 25% higher that the ccw (red) at threshold level.

Figure 4.11 shows the simulation using a ccw pulse with initial threshold condition (P_{ocw}=60W), and the cw at an initial peak power 25% higher. The results show that, because of gain competition, although at threshold initial condition, the ccw pulse is not able to sustain mode-locking, and eventually dies out. The cw, on the other hand, not only sustains mode-locking, but also reaches an energy level up to 50nJ (8 times the energy level when both pulses start at threshold condition) at steady-state. This

tendency to unidirectionality is understandable, because the higher energy pulse will deplete the overall gain for both pulses, and drive the ccw one below threshold. This calculation illustrates an instability of the laser against pump power fluctuations.
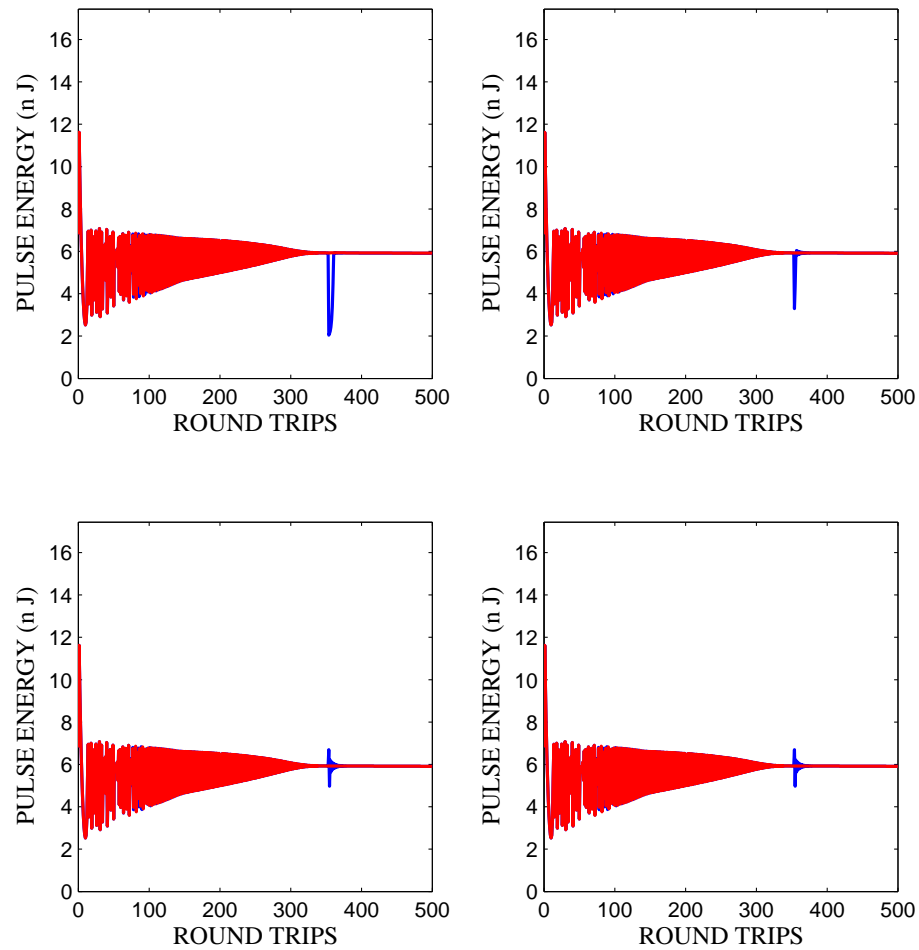
Figure 4.12: Pulse energy characteristics for the cw (blue) pulse, overlapped with the ccw (red) pulse for the simulation results using a noise source at the input to the EDF fiber. The randomly generated noise values are: (a)-1.34rad, (b) -0.83rad, (c) 0.29rad and (d) 0.71rad.

Because the mode-locking mechanism is based on NPR, the system is also very susceptible to instabilities created from disturbances to the polarization state of the pulse. Changes of polarization states in SMF, caused by stress-induced birefringence, can originate even by the smallest of drifts in air currents inside the lab, as they randomly hit a portion of the fiber over and over at the same place. To simulate these changes, a phase noise is introduced to the pulse in the same spot, at randomly chosen round-trips. The noise originates from a normal distribution source with 0 mean value and 0.1 standard deviation.

Figure 4.12 shows the results of the simulation for the case where noise occurs at the input end to the EDF. A single phase jump[3] is set to occur during a 500 round-trips period. It happens around round-trip 350 and it is noticeable in the graphs by its distinct transitory characteristic (the blue "glitch" representing the disturbance on the cw pulse whose uniform energy shape is otherwise completely overlapped by the ccw red line energy). The simulation is run four times, with a different phase noise being introduced each time. It is observed that in all four cases mode-locking was able to recover and sustain.

The simulation was repeated for the case where the point of disturbance occurs at the end of the EDF (Fig. 4.13). In this case, at least one time the cw (blue) pulse failed to maintain mode-locking. This is somewhat expected since at the end of the EDF the effects are more critical, in view of this particular location being right before the absorber (polarizer). Nonetheless, it can be concluded that, for the case of a single phase jump, mode-locking is not drastically affected. In a real scenario, however, not one, but a series of phase shifts, or a constant step phase jump can occur during mode-locking. To simulate that, a sudden 1% drop in the fixed phase value of the cw pulse (at the inverse polarization transformation matrix) was made, well into steady-state.

---

[3]A phase jump may result, for instance, from a single air-current strike on a small section of fiber.
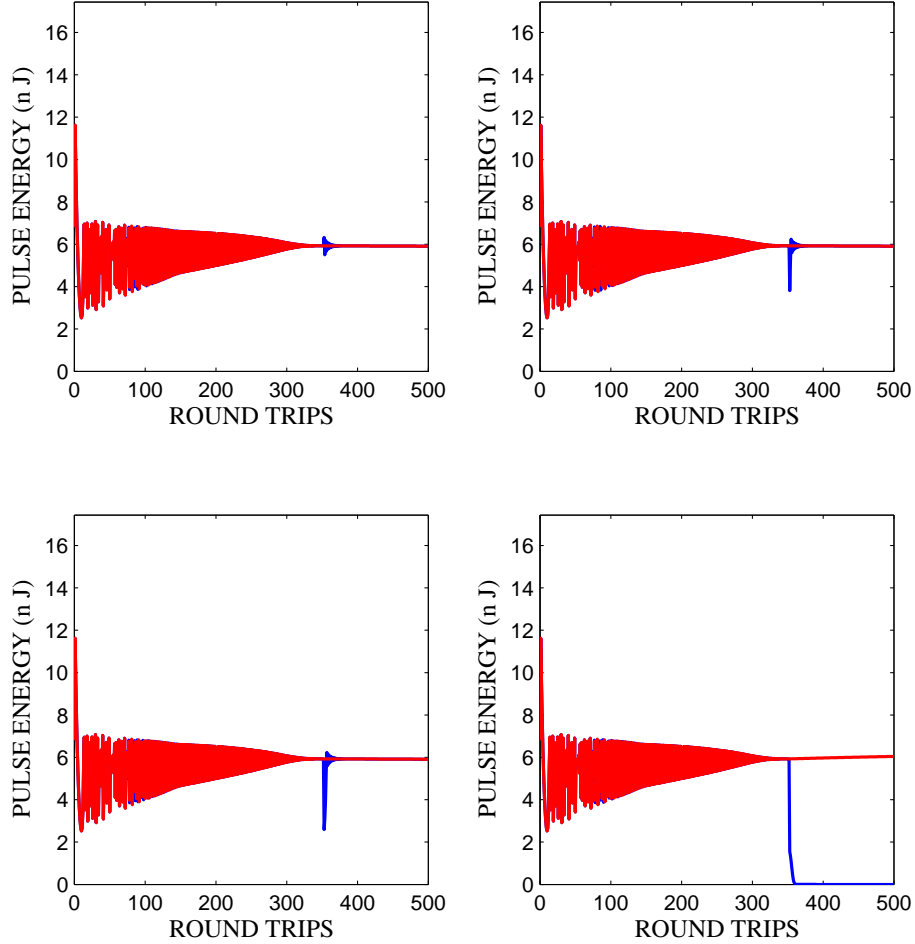
Figure 4.13: Pulse energy values of cw (blue) and ccw (red) pulses for the simulation results using a noise source at the end of the EDF fiber. The randomly generated noise values are: (a)-0.69rad, (b) 0.86rad, (c) 1.25rad and (d) 1.62rad.

As expected, there is a reduction in energy level (a 1nJ drop) of the cw pulse, while the ccw's remained unchanged (Fig. 4.14). The most significant finding, however, is that the center of gravity of the cw pulse undergoes a slight change (Fig. 4.15), while the ccw remained nearly the same. It is an indication of a change in the group-velocity of the cw pulse, which results in a drift of the crossing-point location. For
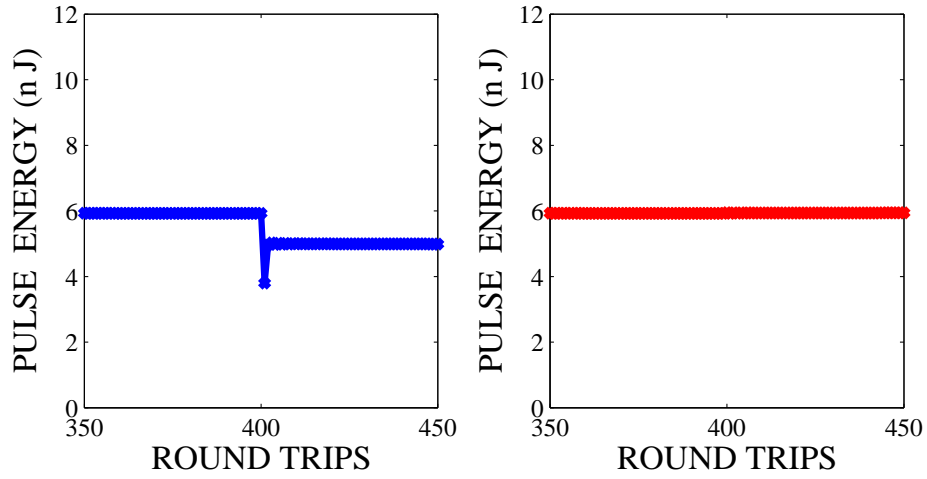
Figure 4.14: Energy change of the cw pulse (blue) associated with a sudden constant step drop in the phase of the inverse polarization transformation matrix.
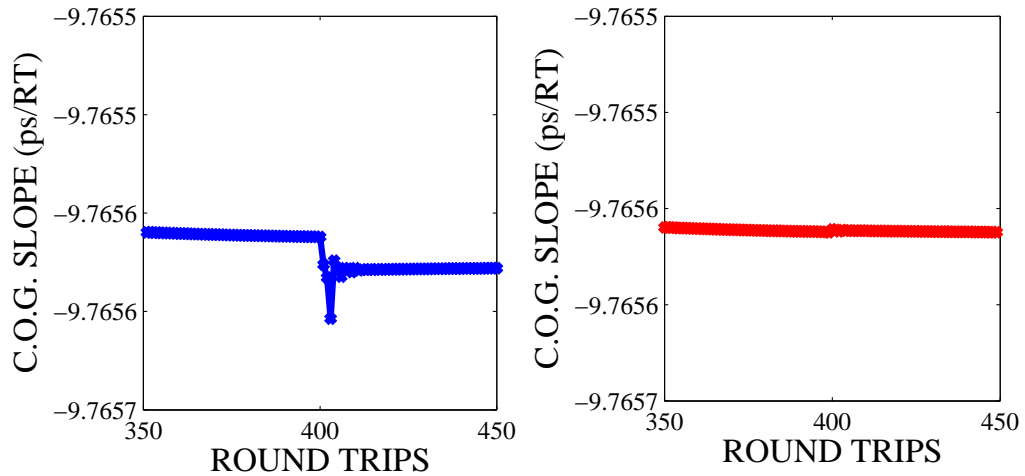
Figure 4.15: Variation of center-of-gravity of cw pulse (blue) in response to a sudden constant step phase drop.

the beat note measurement to be possible, the tolerable drift of the center of gravity is only one pulse duration in a time longer than the beat note period, or 1s (the time window for the measurement, about 5×10^6 round-trips), which corresponds to a stability of 0.04 fs. The simulation indicates a crossing point drift of 1.5×10^{-5}ps

(Fig. 4.16) per round-trip (an accumulated 75ps per measurement) for a 1% phase jump. This implies that a phase change (caused, for instance, by a small motion of a fiber) can not exceed more than 3%, which, in the actual experimental setup, brings instability to the beat note measurement.
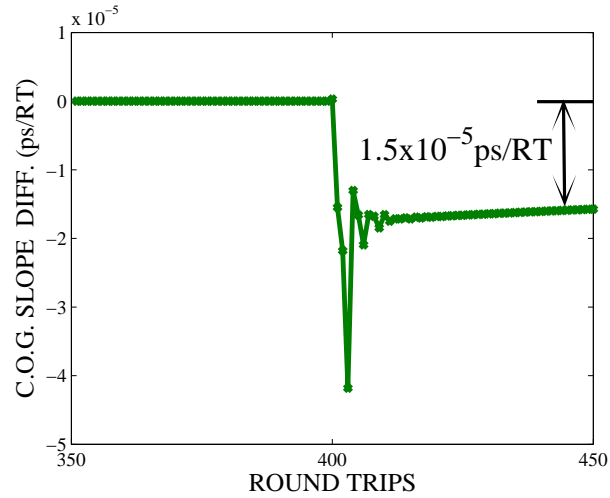
Figure 4.16: Variation difference of the cw and ccw centers-of-gravity.

Chapter 5

The Regenerative System

In a traditional unidirectional fiber ring laser, mode-locking, quite often, requires the insertion of an isolator to start the oscillation. In some cases, mode-locked lasers can self-start without any active element involved [139, 137, 88, 142]. In other cases, an active element must be introduced to give the laser a "kick" in order to get it started [117], or for tunning of the longitudinal modes [91, 49]. Quite often, a feedback system is required to stabilize the laser [37, 86, 113, 156, 20]. For bidirectional mode-locking, an amplitude modulator can be used to block light from either direction at all times, and transmit only at specific desired times. This technique aims to create threshold gating for the oscillating mode, through active modulation of the cavity loss. Such an approach is necessary to bring stability to the laser, or to start the oscillation itself, which may never occur from spontaneous events. Consider, for instance, soliton propagation in an optical fiber laser. To support propagation of the fundamental soliton, a SMF operating on the anomalous-dispersion region, at a wavelength of 1.55μm, would typically require a few Watts of peak power for an input pulse with 1ps width. These levels of magnitude are not easily attainable with simple passive mode-locking mechanisms. Furthermore, most of the time, stabilizing the laser is quite difficult when the repetition rate

is constantly changing due to changes on the cavity's length[1]. In this situation, stabilization requires the introduction of a mechanism to drive the active element using an RF signal generated from the round-trip time of the laser itself. This chapter describes the said system.

5.1   System Description

In recent years, technology has witness an increase in optical system applications to solve electronics problems [118]. The same is true in an opposite sense. During the project, in an attempt to bring initialization and stabilization to the laser, an innovating regenerative system was created [18]. Figures 5.1 and 5.2 show the evolution of the concept.

(a) Isolator   (b) Threshold gate
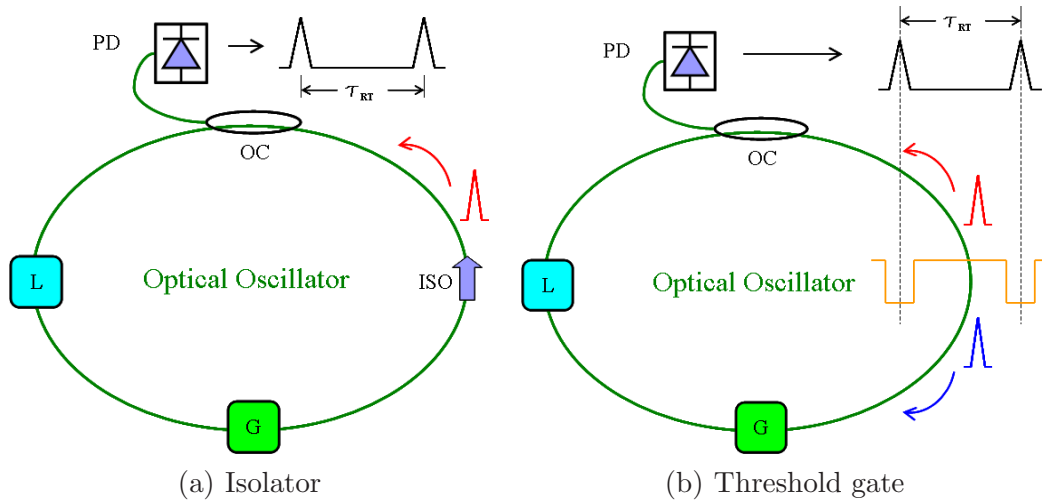
Figure 5.1: Comparison of two ring lasers using (a) an isolator, and (b) a modulator.

It began from the simple unidirectional case (Fig. 5.1a), where an isolator (ISO) is placed inside a generic ring laser represented by the lumped gain (G) and loss

---

[1]Drifts in temperature can change the length of a fiber.

(L) components. The output signal is monitored by a photodetector (PD), which is placed at an output port of an optical coupler (OC). In Fig. 5.1b, the isolator is replaced by a threshold gating device, driven using a fixed round-trip time waveform, which creates a purely active type of mode-locking. This particular condition is called purely active because the waveform is "forced" upon the laser, and does not follow any changes in cavity length, i.e round-trip time changes. In Fig. 5.2a this

(a) Self-regenerative   (b) Modulator Pair
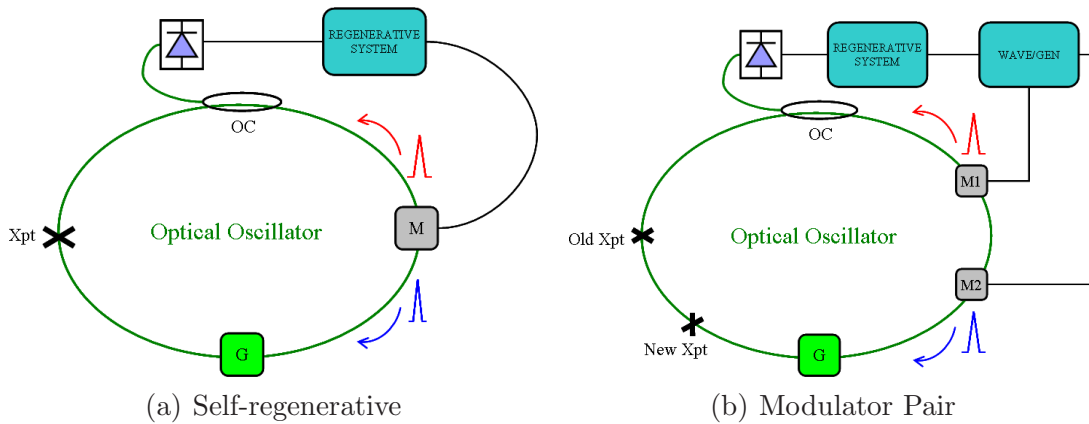
Figure 5.2: Illustration of a self-regenerative system using (a) a single modulator and (b) a modulator pair.

problem is corrected with the gating being controlled by the round-trip time of the cavity, which is regenerated from the laser itself. In this situation, the laser is said to be "passively" controlled by the driving mechanism. Finally, Fig. 5.2b shows the case where two modulators, driven from the regenerated signal, are used for generation of independent pulses and control of their crossing points. This is the case of interested which has been described in section 3.2, and is now explained how it was implemented.

Figure. 5.3 shows a more detailed description of how the setup in Fig. 5.1d works. Here, a fiber ring laser – optical oscillator – spontaneously create "weak" optical pulses, which are not strong enough to sustain themselves in a stable mode-

locked regime, but strong enough to be picked up by a photodetector (PD). A clock-extracting device, such as a Phase-Locked Loop (PLL) circuit, is used to lock-and-track the signal coming out of the PD. After regenerating it, the CLK passes it to the "WAVE GEN" circuitry. These circuits, described in a later section, use the clock of the laser (i.e round-trip time signal) to create the waveforms that are used to drive the modulator pair. The insertion of a low pass filter [2] (LPF), near the band range of the frequency of interest, helps with the conditioning of the driving signal by providing an approximate sinusoidal waveform.
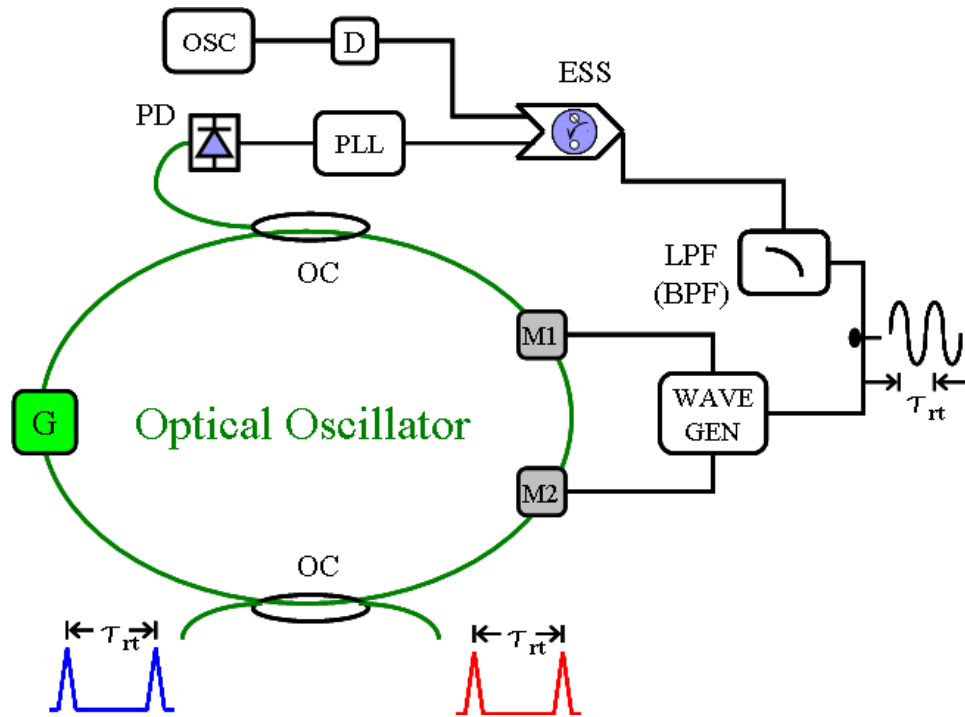
Figure 5.3: Schematics for bidirectional oscillation with self-regenerative system and waveform generator.

---

[2]A low pass filter would work for the fundamental mode. For higher order frequencies, a band pass filter (BPF) could be used instead.

5.2   Electronic-Synchronous Switch

The clock recovery mechanism is one that extracts and regenerates the repetition rate of the mode-locked signal. A popular choice for the device is a Phase-Locked Loop (PLL). These type of devices, which are commercially available in DIP package ICs, use a negative feedback loop system to lock to and regenerate an input frequency signal. It is composed of a phase comparator, a low pass filter/amplifier, a voltage controlled oscillator (VCO), and a frequency divider (or multiplier). They have been extensively used in the context of high frequency applications [31, 32, 33]. They have also been used before as clock recovery mechanism for mode-locking stabilization of fiber lasers [109, 164, 141]. The set back for using these devices is that, in order to lock, they require a steady input signal for at least a round-trip + a settling time. This is not usually available in a laser with "self-starting problems". In this case, an external oscillator can be used to provide an initial "tuning" of the clock-frequency to a "quasi-resonant" frequency. After a few round-trip times, the PLL locks onto the signal and the system can run self-regenerated at that point. In order to ensure a smooth transition of control between the OSC and the PLL, a device, nicknamed the "Electronic Synchronous Switch" (ESS) was designed[3]. This device has a latching characteristic that provides smooth transition (without any loss of synchronization) to switch driving operation of the modulator from the OSC to the PLL.

Figure 5.4 shows the schematics of the circuit. The device, operating on standard TTL input, 50% duty cycle, selects one of two applied input square-waves and sends the selected waveform to the circuit output. In order for the device to work properly, the J-K flip-flop U1A must be triggered on the negative clock edge. This allows switching to occur during the waveform "low" interval which ensures that it does not disturb the output signal during transition. Once switched to the SOSC input, the

---

[3]The device was designed and implemented by Senior Engineer Ronald Kay at the Center for High Technology Material, Univ. of New Mexico.
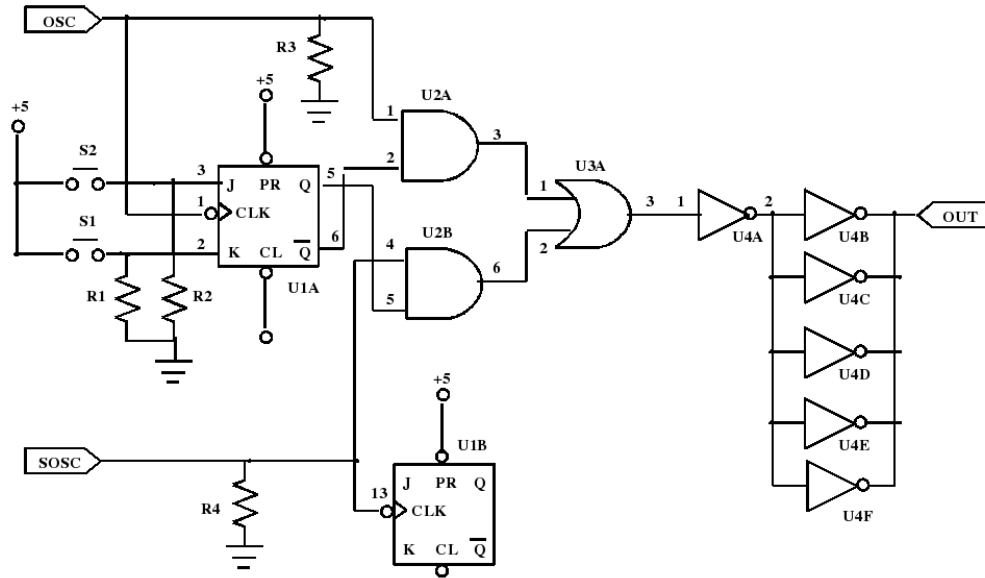
Figure 5.4: Schematics of the Electronic Synchronous Switch (ESS) circuit.

laser system runs free from the external source OSC input, becoming neither phase nor frequency locked to it. At first, switch "S1" is pushed down, ensuring that the device starts up from OSC. The first falling edge of the OSC waveform, which occurs while "S1" is closed, transfers a logical "0" to the output "Q", and a logical "1" to the output "$\overline{Q}$". This operation switches on the AND gate U2A, allowing its output (pin 3) to follow the OSC waveform. Meanwhile, the logical "0" at the "Q" output disables U2B and forces its output (pin 6) to a constant logical "0". Consequently, OR gate U3A only responds to input pin 1 (output of U2A) which is the same as the OSC waveform. Once triggered, U1A will not respond to any additional contact closures from the activated switch. To switch to the SOSC input, S2 must be pressed down. At the first falling edge of the OSC waveform, output "Q" goes high (logical "1") and $\overline{Q}$ goes low (logical "0"). This disables U2A and forces output pin 3 to logical "0", while U2B is now enabled and output pin 6 follows input SOSC. The gate U3A is now constantly low at input pin 1, but at pin 2 it follows the SOSC

input and causes pin 3 to follow it as well. At this point, the switchover between OSC and SOSC sources is complete. Although the "Q" and "$\overline{Q}$" outputs of U1A require time to change state once triggered on the negative edge of the clock input, this change occurs while OSC and SOSC are both "low". Therefore, both U2A and U2B outputs are "low" during the selection transition and keep the output of U3A "low" regardless of the state of U1A outputs ("Q" and "$\overline{Q}$")[4]. Switchover is completed by the time of the first rising edge of input SOSC (after SOSC selection), and the SOSC logical "1" is transferred to the output without any disturbance. Output U3A then transitions from being driven by OSC input to SOSC input during the logical low 1/2 cycle of the waveform. The laser system receives its next input pulse precisely on time but it is now driven by SOSC instead of OSC. The laser fires at the expected time to be picked up by the detector, which then sends an input pulse to SOSC at the correct time to maintain the output repetition rate (positive feedback).

5.3   Synchronous Oscillation

A much simpler circuit architecture, known as the "Synchronous Oscillator" (SOSC) can offer an alternative approach to the self-regenerative system: one that does not need an outside source (OSC) for the initial tuning of the repetition rate. It is said, in many aspects, to outperform the PLL [148]. This type of circuit architecture has been considerably used in strictly electronic applications, but, to the best of our knowledge, up to this day, it has never been used in conjunction with an optical oscillator, and for the purposes described herein. It does require, however, to be carefully designed as to be efficiently able to lock to the repetition rate of the laser.

The basic circuit architecture is shown in Fig. 5.5. With no input, the circuit is essentially an external oscillator, generating a waveform at a fixed designed frequency.

---

[4]This interval corresponds to the "low" state of the input waveforms.
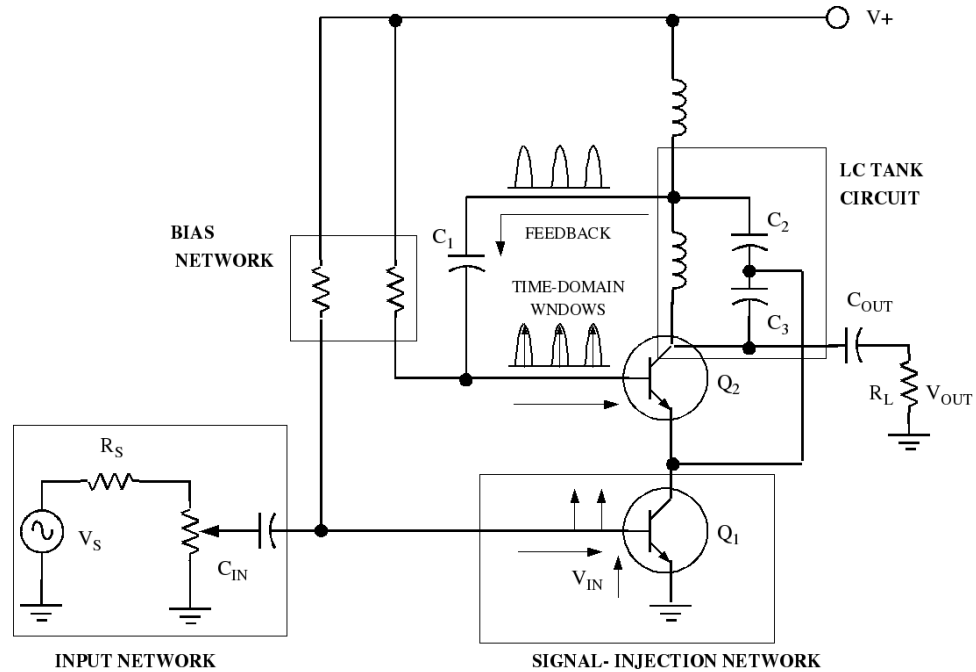
Figure 5.5: Schematics of the typical architecture of a synchronous oscillator (after reference [148]).

This so called center frequency is determined by the parameters of an LC tank circuit (Fig. 5.5). A signal injection network then regulates the current that feeds the tank circuit. It couples the received signal to the oscillator section, forcing it to follow the input frequency. It should be noted that the synchronous oscillator differs from an injection locked oscillator in that the output level is constant over the range of lock frequencies. Although the lock range is a narrow percentage of the free running frequency when compared to typical PLL circuits, this architecture offers the desirable property of enhancing noise rejection. Additionally, lock time is very rapid, typically within a cycle of the free running frequency. The SOSC does not require a sine wave input to obtain lock, an important consideration in this application where the synchronizing input signal is closer to a repetitive pulse outburst. Consequently, the transistors must be carefully selected to preserve beta on the very fast edge spectrum components. The actual SOSC circuit used in the

experiment is the one suggested by Hickman [68], which more robustly defines the DC operating parameters.
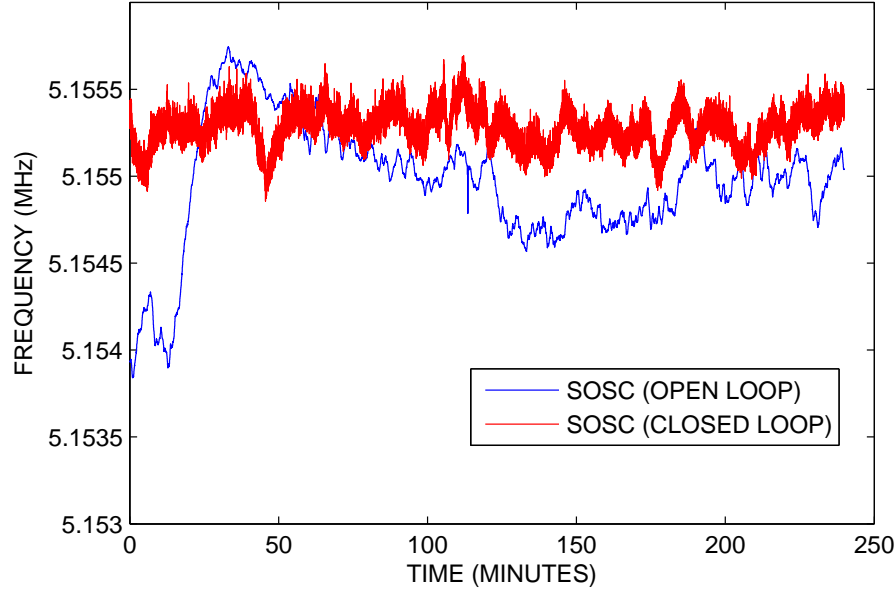
Figure 5.6: Curves of performance of SOSC in OPEN (no input signal) and CLOSED (feedback signal from laser "on") operation modes. In CLOSED loop operation, the detected signal represents a measure of the stability of the ccw mode-locked pulse pattern.

   The performance of the SOSC was evaluated with the instrument operating both in OPEN (no input), and CLOSED (laser on) loop modes. In the open loop mode, the instrument was kept running directly connected to the modulator via a buffer with no input. In the closed-loop mode, the laser was turned on, and the signal (the ccw mode-locked pattern) from the photodetector was fed into the instrument, and a frequency of (5.15525 ± 0.00010)MHz was detected. In both cases, data was recorded over a period of four hours (Fig. 5.6).

5.4   Waveforms Generation

As mentioned earlier, the introduction of an electro-optical modulator to the cavity facilitates bidirectional mode-locking, as it synchronizes the counter-propagating pulses in such a way that their crossing point is controlled. The timing of the waveforms that drive the modulator pair are constructed from the signal regenerated from the laser itself and must mimic the shape of the modulated loss described in Section 3.2.2. In one approach, nicknamed "serial approach", the regenerated RF signal is fanned out, with one branch passing an adjustable delay line (D_1). The signals are recombined using an OR gate and the output fanned out again. One branch drives one modulator whereas the other is once again delayed (D_2), and then used to drive the second modulator. The resulting two waveforms must fall into an "interleaved pattern", exactly as described in 3.2.2, where one modulator must always receive a signal a time later, corresponding to the travel time between the modulators. Figure 5.7 details the mechanism.
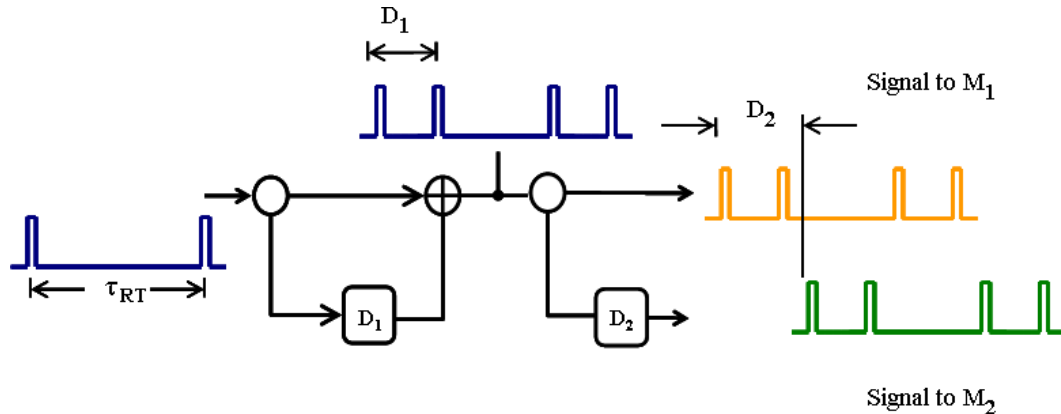
Figure 5.7: Modulator pair driving signals (serial approach).

The idea of converting electrical-to-optical, or, conversely, optical-to-electrical oscillation is not new. In the past, experiments demonstrated that light energy can be successfully converted into spectrally pure microwave signals [159, 160, 163, 43].

Experiments where microwave and optical oscillators are coupled with each other have been often reported [158, 161, 163]. These types of regenerative systems may become a useful tool for high-repetition rate optical pulse generation [153, 1, 36] and harmonic mode-locking lasers [95, 67, 15, 146].

Chapter 6

The Experimental Setup

This chapter explains the laser implementation within the actual experimental setup. It describes the experimental passive laser with all the control electronics of the regenerative system integrated to it. Then it shows the mode-locked waveform data and the results from the crossing between the counter-propagating pulses through the beat-note measurements [17].

6.1   Experimental Passive Laser System

Section 3.1 introduced a simple model description of a passive laser capable of sustaining bidirectional mode-locking using nonlinear polarization rotation. The actual experimental passive fiber ring oscillator is shown in Fig. 6.1. It was build using approximately 15m of low doping EDF[1] with peak absorption 6.4dB/m (at nearly 1530nm), $\sim$ 5m of SMF (Corning$^©$ SFM-28 standard), 7m of DSF (Corning$^©$ SMF/DSF standard), and 10m of PMF (Fujikura$^©$ SM-15-P8 family standard). The DSF was used to balance the average GVD.L_T of the laser, which is -0.08ps^2, where

---

[1]Estimated ion concentration N_0=10.5x10^{24}m^{-3}.

L_T is the total length of the cavity. The EDF is pumped using a pair of 980nm laser diodes (JDSU[©] butterfly package type) – each with an estimated 100mW output power– via a pair of 1550/980 WDMs (Thorlabs[©] type) spliced to the EDF and SMF sections of the laser, and connected to the pump port using FC/APC standard type connectors. Two SMF 2x2 1% Optical Couplers (OCs), Thorlabs[©] type, placed at the outputs of the EDFs were used to monitor the signal, as well as feed the self-regenerative system, and one PMF 2x2 2% OC, at the PMF section, to monitor the output counter-propagating signals. Two Polarization Controllers (PCs) provided the necessary linear rotation of the cw and ccw pulses' polarization states, and two Polarization Beam Splitters (PBS), spliced at the end points of the PMF section and aligned to its slow axis[2], provided the absorption. The entire ring laser was spliced together as an "all fiber" laser system except for a single 3cm long airgap section, right before the a PBS, where a LiNbO$_3$ phase modulator (Φmod) was inserted (Fig. 6.2) for the beat note measurements (Section 6.4). Furthermore, two high intensity, high performance amplitude modulators, custom build for no transmission at 0 DC bias (JDSU[©] types) were placed in the PM section for threshold gating controlled by the regenerative system.

As described in Chapter 3, the laser is mode-locked by a combination of nonlinear polarization rotation (passive), and threshold gating (passively controlled, active mechanism). Figure 6.2 shows the entire system. On the left, the gain is provided by an erbium doped fiber (EDF) pumped by a pair of laser diodes. Polarization controllers (PC) bias the polarization of the pulses' low intensity components to match the rejection axis of an absorbing element (in this case, a polarization beam splitter (PBS)), emulating a fast saturable absorption effect which "narrows" the pulse. At each round trip, this process is balanced by broadening due to the net group-velocity dispersion of the laser. On the right side of the ring laser, two amplitude modulators

---

[2]Soliton propagation along the fast axis faces problems created from XPM induced modulation instabilities [3, 150, 124, 4, 7].
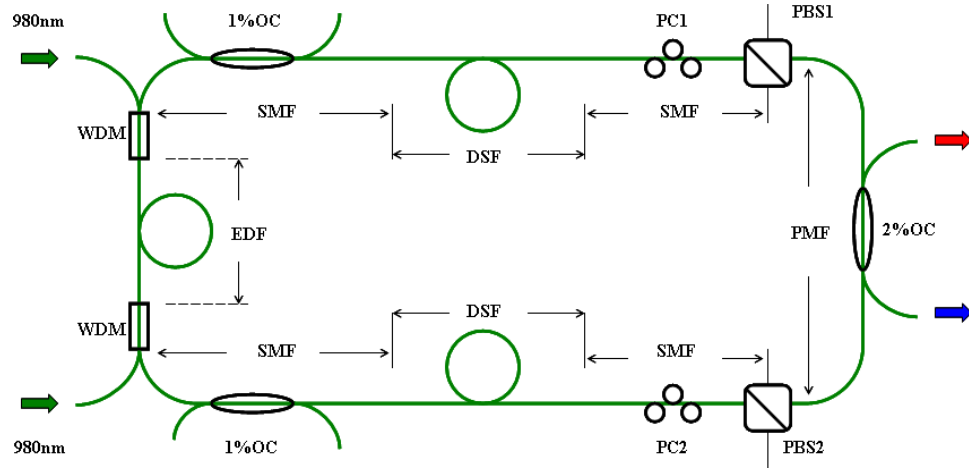
Figure 6.1: Schematics of the actual passive fiber ring laser used experimentally.

are driven in cascade to create two independent counter-circulating pulses. The following section describes the self-regenerative mechanism used to create the driving waveforms of the modulator pair.
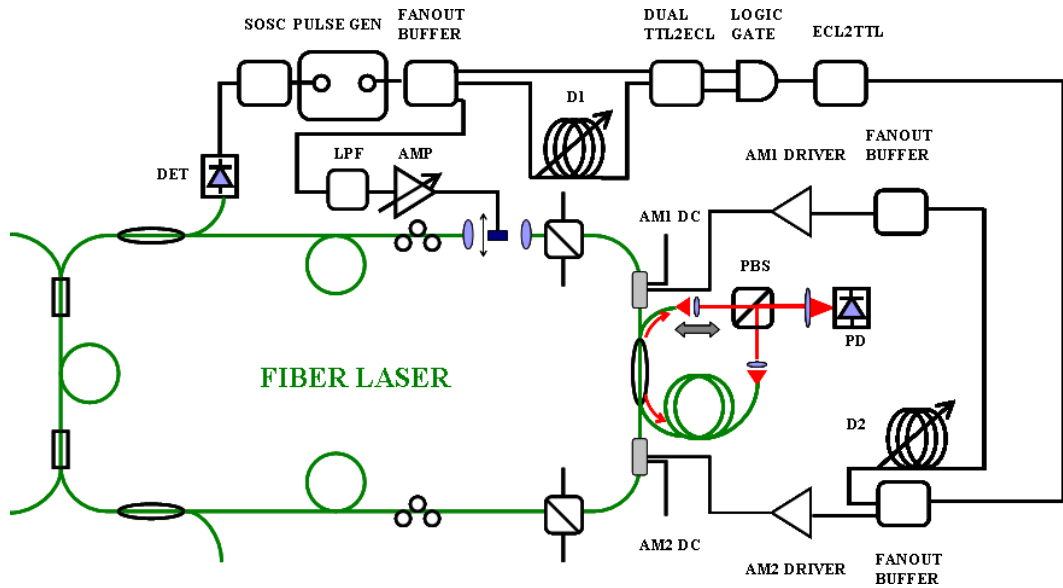
Figure 6.2: Schematics of the entire experimental setup for bidirectional mode-locking of the fiber ring laser.

6.2   Synchronization Scheme

To assist with the starting of mode-locking itself, two amplitude modulators are used
to promote a passively controlled mode-locking mechanism. In addition to providing
the necessary control of the nonlinear loss of the cavity, by direct modulation of the
loss, they serve as a tool to control the crossing points of the counter-propagating
pulses, by means of adjusting the relative delay of their start off time. Figure 6.2
shows how this control is attained. An optical signal is picked up by a fast response
photodetector (PD) (Thorlabs$^{©}$ DET01CFC), attached to one of the 1%OCs. It is
converted to an RF signal and sent to the Synchronous Oscillator (SOSC), which
locks onto it and provides a reference, at the round trip time of the cavity τ_{RT}, to
trigger a pulse generator, "PULSE GEN" (E-H Research Laboratories, Inc., Model
136A). The output signal, regenerated from the laser itself, is sent to a 1:4 50Ω
line driver fannout buffer (PRL-414B from Pulse Instruments.). The buffer, a high
bandwidth device, fans out the signal, in TTL standard levels, at four separate
ports, in sharp rising edge versions of it, i.e 10nsec width "square" waves. Two of
the output signals are used in the regenerative system, one, as describe later, is used
to drive the phase modulator (Φmod) for the beat note measurements. The two
signals are sent to an OR gate (PRL-436N from Pulse Instruments). Before going to
the gate, one of the pulses is delayed (D_1) using coax cables[3] plus a programmable
delay line (Hamamatsu C1097) which provides coarse delay step adjustments (up
to 31.75ns range). Before added at the OR gate, which uses ECL standard levels,
the signal passes through a dual input voltage level translator (PRL-420ND from
Pulse Instruments) to go from TTL to ECL logic level. Similarly, after passing the
gate, it goes through another translator (PRL450ND from Pulse Instruments) to go
from ECL back to TTL. This signal is fanned out once more using a second buffer

---

[3]Issues with coax cable distortion of high bandwidth signals at long transmission lengths
are overcome by the signal being regenerated several times through several fannout buffers.

of the same type. One of the signals is sent to a driver[4] to the modulator (MPI).
The other signal is first delayed D$_2$ using a second fine tuning (0-10.23ns range at
10ps steps) programmable delay line (HPDL-100A-10.23NS by Colby Instruments)
and then sent to another driver to the modulator of the same type of the first.

6.3   Mode-locked waveforms

With nearly 40m of total cavity length mode-locked pulses were created at a fun-
damental repetition rate on the order of 5.1MHz, with an estimated intra-cavity
average power/pulse of 142mW. Initially the two pumps were turned on with no
electronics connected to the system, i.e no active control mechanisms, or RF wave-
forms driving the modulators. With only CW light circulating inside the cavity
(the counter-propagating signals were monitored at the output PM 2% OC with two
DET01CFC photodetectors terminated at 1MΩ load input to the scope), the DC
bias was adjusted at each modulator for no light transmission. Once the biases were
set correctly, all the electronics were turned on, and the driving current of the pumps
were adjusted until pulse patterns were beginning to be visible at the output scope
(now set at 50Ω input termination). At first, the system showed a strong tendency
to "Q-switching", but as the polarization controllers were adjusted it gradually be-
gan to display normal CW mode-locking characteristics. After adjusting the delay
lines, the crossing point of the pulses moved inside the cavity, the open/close delay
sequences between the modulators were corrected, and mode-locking settled into a
stable state. The mode-locked patterns were monitored using a 2.5Ghz, 20Gsam-
ples/sec, digital scope[5] and recorded at several time references. Figure 6.3 shows the
mode-locked waveforms at two different time resolutions.

---

[4]A high bandwidth amplifier, with offset and amplitude controls, that is capable of
maintaining sharpness of the signals' edges.

[5]Agilent Infiniium Series, Model DSO90254A.

(a) 100nsec/div.

(b) 1μsec/div.
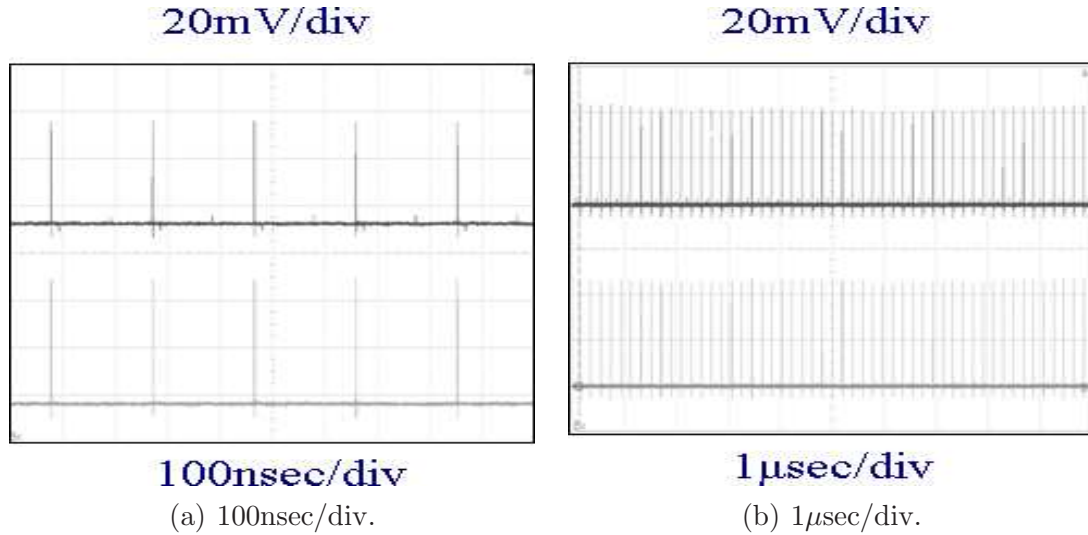
Figure 6.3: Mode-locked waveforms for cw (top waveforms) and ccw (bottom waveforms) pulse trains at two different time scales.

To get a better idea of how narrow the pulses were, a sampling scope was used. The measured pulse widths are shown in Fig. 6.4. Both cw and ccw pulses displayed pulse widths very close to 288ps.

(a) Clockwise pulse width.

(b) Counter-clockwise pulse width.
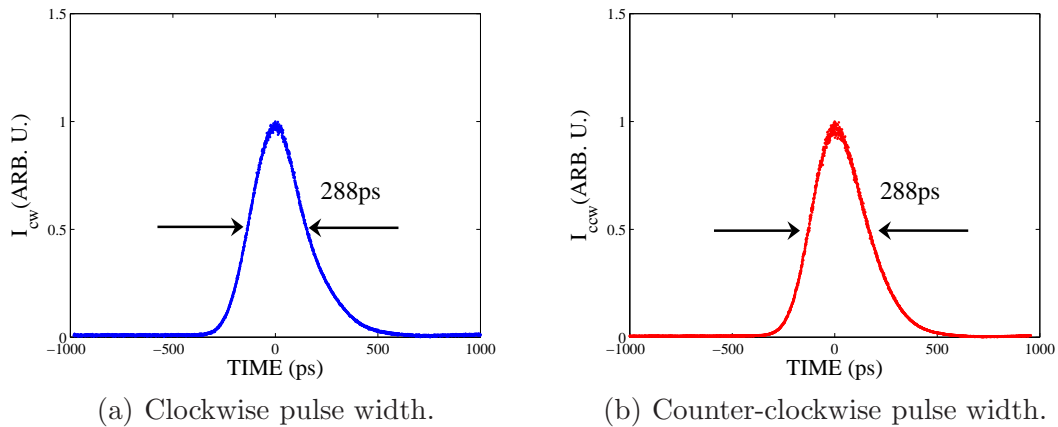
Figure 6.4: Measurements of pulse widths for (a) cw, and (b) ccw mode-locked waveforms.

6.4 Beat-Note Measurement

To measure the beat-note, the counter-propagating pulses were crossed in air at the input to an InGaAs photodetector (Thorlabs©' DET10C) using a 50/50 beam splitter as heterodyning junction. In order to perfectly overlap the pulses, the ccw had to be delayed ∼90nsec, relative to the cw, to compensate for the difference in their arrival time at the output of the 2% optical coupler. In air, that difference would require a travel distance of ∼27m. Using a PM optical fiber, however, that distance was reduced to ∼18m, with the advantage of maintaining both the pulse confined to the fiber, which avoids diffraction problems, and its linear polarization state. An 18m PM optical fiber patchcord was then customer build to delay the ccw pulse, placing it to within ± 1 nsec of the cw pulse.
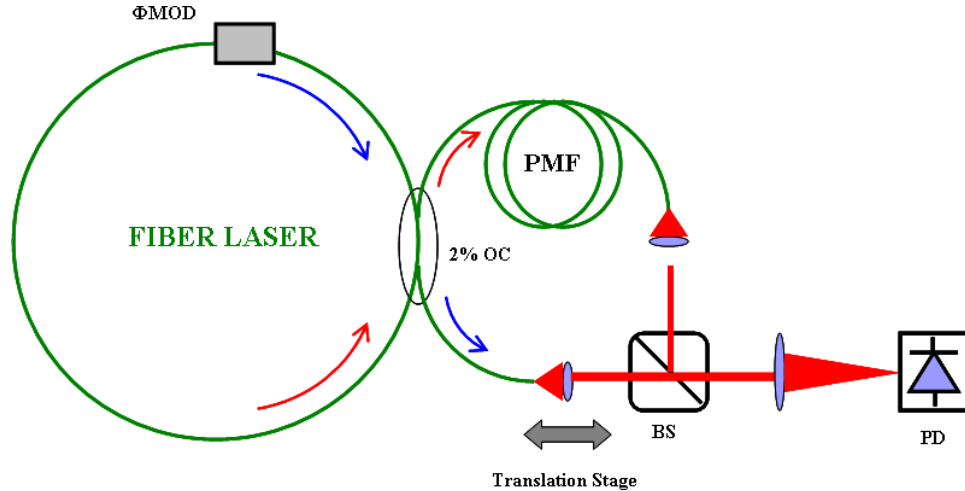
Figure 6.5: Schematics of the experimental setup to measure the beat-note.

The schematics of the experiment are shown in Fig. 6.5. The beams were launched in air using two "FC ready" type collimators connected at the end of the output fibers. The collimators were mounted on a rotating frame to optimize the polarization angle of the linearly polarized light coming out of the PM fibers relative to the 50/50 Beam

Splitter (BS). The two beams were aligned to perfectly overlap both on the detector's and at the beam splitter's surface. Immediately, a "Doppler Effect" fringe pattern could be seen, at a scope channel ($1M\Omega$ terminated input) as the micrometer on the translation stage of the mount directly facing the detector was moved back and forth. This translation confirmed that the pulses, indeed broad, were overlapping well[6].
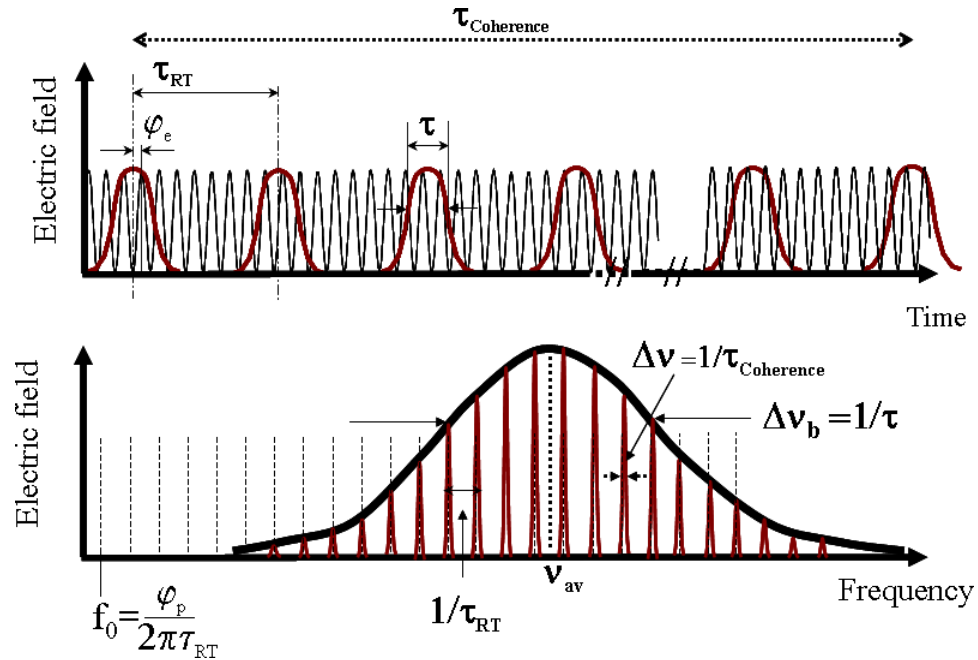
Figure 6.6: Illustration of the origins of the CEO concept, from the pulse train configuration in time domain (top) to its frequency domain representation (bottom). Because the group-velocity (v_g) of the envelope does not match the phase-velocity of the carrier (v_p), an offset frequency appears (f_0 in the frequency domain graph).

In order to see a beat note, a sinusoidal RF signal, locked to the round-trip time of the cavity, was applied to a phase modulator (ΦMOD), for the purpose of originating a carrier-to-envelope (CEO) bias between the counter-circulating pulses, i.e a difference in φ_p (see Fig. 6.6), thus artificially creating a beat $\Delta f_b = f_{0cw} - f_{0ccw}$

---

[6]Fringes could also be seen at the detector's active area which was imaged using a CCD camera.

between them. The "0" frequency associated to the CEO is defined as,

$$\Delta f_0 = \frac{(\frac{P}{v_g} - \frac{P}{v_p})\omega_0}{2\pi\tau_{rt}},$$
(6.1)

where "P" is the perimeter of the cavity, "v_g" and "v_p" the group and phase velocity, respectively, and "ω_0" the carrier frequency.

The regenerated RF signal, provided by the third port of the first fannout buffer (Fig. 6.2), converted to a sine wave using a low pass filter (LP), was amplified using an RF power amplifier (EIN, Model 325LA) with a step attenuator (Kay Electric Co., Model 30-0) at its input to control the levels of amplification. In order to ensure maximum modulation, the voltage difference between the pulses (ΔV_{cw-ccw}) had to line up symmetrical with respect to the "0" crossing point of the RF sinusoidal wave (Fig.6.7). Consequently, the RF wave had to be precisely delayed, relative to the two pulses, to be positioned halfway between them.
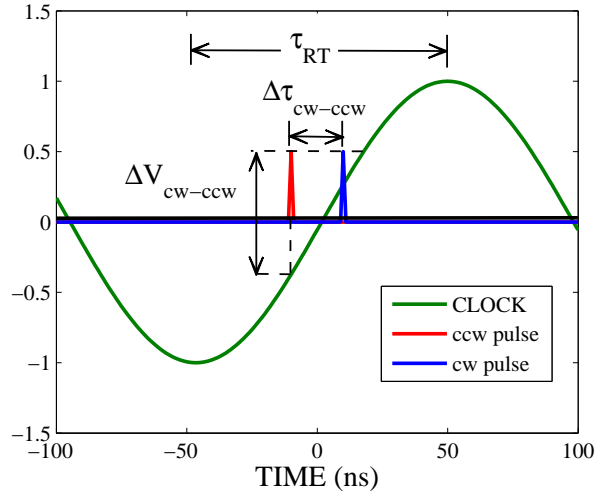
Figure 6.7: RF signal applied to phase modulator for beat note measurement control.

Information on the relative delay time between the pulses $\Delta\tau_{cw-ccw}$, as they crossed the modulator, was inferred from the monitoring of the cw and ccw pulse

trains at the cw and ccw rejection ports of the PBS closest to ΦMOD, as well as knowledge of the pulse travel time between them. The relative position of the counter-circulating pulses to the sinusoidal waveform was set to correspond to the highest achievable voltage difference ΔV_{cw-ccw} between them. Figure 6.8 shows some of the measured waveforms, corresponding to different values of input "rms" voltage. Most of the detected signals displayed close to 50% modulation which indicates good interference (overlap) between the waveforms.

(a) 13.5Vrms.

(b) 4.7Vrms.

(c) 2.5Vrms.

(d) 1.25Vrms.
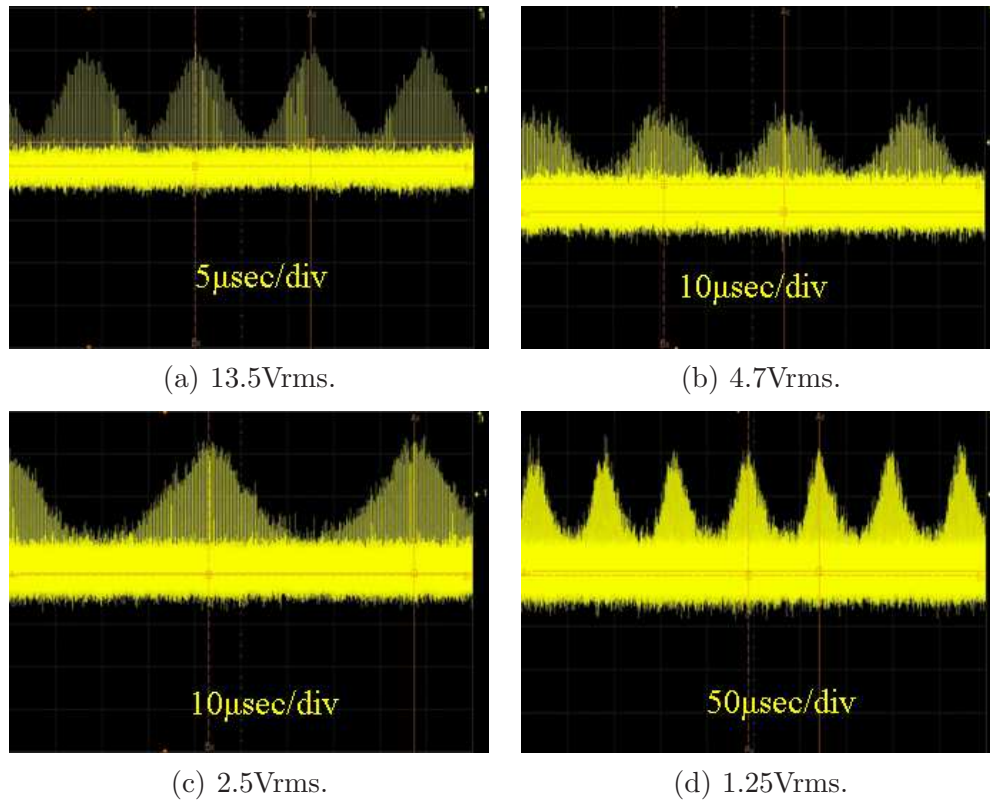
Figure 6.8: Beat note waveforms detected at different levels of rms input voltages.

6.5   Gyroscopic Response

To evaluate the gyroscopic response of the system, the beat note frequency values were plotted as a function of input "rms" values of voltage applied to the phase modulator. The rms values were varied step-wise from as high as 45V to as low as 500mV. Figure 6.9 shows the graph of beat note versus rms voltage together with a linear trend line that best fits the data. The linear fit has a beat note change rate of $\simeq 5.3\text{KHz}/\text{V}_{rms}$ and a response bias "$\Delta\nu_{bias}$" of approximately 10KHz.
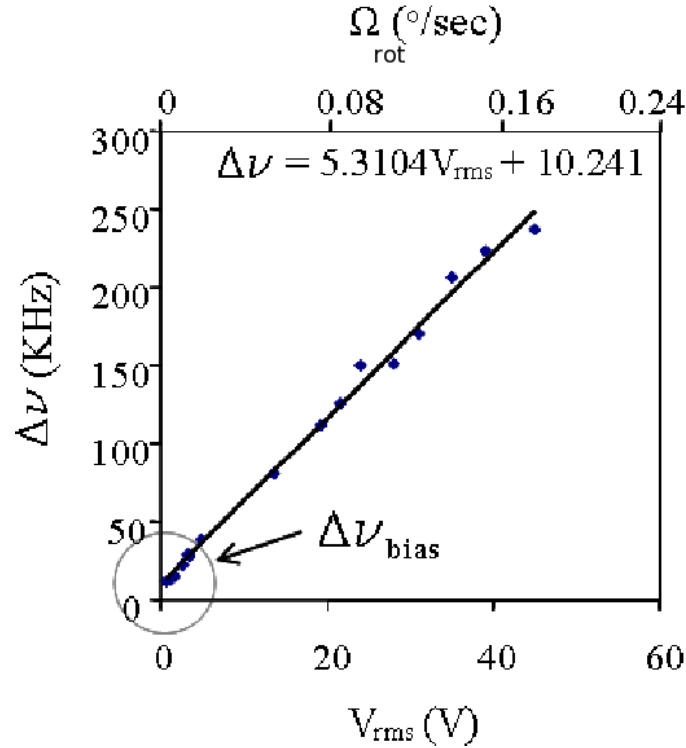
Figure 6.9: Beat-note versus rms input voltage to phase modulator.

This bias can be explained by the existence of an intra-cavity intensity difference "ΔI" between the counter-propagating pulses [98], and estimate from the equation:

$$\Delta\nu_{bias} = \frac{2\pi(n_2\Delta I)P}{\lambda}\frac{c}{2\pi P} = \frac{n_2 c}{\lambda}\Delta I, \tag{6.2}$$

where, as before, "P" is the perimeter of the ring laser, and "n_2" the nonlinear index. For an estimated average intra-cavity intensity per pulse of $0.57\text{MW}/\text{cm}^2$, the calculated intensity difference would be only $\%\Delta I/I = 0.3\%$, which demonstrates a remarkable bidirectional mode-locking performance of the system.

Beat Note Measurement: $\Delta\nu$	Detectable Rotation: Ω_{det} (^{o}/sec)
10KHz	$1.18\text{x}10^{-3}$
1KHz	$1.18\text{x}10^{-4}$
1Hz	$1.18\text{x}10^{-7}$

Table 6.1: Comparison of several values of beat note and their corresponding capacity for rotation detection in a 40m perimeter circular ring laser.

In order to have a better assessment of the significance of the gyroscopic response, the values of rotation "Ω_{rot}", in ^{o}/sec, corresponding to the V_{rms} values, are displayed in the upper axis of Fig. 6.9. These values correspond to the response of the ring laser as if it had been stretched into a circular loop whose radius "R" equals $P/2\pi$, where "P" is it perimeter (i.e 40m). In such a loop laser, the rotation sensitivity would be given by:

$$\Omega_{det} = \frac{\lambda/2}{R}\Delta\nu_{meas.}, \tag{6.3}$$

where "Ω_{det}" represents the "detectable" rotation for a given measured beat note "$\Delta\nu_{meas.}$". Table 6.1 shows a few calculated values of "Ω_{det}" over different "$\Delta\nu_{meas.}$" ranges. To get a sense for what the system represents in terms of sensitivity, consider the fact that a beat note measurement of 10KHz would be sufficient to detect the rotation of the earth, which is $4.2\text{x}10^{-3}$ ^{o}/sec. At lower "$\Delta\nu_{meas.}$", this system could make a powerful sensing tool for geodesic applications.

Chapter 7

Conclusions

Bidirectionality has seldom been observed in the past in both continuous [76] and mode-locked fiber lasers [84, 80]. In one experiment, a 90° Faraday rotator was used as non-reciprocal element to create orto-conjugated and complex-conjugated counter propagating pulse pairs [84]. In the same experiment, it has been reported that the bias frequency of the laser (beat note), in some cases, was sensitive to phase changes due to fluctuations in the birefringence and angle of rotation of the Faraday rotator. In addition to that, performance was limited by the need of a large Free Spectral Range (FSR) resonator to guarantee satisfactory longitudinal selection, and the minimum detectable beat note was 100KHz. In another, more recent experiment, a carbon nanotubes/polymer composite was used as saturable absorber to produce bidirectional mode-locking in a fiber laser [80]. As mentioned earlier, the idea of using carbon nanotubes as SA was initially considered in this project, but dismissed since the crossing-point at the SA will inevitably enlarge the deadband of the system. That is possibly the reason why, in the said report, a large beat note of 2MHz was observed. In fiber lasers, to this day, bidirectional mode-locking had never been achieved using a passively controlled active mechanism to stabilize the laser, as described in this project. This chapter summarizes all the important aspects of the research, and the

advantages of the designed mechanism. Comments on the significance of the findings, and the outlook for future developments, pointing to some aspects of it that may be improved, follows.

7.1   Summary

During the project, stable bidirectional mode-locking of a fiber ring laser using a passively controlled active mechanism was achieved. The entire project evolved around three major areas of research that can be summarized as follows:

- **Numerical Model of Passive Laser System:** A computer model was created to understand the passive mechanisms responsible for the sustaining of bidirectional mode-locking in a fiber ring laser. The model was implemented with the objective of studying the role of the polarization controllers, as well as gain competition, on the counter-circulating pulses, in a NPR based mode-locking system. The results showed that, for a fixed initial phase and azimuth angle values of the transformation matrices, which represent the controllers, mode-locking was only sustained under certain threshold conditions. It has been observed that for the case where the input pulses had unequal initial peak power, even when one of the pulses is only 25% above threshold, gain competition forces mode-locking to unidirectionality as the pulse with a lower initial energy falls below threshold condition. To simulate the effects of air current flow on the birefringence of a fiber, as occurs in a real experimental situation, a 1% drop in the fixed phase value of the cw pulse inverse polarization transformation matrix was made, while the pulse was well into steady-state. A reduction in energy level (1nJ drop) was observed on the cw pulse, while the ccw's remained unchanged. The center of gravity, and consequently the group-velocity, of the cw pulse, changed relative to the ccw's, indicating an ac-

cumulative drift of the crossing-point location at every round-trip. This finding illustrates an aspect of the system which is observed experimentally: to measure the beat note, the phase jump caused by a small motion of a fiber, must be a tiny fraction of the phase amount introduced by polarization controller that regulate the birefringence of a given pulse. Therefore, measures of confinement for the laser must be taken in the future to improve the stability of the system.

- **Self-Regenerative System:** An innovative electronics system has been created using a signal regenerated from the laser's own clock (round-trip time τ_{RT}) with the purpose of driving a modulator pair operating as threshold gating devices inside the laser. The modulator pair itself is a new idea[1] whose primary purpose is to create two independent (phase unlocked) counter-propagating pulses, providing active control of their crossing points along the cavity by means of modulating their loss per round-trip. This system was successfully tested and the idea eventually filled for a patent application [18].

- **Experimental Implementation of Passive/Active Laser:** a passively controlled active bidirectional mode-locking was demonstrated experimentally for the first time by integrating the NPR based passive mechanism with the electronic regenerative system. Stable mode-locked counter-propagating pulses were observed at a repetition rate of 5.1MHz, an estimated average output[2] energy of ~ 0.58nJ per pulse, corresponding to an estimated average output power of 2.9mW/pulse.

---

[1]Envisioned by Dr. Diels from the Physics Dept. at the Univ. of New Mexico.
[2]Measured at the output ports of the 2% PM OC.

7.2 Recommendations for future work

A few improvements which can be made on the numerical model, regenerative system, and experimental setup are described next.

7.2.1 Improvements on Numerical Model

The numerical model used is a very simple model where lots of assumptions were made. For instance, it was assumed that in the propagators, the net saturated gain, and for that matter, gain or losses in all fibers, were the same in both orthogonally polarized directions of propagation. A more refined model of the EDF, for example, would have to take into account the polarization-dependent character of the gain. In [89], a rate equation model that accounts for polarization hole burning in EDFs is presented. This model, as well as others well documented [62, 93], could be incorporated to the current numerical model. Also, in the current model, it was expected that in the actual laser (as it turned out to be the case) the pulse width would be relatively broad. Under a different assumption, i.e of a cavity that can support pulses on the fs range [140], the Raman response of the medium, and higher order GVD effects, would have to be included in the propagator as well. Simulation of fs mode-locked erbium-doped fiber lasers using NPR, for the unidirectional case, has been successfully studied in the past [21]. A similar model can also be extended to the bidirectional case. Furthermore, in a more realistic model, other types of fiber inevitably become a part of the system – e.g SMFs at the input/output ports of OCs, DSF fibers, etc...– and their presence, particularly in the context of the interfaces between different types, brings the issue of the orthogonally polarized (slow and fast) axis misalignment. In other words, at each intersection (splice), a change in basis must be performed before a propagator can be used so that the slow and fast axis are decomposed correctly to the basis of the particular fiber in which the pulse

propagates. Extensive studies of this type of propagation, as well as propagation with more generalized birefringence types have become available for quite some time now [99, 100, 101, 102]. Incorporating one such propagator in this system can be quite challenging and, for the moment, beyond the scope of this work. Finally, in addition to using the Split-Step Fourier Method, other types of numerical computation are available and one can only benefit by using it for the simulation of bidirectional mode-locked fiber lasers. The finite differences method, for instance, is very popular, and it has been used in the past to study pulse propagation in fibers [147].

7.2.2 Improvements on Regenerative System

A second approach (Fig. 7.1), nicknamed the "parallel approach", for the driving waveforms generation is currently under investigation. In this approach the regenerated signal is initially fanned out in three separate ports. One provides a signal which directly goes to a modulator to start a pulse in one direction. A second, delayed the exact travel time between the modulators, is sent to the second modulator to open for the pulse coming from the first modulator to pass through. The third one, delayed of an arbitrary amount, is responsible for creating the counter-propagating sequence. It first goes to a second fannout device. From this device, one of its port signals will directly drive the second modulator to initiate the pulse in the opposite direction. Another port, delayed the precise travel time between the modulators, will go to the other one to open for the pulse to go through. This second approach, as compared to the first, offers the advantage of independently moving the crossing-point of the counter-circulating pulses around the ring laser using a single adjustable delay line (the first one). The only disadvantage of this approach is that the travel distance between the modulators is kept fixed and can not be adjusted without the introduction of two extra programmable delay lines.
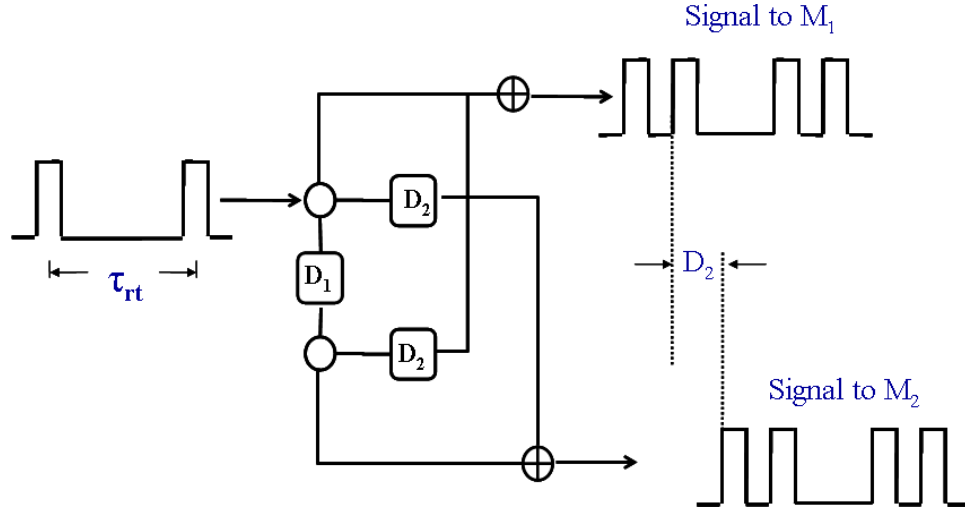
Figure 7.1: Modulators' driving signals (parallel approach).

Further improvements in the regenerative system can yet be made with an introduction of a circuit which can automatically control any adjustments to D_1 and D_2 to correct for variations on the repetition rate of the regenerated RF signal. One such a circuit would not be so trivially implement as, for instance, any adjustment of D_2 would require knowledge of the change in the time travel between the modulators. Not so critically, however, would be the adjustment of D_1 as, once D_2 is fixed, it can be derived from the round trip time τ_{RT}, using some simple logic circuitry.

7.2.3 Improvements on the Experimental Setup

Experimental implementation of the second RF driving signals scheme (Section 7.2.2) is currently under development. The experimental setup is shown in Fig. 7.2. In this case, the first buffer fans out the signal in two separate ports: one is used to drive the phase modulator, for beat note measurements, and the other sent to a second buffer. The second buffer fans out the signal in three separate ports: one goes to one input of an OR gate whose output will drive one of the modulators, and the
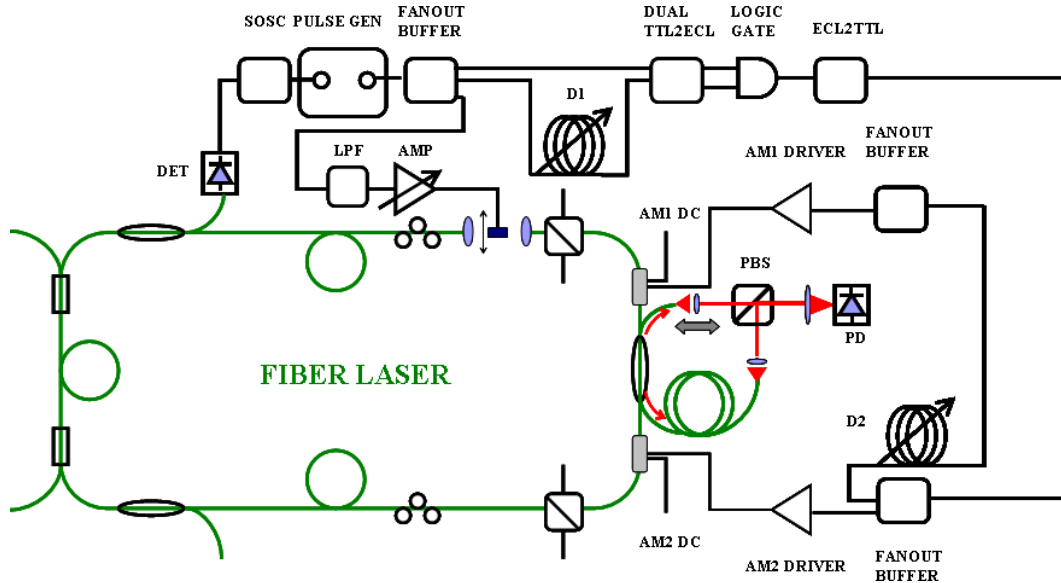
Figure 7.2: Schematics of the experimental implementation for the RF driving signals using the "parallel approach".

second, delayed a fixed "travel-between-modulators" time, will go to a second OR gate whose output will drive the other modulator. In conjunction, the two signals create a sequence for mode-locking in a certain direction. A third port provides the signal, whose adjustable delay controls the pulses' crossing point across the laser, to a third fannout buffer. The outputs of this buffer provide the sequence for the pulse in the opposite direction. One port sends the signal directly to the OR gate associate with the modulator where the pulse will start, and the second, delayed the fixed "time-between-modulators" travel time, sends the signal to the other modulator. All the parts used are essentially the same used in the first driving scheme, except for the addition of a second OR gate (ECL-to-TTL and TTL-to-ECL logic translators as well). It is, however, conveniently reduced by one programmable delay line.

Appendices

Appendix A

Properties of Optical Fibers

A.1 Dispersion

The term dispersion has often been used to describe two distinct properties of optical fibers, i.e chromatic, and modal dispersions. The first is related to the Taylor Series expansion of the field's wave-vector, whereas the second is related to the velocity of propagation of the orthogonally polarized components of the field.

A.1.1 Chromatic Dispersion

Fused silica fibers typically have a negative dispersion value of -25$(ps)^2$/Km at the wavelength $\lambda \simeq 1.55\mu$m. This value corresponds to the second order coefficient of the Taylor series expansion of the wave vector, as shown in the equation below:

$$k(\Omega) = k_o(\omega_l) + k_1(\omega_l)(\Omega - \omega_l) + \frac{1}{2}k_2(\omega_l)(\Omega - \omega_l)^2 + ..., \tag{A.1}$$

where $k_n = d^n k/d\Omega^n$, $v_g = 1/k_1$ is the pulse's group velocity, and "k_2" is known as the group velocity dispersion (GVD). In EDFs, additional chromatic dispersion is introduced due to the presence of the dopants [61].

A.1.2 Polarization Mode Dispersion (PMD)

Polarization mode dispersion is related to the birefringence of the fiber, and it describes the amount at which one of the two orthogonal eigen-modes lags in phase with respect to the other. Figure A.1 shows how the polarization evolves inside a fiber as a consequence of birefringence.
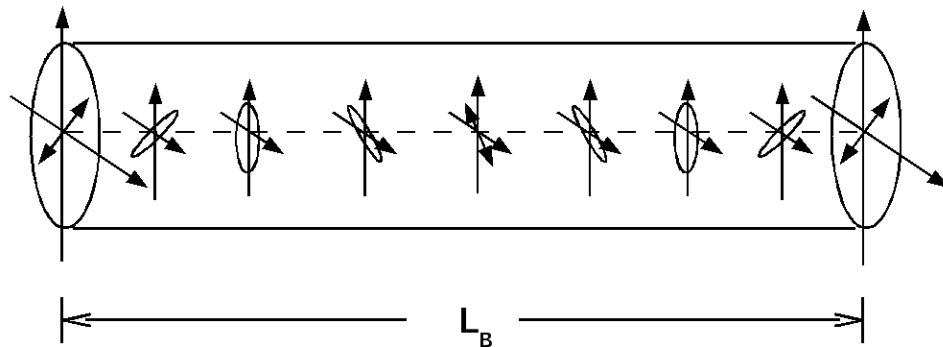
Figure A.1: Polarization evolution in a linearly birefringent fiber of beat length L_B.

The beat length is a parameter that describes the polarization evolution inside the fiber. It represents the length of fiber it takes for the input light beam to return to its original polarization state. It is defined as:

$$L_B = \frac{2\pi}{|k_x - k_y|} = \frac{2\pi}{k_0|n_x - n_y|} = \frac{\lambda_0}{B}, \tag{A.2}$$

where $k_{x,y}$ and $n_{x,y}$ are the propagation constants and indexes of refraction on the x and y direction respectively, k_0 the wavenumber, and $B = |n_x - n_y|$ represents the degree of modal birefringence. A technique to measure the beat length in a low birefringence fiber using an optical loop mirror has been reported in the past [46].

Polarization mode dispersion has been the subject of intense study in the context of its effects on pulse propagation in optical fibers [59, 34, 90], and in relation to its impact on signal degradation in optical transmission systems [79, 48, 134, 16].

Several techniques for detection [111, 114, 115], and compensation [130, 27, 135] have been proposed and evaluated [81].

A.2   Distributed Gain Medium

In an all-fiber ring laser, gain is mostly likely provided by a rare earth doped fiber such as YtEr-, or Er+3- doped fibers. Ultrashort pulse sources based on rare-earth-doped fibers have been the subject of extensive study in the past [23, 71, 52, 51, 50, 54]. In one experiment, an environmentally stable Kerr-type mode-locked erbium fiber laser produced 360fs near bandwidth-limited pulses [55]. In another experiment, passive mode-locking based on an active nonlinear directional coupler concept, used a dual-core-erbium-doped fiber laser [152]. In order to understand the dynamics of mode-locking, an understanding of how an erbium doped fiber works as a distributed gain medium is necessary. This section discusses some of the equations that govern the behavior of signal, pump and population inversion inside an erbium-doped fiber.

A.2.1   Homogeneously Broadened Gain Medium

In a homogeneously broadened gain medium, the spectral gain has the Lorentzian form given by:

$$g(\Omega) = \frac{g_o}{1 + (\Omega - \omega_a)^2 T_2^2 + \frac{E}{E_s}}, \tag{A.3}$$

where g_o is the peak gain at the light frequency ω_l, ω_a is the atomic transition frequency, T_2 the dipole relaxation time of the 3 level system, which is on the order of 0.1ps, and E and E_s the input energy and saturation energy, respectively.

A.2.2 Simplified Two-Level Rate Equation

If one neglects the effects of amplified spontaneous emission and absorption of the excited state – i.e assumes $T_2 \simeq 0$ – one can use the simplified rate equation of a 2 level system [131]:

$$\frac{\partial}{\partial t} N_2(z) = R_p N_1(z) - R_s(N_2(z) - N1(z)) - \frac{N_2(z)}{T_1}, \tag{A.4}$$

with $N_2(z)$ and $N_1(z) = N_T - N_2(z)$ being the populations of levels 2 and 1 (N_T the ion doping concentration), respectively, and T_1 the relaxation (or fluorescence) time of level 2, which is on the range of 1μsec to 10msec. Also, $R_p = \sigma_p P_p/(a_p h \nu_p)$ and $R_s = \sigma_s P_s/(A_s h \nu_s)$ are the transition rates of pump and signal, with $\sigma_{p,s}$, $a_{p,s}$, and $\nu_{p,s}$ being the pump and signal's transition cross-section, mode area, and frequency, respectively.

A.2.3 Steady-State Population Inversion

The steady-state solution to Eq. (A.4), i.e $\partial N_2(z)/\partial t = 0$, leads to a population at level two given by:

$$N_2(z) = \frac{\overline{I_p}(z) + \overline{I_s}(z)}{1 + \overline{I_p}(z) + 2\overline{I_s}(z)} N_T. \tag{A.5}$$

Here, $\overline{I_p}(z) = I_p(z)/I_p^{sat}$ and $\overline{I_s}(z) = I_s(z)/I_s^{sat}$ are the pump and signal normalized intensities, with $I_p^{sat} = h\nu_p/(\sigma_p T_1)$ and $I_s^{sat} = h\nu_s/(\sigma_s T_1)$ being the pump and signal saturated intensities, respectively. Using Eq. (A.5) and the relation $N_1(z) = N_T - N_2(z)$, the steady-state population inversion, defined as $W_{ss}(z) = N_2(z) - N_1(z)$ is found to be:

$$W_{ss}(z) = \frac{\overline{I_p}(z) - 1}{1 + \overline{I_p}(z) + 2\overline{I_s}(z)} N_T, \tag{A.6}$$

where, $\overline{I}_p(z) = \sigma_p T_1 I_p(z)/h\nu_p$ and $\overline{I}_s(z) = \sigma_s T_1 I_s(z)/h\nu_s$ are the average pump, and signal, intensities, respectively. Another, more elaborate, analytical model for two-, three-, and four-level system rare earth doped fiber amplifiers is presented in [13].

A.2.4 Evolution of Signal and Pump Intensities

Neglecting the effects of spontaneous emission and assuming forward pump propagation (i.e in the same direction as the signal), the equation for the evolution of the pump intensity becomes:

$$\frac{1}{I_p(z)}\frac{dI_p(z)}{dz} = -\sigma_p N_1(z) - \alpha_p \tag{A.7a}$$

$$\frac{1}{I_s(z)}\frac{dI_s(z)}{dz} = -\sigma_p(N_2(z) - N_1(z)) - \alpha_s, \tag{A.7b}$$

where α_p and α_s are the fiber's intrinsic loss at the pump and signal wavelengths, respectively.

It is worth mentioning that the erbium ions do not respond to the fast variation of signal pulses with widths much less than the fluorescence time T_1. Because the energy of a single pulse is usually much smaller than the saturation energy of the EDFA (typically 1-10μJ), the amplifier will only respond to the average power of the signal pulse train.

A.3 The Fast Saturable Absorption (FSA)

A Fast Saturable Absorber (FSA) is an element that is used for compression of an optical pulse. As illustrated in Fig. A.2, a pulse approaches an FSA at time t_1. At time t_2, the leading edge of the pulse, which is propagating inside the FSA, is absorbed, causing the medium to saturate at t_3. At t_4, the medium is fully saturated

and the peak portion of the pulse is not absorbed. Because the saturation process is very fast, the relaxation of the upper level carriers occur while the pulse is still propagating inside the medium (t_4). That causes the tail of the pulse to be absorbed as well (t_5), resulting in an overall pulse compression effect (t_6).
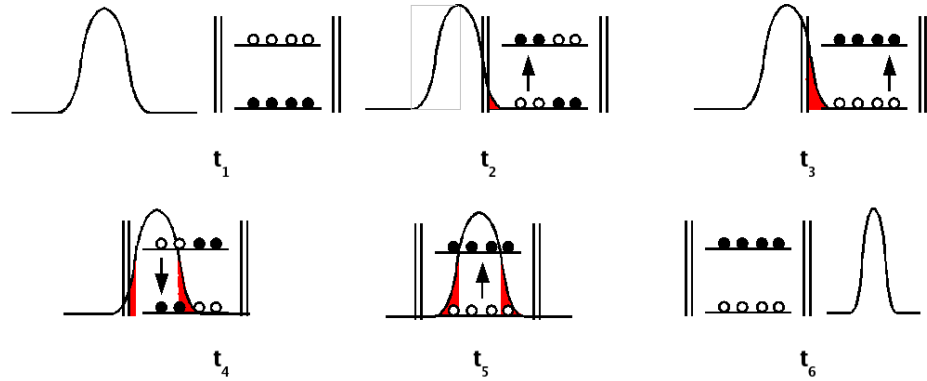
Figure A.2: Principle of pulse compression using a fast saturable absorber (FSA).

A.4 Nonlinear Polarization Rotation (NPR)

When both the SPM and XPM effects are present, an interesting phenomenon is manifested on the polarization state of the pulse as it propagates inside the fiber. As SPM and XPM are intensity dependent effects, the pulse experiences a nonlinear phase change which is also intensity dependent, and acts differently on the slow and fast axis of the fiber in the case where the orthogonal components have an initial phase difference, i.e an initial elliptical State-of-Polarization (SOP). As a result, the elliptical angle becomes intensity dependent as well. This phenomenon is referred to by several names in different articles, but is most commonly referred to as "nonlinear polarization rotation", or simply "NPR".

Appendix A. Properties of Optical Fibers

In order to understand the phenomenon mathematically, consider an optical pulse described by the electric field:

$$\mathbf{E}(z,t) = \begin{pmatrix} E_x(z,t) \\ E_y(z,t) \end{pmatrix} = \Re\{ \begin{pmatrix} A_x e^{-i\Delta k_x z} \\ A_y e^{-i(\Delta k_y z + \phi)} \end{pmatrix} \} e^{-ik_z z}, \tag{A.8}$$

where $\Delta k_{x,y} = k_0 \gamma(|A_{x,y}|^2 + (2/3)|A_{y,x}|^2)$, contains the nonlinear terms (i.e SPM and XPM, respectively), as before "$\Re$" represents real part, and "ϕ" is the phase difference between the "x", and "y" components.

Taking the real part leads to two equations, one in "x" and one in "y", which, after taking the squares on each side, and adding them together leads to:

$$(\frac{E_x}{A_x})^2 + (\frac{E_y}{A_y})^2 - 2(\frac{E_x}{A_x})(\frac{E_y}{A_y})\cos([\Delta k_y - \Delta k_x]z + \phi) = \sin^2([\Delta k_y - \Delta k_x]z + \phi). \tag{A.9}$$

Equation (A.9) is the representation of an ellipse at a coordinate system "$\overline{E_x E_y}$" which is rotated relative to its "*major axis*" of an angle "α" given by:

$$\alpha_{1,2} = \frac{1}{2}\tan^{-1}[(\frac{A_x(z_{1,2}, t_{1,2})A_y(z_{1,2}, t_{1,2})}{A_x^2(z_{1,2}, t_{1,2}) - A_y^2(z_{1,2}, t_{1,2})})\cos([\Delta k_{y1,2} - \Delta k_{x1,2}] - \phi)], \tag{A.10}$$

where the subscripts 1 and 2 indicate different spatial and time positions (Fig. A.3).

(a) Position 1.

(b) Position 2.
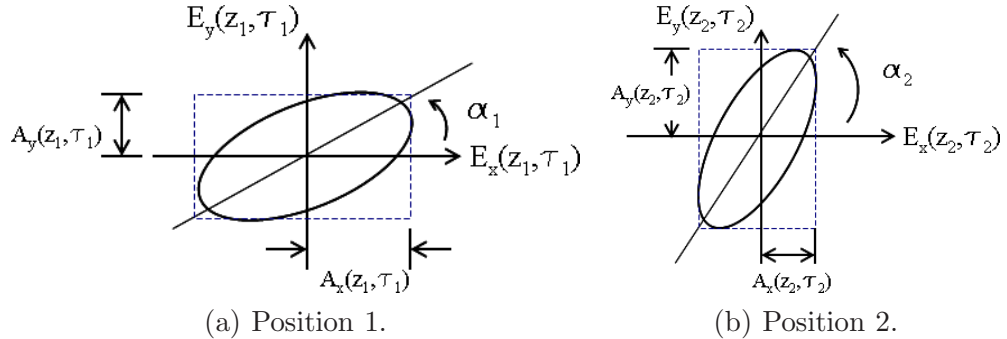
Figure A.3: Nonlinear elliptical angle of rotation at two different points in space (z) and time (t).

Figure A.4 illustrates the effect of NPR on the SOP of an elliptically polarized light traveling on the z-axis. As the light travels, the SOP of its high intensity components (red) rotates relative to the SOP of its low intensity components (blue). The role of NPR on mode-locked fiber lasers has and continues to be the subject of extensive studies [72, 82]. It has been modeled numerically [9], and its interplay with XPM for two components of different frequencies studied theoretically [92]. In a 2000 article [149], studies of NPR in highly birefringent fibers were presented both theoretically and experimentally. Recently, NPR associated to frequency-shifted feedback was used in an experiment to produce 9.3MHz repetition rate pulses, at 1050nm [8].
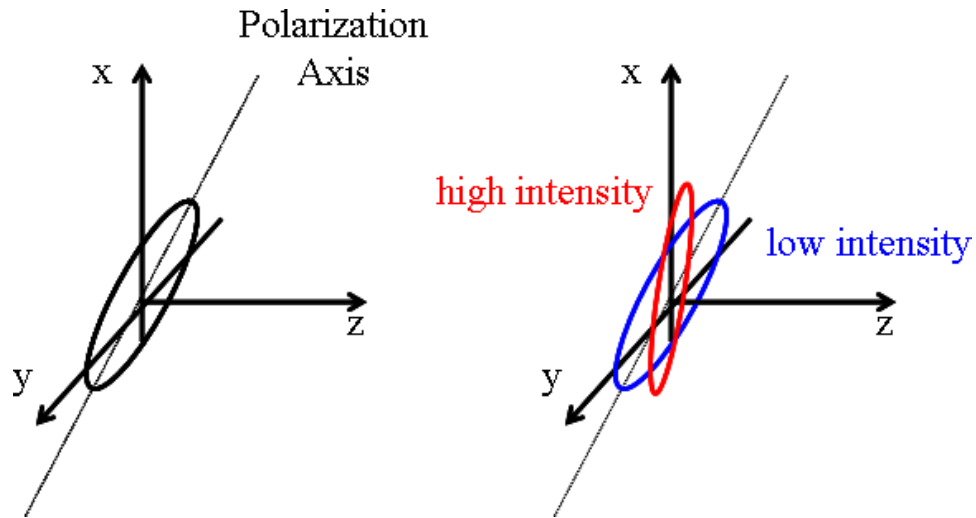
Figure A.4: Nonlinear rotation of elliptical polarization at higher (red), and lower (blue) intensity components of the optical pulse.

Appendix B

Optical Fiber Types

There are essentially four types of fiber used in the experiment: single mode fiber (SMF), erbium-doped fiber (EDF), dispersion-shifted fiber (DSF), and polarization maintaining fiber (PMF). Following is a brief description of each type, with some of the specifications which were provided by the manufacturer.

- **Single Mode Fiber (SMF):** it is the fiber type most commonly found in any fiber laser experiment, and used in most fiber coupled optical components. The standard SMF is Corning$^{\copyright}$ SMF-28$^{\text{TM}}$ Optical Fiber.

- **Dispersion-Shifted Fiber (DSF):** as the name suggests, it is a fiber with the zero dispersion wavelength shifted relative to the value of 1.31μm of typical fibers. The fiber used in the experiment was Corning$^{\copyright}$ SMF/DS$^{\text{TM}}$.

- **Erbium Doped Fiber (EDF):** as discussed before, the erbium-doped fiber is a type of fiber doped with rare-earth ions which provides the gain for the laser. The EDF used in this experiment was OFS$^{\copyright}$ EDF-MP980.

- **Polarization Maintaining Fiber (PMF):** polarization maintaining fibers are highly birefringent fibers types, some with beat lengths on the order of a
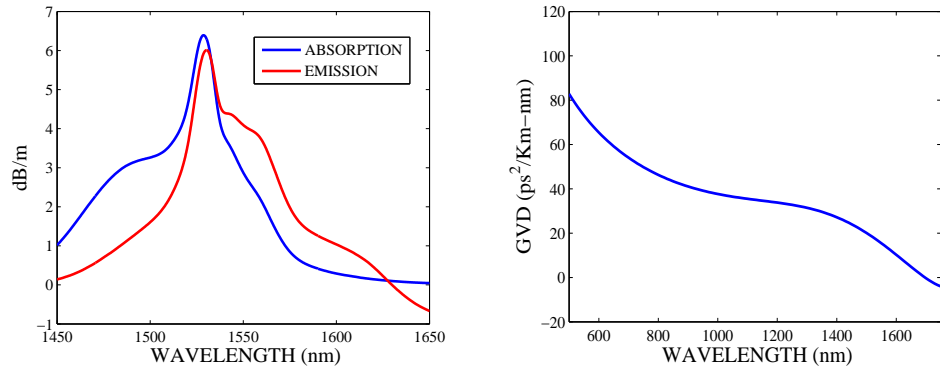
(a) Absorption coefficient and small signal gain parameters.

(b) Group-velocity-dispersion coefficient.

Figure B.1: Parameters for the OFS MP980 erbium-doped fiber: (a) Giles Parameters, and (b) GVD coefficient.

few milimeters. Figure B.2 shows the cross-section shapes of the three PMF types most commonly found in the market. The one used in the experiment was Fujikura© SM-15-P8, which is a "PANDA" type.

PANDA   BOW-TIE   3M
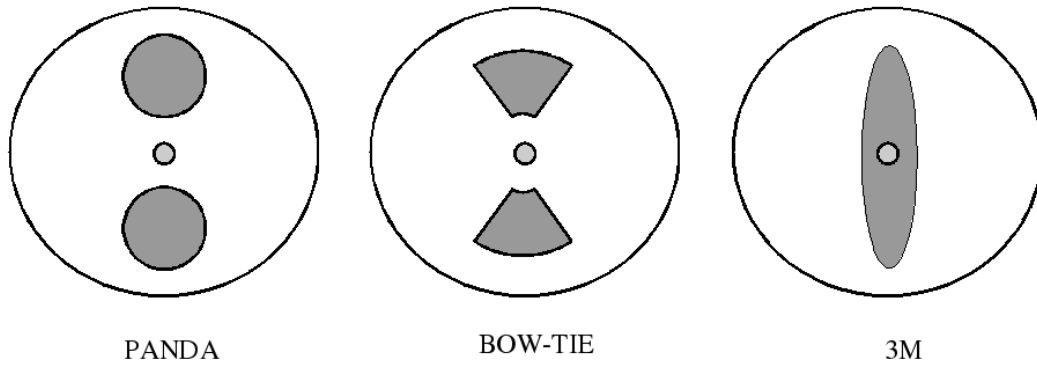
Figure B.2: Stress-rod structures for the most common types of polarization maintaining fibers.

Appendix B. Optical Fiber Types

Some of the most relevant specifications for the fibers used in the experiment, as provided by the manufacturers, are summarized in Table B.1.

Parameter	SMF	DSF	EDF	PMF
Mode-field diameter at 1550nm (μm)	9.2	8.10	6.01	10.5
Zero dispersion wavelength (nm)	1313	1550	-	-
Numerical aperture (NA)	0.14	0.17	0.23	-
Effective group index at 1550nm	1.4682	1.4711	1.4751	1.4948

Table B.1: Some specifications for the fibers used in the experimental setup.

Another important parameter, which is sometimes provided by the manufacturer, and, for this particular project, most relevant, is the Rayleigh back-scattering coefficient "r" of the fiber. Several techniques to determine an accurate value for "r" [63, 120, 44], and other theoretical studies of it [19, 108, 103] have been reported in the past. For an input intensity "I_{in}", the back-scattered intensity "I_{sc}" is given by:

$$I_{sc} = (1 - e^{\alpha l_{int}})I_{in} \simeq -(\alpha l_{int})I_{in}, \tag{B.1}$$

where "l_{int}", in the case of a bidirectional mode-locked fiber laser, is the length over which two counter-propagating pulses interact in the medium. Likewise, in terms of the input "E_{in}" and scattered "E_{sc}" optical fields:

$$E_{sc} = rE_{in} - \simeq -\frac{\alpha}{2}l_{int}E_{in}, \tag{B.2}$$

where the back-scattering coefficient $r = -\alpha l_{int}/2$, with "α" converted from dB/Km to Km^{-1}. For typical SMF, the intrinsic loss which results from Rayleigh scattering

is $\alpha \simeq$-0.12dB/Km at a wavelength of 1550nm [77]. For instance, if the medium is a SMF, and the pulses interact over a 1ns period (i.e l_{int}=0.2m), then $r = \ln(10) \cdot 0.012/(2 \cdot 5000) = 2.76 \cdot 10^{-6}$. The dead band can then be estimated for 1ns, 100ps, and 100fs pulses using Eq. (1.11).

Appendix C

Net GVD Measurements

During the experimental part of the project, one of the most important parameters, which influences considerably the functionality of the laser, was the cavity's net Group-Velocity-Dispersion (GVD). Tables C.1- C.4 show the components of the cavity, their physical length, the accumulated GVD over the length of each element, and the accumulated travel time over them.
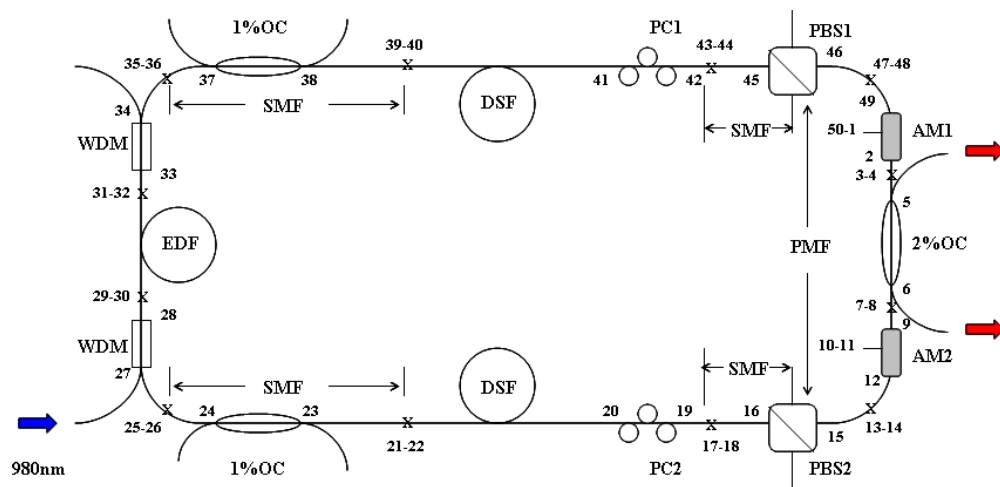
Figure C.1: Fiber types distribution of the two-modulator ring laser.

With the measured parameters from Tables C.1-C.4 is possible to obtain an estimate of the locations of the counter-propagating pulses' crossing points. From the accumulated travel time T_p, the location of a given pulse (cw or ccw) can be pin-pointed to an specific component of the laser. The same is true for the pulse propagating in the opposite direction using an accumulated travel time which counts propagation through the laser's elements in a reverse sense. To illustrate the idea, consider the example below, where a cw pulse fires at a time T=0 from M_1, and a ccw 97ns later from M_2.

$L_{X1} \approx 33.2$ m

M_1 L_0, $T_1 = 0$ sec

$L_{T2} \approx 20$ m

$P \approx 40.14$m, $T_{RT} \approx 197$ns

$\Delta\tau_{M1\text{-}M2} \approx 31$nsec

M_2, $T_2 = 97.5$nsec

$L_{X2} \approx 13$ m
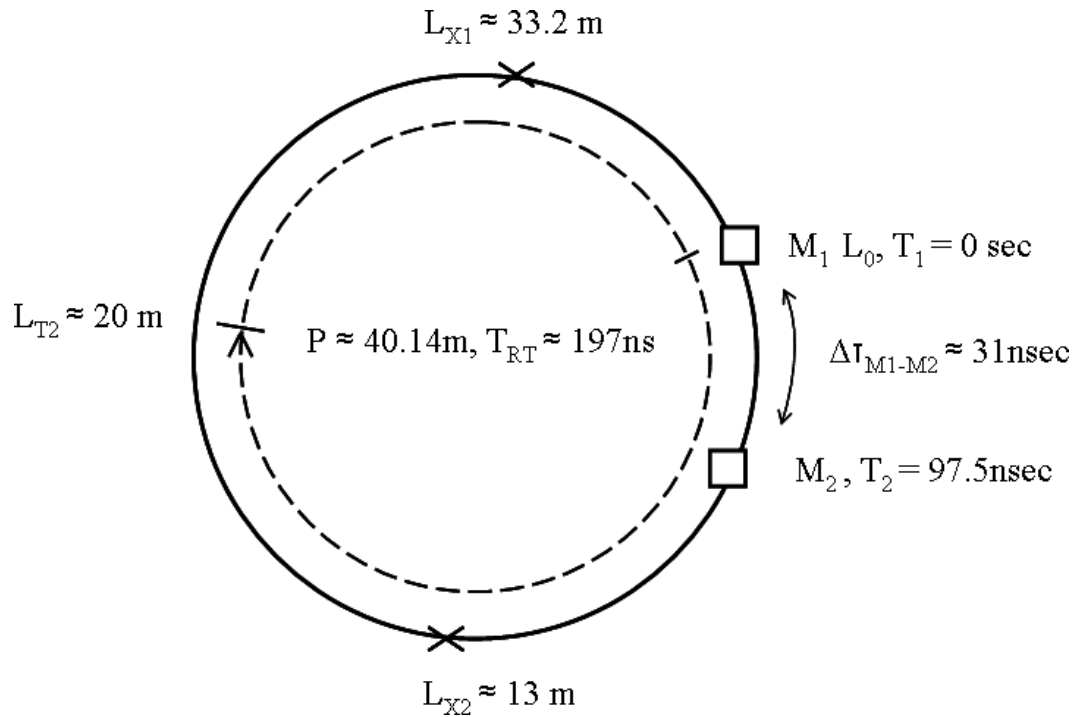
Figure C.2: Ring laser schematics to estimate the locations of the counter-propagating pulses' crossing points. M_1 and M_2 represent the amplitude modulators, "P" the perimeter, and "T_{RT}" the round-trip time. $\Delta\tau_{M1-M2}$ is the travel time between the modulators.

In Figure C.2, L_{T2} is the location of the cw pulse at time T_2 when M_2 fires for the ccw pulse. L_{X1} and L_{X2} are the locations of the two crossing points. At

Appendix C. Net GVD Measurements

$T_2 \simeq 97.5$ns, the cw pulse will have traveled a distance $L_{T2} = T_2\overline{v_g}$=20m, from M$_1$, out of the entire perimeter "P", when M$_2$ opens for the ccw pulse[1]. The two pulses will, therefore, cross at:

$$L_{x1} = \frac{1}{2}(P - L_{T2} + \Delta v_{pmf}T_{M1-M2}) \simeq 33.2m, \qquad (C.1)$$

from M$_1$ in a clockwise sense of direction, where v_{pmf} is the propagation velocity of the pulse at a PMF section (between the modulators). That puts one of the crossing points at branch 38-39 of Fig. C.1, i.e in a SMF section. Consequently, the second crossing point will be located at:

$$L_{x2} = L_{x1} - \frac{1}{2}P \simeq 13.13m, \qquad (C.2)$$

from M$_1$, which is in branch 22-23, i.e also a SMF section.

Tables C.1 through C.4 show the measured parameter values for each individual component of the actual laser. Parts where the number "2" appears represent splices between two sections of fiber (for instance "SMF2SMF/DS" is a splice between a single mode and a dispersion-shifted fiber).

---

[1]$\overline{v_g}$ is the average group velocity of the pulse as it travels through the laser's elements.

Branch	Component	Length (cm)	GVD (ps^2)	Travel Time (ns)
1-2	MOD	6.25 ± 0.10	0.00	0.31
2-3	PMF	171.70 ± 1.00	-0.0384	8.72
3-4	PMF2PMF	6.00 ± 0.10	-0.0013	9.01
4-5	PMF	72.80 ± 1.00	-0.00163	12.58
5-6	2%OC	2.00 ± 0.10	0.00	12.68
6-7	PMF	194.80 ± 1.00	-0.0436	22.22
7-8	PMF2PMF	6.00 ± 0.10	-0.0013	22.52
8-9	PMF	177.80 ± 1.00	-0.0398	31.23
9-10	MOD	6.25 ± 0.10	0.00	31.54
10-11	NONE	0.00 ± 0.00	0.00	31.54
11-12	MOD	6.25 ± 0.10	0.00	31.84
12-13	PMF	121.30 ± 1.00	-0.0271	37.79
13-14	PMF2PMF	6.00 ± 0.10	-0.0013	38.08
14-15	PMF	68.20 ± 1.00	-0.0152	41.42

Table C.1: GVD over a component's length and accumulated propagation times T_p for laser's components 1-15.

Branch	Part	Length (cm)	GVD (ps^2)	Tp (ns)
15-16	PBS	5.00 ± 0.50	0.00	41.67
16-17	SMF	97.10 ± 1.00	-0.0182	46.43
17-18	SMF2SMF/DS	6.00 ± 0.10	-0.0005	46.72
18-19	SMF/DS	44.60 ± 1.00	0.00094	48.90
19-20	PC	7.50 ± 0.25	0.00016	49.27
20-21	SMF/DS	287.20 ± 1.00	0.0061	63.34
21-22	SMF/DS2SMF	6.00 ± 0.10	-0.0005	63.64
22-23	SMF	16.90 ± 0.25	-0.0032	64.47
23-24	1%OC	5.50 ± 0.20	0.00	64.74
24-25	SMF	46.20 ± 1.00	-0.0086	67.00
25-26	SMF2SMF	6.00 ± 0.10	-0.0011	67.29
26-27	SMF	87.80 ± 1.00	-0.0164	71.60
27-28	980/1550 WDM	7.75 ± 0.25	0.00	71.98
28-29	SMF	35.30 ± 0.50	-0.0066	73.71
29-30	SMF2EDF	6.00 ± 0.10	-3.9E-05	74.00

Table C.2: GVD over a component's length and accumulated propagation times T_p for laser's components 15-30.

Branch	Part	Length (cm)	GVD (ps^2)	Tp (ns)
30-31	EDF	1491.30 ± 10	0.2595	147.07
31-32	EDF2SMF	6.00 ± 0.10	-3.9E-05	147.37
32-33	SMF	31.70 ± 0.50	-0.0059	148.92
33-34	980/1550 WDM	7.75 ± 0.25	0.00	149.30
34-35	SMF	17.80 ± 1.00	-0.0033	150.17
35-36	SMF2SMF	6.00 ± 0.10	-0.0011	150.47
36-37	SMF	124.20 ± 1.00	-0.0232	156.55
37-38	1%OC	5.50 ± 0.20	0.00	156.82
38-39	SMF	120.70 ± 1.00	-0.0226	162.74
39-40	SMF2SMF/DS	6.00 ± 0.10	-0.0005	163.03

Table C.3: GVD over a component's length and accumulated propagation times T_p for laser's components 30-40.

Branch	Part	Length (cm)	GVD (ps^2)	Tp (ns)
40-41	SMF/DS	58.80 ± 1.00	0.00124	165.91
41-42	PC	7.50 ± 0.25	0.00016	166.28
42-43	SMF/DS	278.30 ± 0.10	0.00588	179.92
43-44	SMF/DS2SMF	6.00 ± 0.10	-0.0005	180.21
44-45	SMF	100.50 ± 1.00	-0.0188	185.13
45-46	PBS	5.00 ± 0.50	0.00	185.38
46-47	PMF	80.10 ± 1.00	-0.0179	189.30
47-48	PMF2PMF	6.00 ± 0.10	-0.0013	189.60
48-49	PMF	138.40 ± 1.00	-0.0309	196.38
49-50	MOD	6.25 ± 0.10	0.00	196.69
TOTAL:		35.51	0.01	-0.05

Table C.4: GVD over a component's length and accumulated propagation times T_p for laser's components 40-50.

References

[1] K. S. Abedin and F. Kubota. Erbium-doped modelocked fiber laser generating sub-picosecond soliton pulses at 154 ghz rate. In *CLEO, CThO7*, pages 1707–1709. Opt. Soc. Am., 2003.

[2] F. Adler, K. Moutzouris, A. Leitenstorfer, H. Schnatz, B. Lipphardt, G. Grosche, and F. Tauser. Phase-locked two-branch erbium-doped fiber laser system for long-term precision measurements of optical frequencies. *Opt. Express*, 12:5872–5880, 2004.

[3] G. P. Agrawal. Modulation instability induced by cross-phase modulation. *Phys. Rev, Lett.*, 59:880–883, 1987.

[4] G. P. Agrawal. Agrawal replies. *Phys. Rev. Lett.*, 64:814, 1990.

[5] G. P. Agrawal. Amplification of ultrashort solitons in erbium-doped fiber amplifiers. *IEEE Phot. Tech. Lett.*, 2:875–877, 1991.

[6] G. P. Agrawal. Optical pulse propagation in doped fiber amplifiers. *Phys. Rev. A*, 44:7493–7501, 1991.

[7] G. P. Agrawal. Modulation instability in erbium-doped fiber amplifiers. *IEEE Phot. Tech. Lett.*, 4:562–564, 1992.

[8] A. Albert, V. Couderc, L. Lefort, and A. Barthelemy. High-energy femtosecond pulses from an Ytterbium-doped fiber laser with a new cavity design. *IEEE Phot. Tech. Lett.*, 16:416–418, 2004.

[9] J. Ares, M. T. Flores-Arias, V. Kermne, A. Desfarges-Berthe1emot, and A. Barthlmy. Numerical modelling of nonlinear ellipse rotation. In *SPIE Conference Series*.

References

[10] L. Arissian and J. C. Diels. Investigation of carrier to envelope phase and repetition rate — fingerprints of mode-locked laser cavities. *J. Phys. B: At. Mol. Opt. Phys*, 42:183001, 2009.

[11] M. Asobe, T. Kanamori, and K. Kubodera. Applications of highly nonlinear chalcogenide glass fibers in ultrafast all-optical switches. *IEEE J. Quantum Elect.*, 29:2325–2333, 1993.

[12] C. A. Balanis. *Advanced Engineering Electromagnetics*. John Wiley & Sons, Inc., New York, 1989.

[13] C. Barnard, P. Myslinski, J. Chrostowski, and M. Kavehrad. Anaytical model for rare-earth-doped fiber amplifiers and lasers. *IEEE J. Quantum Elect.*, 30:1817–1829, 1994.

[14] R. A. Bergh, H. C. Lefevre, and H. J. Shaw. An overview of fiber-optic gyroscopes. *J. Lightwave Tech.*, LT-2:91–107, 1984.

[15] N. H. Bonadeo, W. H. Knox, J. M. Roth, and K. Bergman. Passive harmonic mode-locked soliton fiber laser stabilized by an optically pumped saturable bragg reflector. *Opt. Lett.*, 25(19):1421–1423, October 2000.

[16] A. Bononi, A. Vannucci, A. Orlandini, E. Corbel, S. Lanne, and S. Bigo. Degree of polarization degradation due to cross-phase modulation and its impact on polarization-mode dispersion compensators. *J. Lightwave Tech.*, 21:1903–1913, 2003.

[17] A. Braga and R. Kay L. Wang J. C. Diels, R. Jain. Bidirectional mode-locked fiber ring laser using passively controlled threshold gating. In *CLEO 2010*, San Jose, Ca, 2010. Optical Society of America.

[18] A. B. Braga, J-. C. Diels, R. Jain, and R. Kay. Radio frequency self-regenerated locked optical oscillator. U.S. Patent Application 61/203,091, 2008.

[19] E. Brinkmeyer. Backscattering in single-mode fibres. *Electron. Lett*, 16:329–330, 1980.

[20] T. F. Carruthers, I. N. Duling, and M. L. Dennis. Active-passive modelocking in a single-polarisation erbium fiber laser. *Electron. Lett.*, 30:1051–1053, 1994.

[21] C. W. Chang and S. Chi. Mode-locked erbium-doped fibre ring laser using nonlinear polarization rotation. *J. Mod. Opt.*, 45:355–362, 1998.

[22] C. W. Chang and S. Chi. Ultrashort pulse generation from mode-locked erbium-doped fibre ring lasers. *J. Mod. Opt.*, 46:1431–1442, 1999.

References

[23] Y. Chaoyu, P. Jiangde, and Z. Bingkun. Tunable Nd3+-doped fiber ring laser. *Electron. Letters*, 25:101–102, 1989.

[24] C.-J. Chen, P. K. A. Wai, and C. R. Menyuk. Self-starting of passively mode-locked lasers with fast saturable absorbers. *Opt. Lett.*, 20(4).

[25] J. Chesnoy. Picosecond gyrolaser. *Opt. Lett.*, 14(18).

[26] S. Chi, C.-W. Chang, and S. Wen. Femtosecond soliton propagation in erbium-doped fiber amplifiers: the equivalence of two different models. *Opt. Comm.*, 106:193–196, 1994.

[27] P. C. Chou, J. M. Fini, and H. A. Haus. Demonstration of a feed-forward PMD compensation technique. *IEEE Phot. Tech. Lett.*, 14(2):161–163, 2002.

[28] W. W. Chow, J. Gea-Banacloche, L. M. Pedrotti, V. E. Sanders, W. Schleich, and M. O. Scully. The ring laser gyro. *Rev. Mod. Phys.*, 57(1):61–104, 1985.

[29] D. N. Christodoulides and R. I. Joseph. Vector solitons in birefringent nonlinear dispersive media. *Opt. Lett.*, 13(1).

[30] B. Culshaw. The optical fibre sagnac interferometer: an overview of its principles and applications. *Meas. Sci. Technol.*, 17:R1–R16, 2006.

[31] M. Curtin and P. O'Brien. Phase-locked loops for high-frequency receivers and transmitters: Part 1. *Analog Dialogue*, 33(3):1–4, March 1999.

[32] M. Curtin and P. O'Brien. Phase-locked loops for high-frequency receivers and transmitters: Part 2. *Analog Dialogue*, 33(5):1–4, May 1999.

[33] M. Curtin and P. O'Brien. Phase-locked loops for high-frequency receivers and transmitters: Part 3. *Analog Dialogue*, 33(7):1–5, July/August 1999.

[34] A. O. DalForno, A. Paradisi, R. Passy, and J. P. von der Weid. Experimental and theoretical modeling of polarization-mode dispersion in single-mode fibers. *IEEE Phot. Tech. Lett.*, 12(3):296–298, 2000.

[35] T. T. Dang. *Towards a compact mode locked laser gyroscope: Study of a fiber ring laser and a Nd:YVO4 ring laser.* Doctoral dissertation, University of New Mexico, Albuquerque, NM, USA, Jan 2005.

[36] Y. Deng, M. W. Koch, F. Lu, G. W. Wicks, and W. H. Knox. Colliding-pulse passive harmonic mode-locking in a femtosecond Yb-doped fiber laser with a semiconductor saturable absorber. *Opt. Express*, 12:3872–3877, 2004.

References

[37] D. J. Derickson, R. J. Heikey, A. Mar, P. A. Morton, and J. E. Bowers. Self-mode-locking of a semiconductor laser using positive feedback. *Appl. Phys. Lett.*, 56:7–9, 1990.

[38] J. C. Diels. Detection of groundwater through ultra-sensitive magnetic measurements with ultra-short pulse lasers. WWRI Technical Report No. 313.

[39] J. C. Diels. Instrumentation for measurement of femtotesla magnetic fields and small changes of magnetic susceptibility. Technical Report.

[40] J. C. Diels and I. C. McMichael. Influence of wave-front-conjugated coupling on the operation of a laser gyro. *Optics Lett.*, 6:219–221, 1981.

[41] J. C. Diels and W. Rudolph. *Ultrashort Laser Pulse Phenomena, Second Ed.* Academic Press, Burlington, MA, 2006.

[42] N. J. Doran and D. Wood. Nonlinear-optical loop mirror. *Opt. Lett.*, 13:56–58, 1988.

[43] D. Eliyahu and L. Maleki. Novel tunable opto-electronic oscillator. In *GOMATEch03 Conference*, Tampa, FL, 2003. OEWaves, Inc.

[44] R. Ellis. Explanation of reflection features in optical fiber as sometimes observed in OTDR measurement traces. Corning, Inc., May 2007.

[45] B. I. Escamilla, E. A. Kuzin, D. E. G. Garcia, F. G. Zainos, S. M. Vazquez, and J. W. Haus. A mode-locked fibre laser using a sagnac interferometer and nonlinear polarization rotation. *J. Optics A*, 5:S225–S230, 2003.

[46] B. I. Escamilla, E. A. Kuzin, F. G. Zainos, R. T. Garcia, J. W. Haus, R. R. Laguna, J. M. E. Ayala, and J. W. Haus. Measurement of beat length in short low-birefringence fibers using the fiber optical loop mirror. *Opt. Comm.*, 217:211–219, 2003.

[47] S. G. Evangelides, L. F. Mollenauer, J. P. Gordon, and N. S. Bergano. Polarization multiplexing with solitons. *J. Lightwave Tech.*, 10:28–35, 1992.

[48] A. Eyal. Polarization dependence of the intensity modulation transfer function of an optical system with PMD and PDL. *IEEE Phot. Tech. Lett.*, 14:1515–1517, 2002.

[49] X. Fang, D. N. Wang, W. Jin, H. L. Ho, and F. W. Tong. Combined mutual pulse injection-seeding and active mode locking system for wavelength tunable optical short pulse generation. *Opt. Express*, 13:3872–3877, 2005.

References

[50] M. E. Fermann. Ultrashort-pulse sources based on single-mode rare-earth-doped fibers. *Appl. Phys. B*, 58:197–209, 1994.

[51] M. E. Fermann, M. J. Andrejco, Y. Silberberg, and M. L. Stock. Passive mode locking by using nonlinear polarization evolution in a polarization-maintaining erbium-doped fiber. *Opt. Lett.*, 18:894–896, 1993.

[52] M. E. Fermann, M. J. Andrejco, M. L. Stock, Y. Silberberg, and A. M. Weiner. Passive mode locking in erbium fiber lasers with negative group delay. *Appl. Phys. Lett.*, 62:910–912, 1993.

[53] M. E. Fermann, F. Haberl, M. Hofer, and H. Hochreiter. Nonlinear amplifying loop mirror. *Opt. Lett.*, 15:752–754, 1990.

[54] M. E. Fermann, K. Sugden, and I. Bennion. High-power soliton fiber laser based on pulse width control with chirped fiber bragg gratings. *Opt. Lett.*, 20:172–174, 1995.

[55] M. E. Fermann, L.-M. Yang, M. L. Stock, and M. J. Andrejco. Environmentally stable kerr-type mode-locked erbium fiber laser producing 360-fs pulses. *Opt. Lett.*, 19:43–45, 1994.

[56] R. A. Fisher and W. Bischel. The role of linear dispersion in plane-wave self-phase modulation. *Appl. Phys. Lett.*, 23:661–663, 1973.

[57] R. A. Fisher and W. K. Bischel. Numerical studies of the interplay between self-phase modulation and dispersion for intense plane-wave laser pulses. *J. Appl. Phys.*, 46:4921–4934, 1975.

[58] J. A. Fleck, J. R. Morris, and M. D. Feit. Time-dependent propagation of high energy laser beams through the atmosphere. *Appl. Phys.*, 10:129–160, 1976.

[59] C. Francia, F. Bruyere, D. Penninckx, and M. Chbat. PMD second-order effects on pulse propagation in single-mode optical fibers. *IEEE Phot. Tech. Lett.*, 10(12):1739–1741, 1998.

[60] C. S. Gardner, J. M. Green, M. D.Kruskal, and R. M. Miura. Method for solving the Korteweg-deVries equation. *Phys. Review Lett.*, 19(19).

[61] D. S. Gasper, P. F. Wysocki, W. A. Reed, and A. M. Vengsarkar. Evaluation of chromatic dispersion in erbium-doped fibers. In *LEOS'93 Conference Proceedings*, pages 167–168. IEEE, USA, ISBN 0-7803-1263-5, 1993.

[62] C. R. Giles and E. Desurvire. Modeling erbium-doped fiber amplifiers. *J. Lightwave Tech.*, 9:271–283, 1991.

References

[63] M. P. Gold and A. H. Hartog. Measurement of backscatter factor in single-mode fibres. *Electron. Lett.*, 17:965–966, 1981.

[64] L. A. Gomes, L. Orsila, T. Jouhti, and O. G. Okhotnikov. Picosecond SESAM-based Ytterbium mode-locked fiber lasers. *IEEE J. Select. Top. Quant. Electron.*, 10:129–136, 2004.

[65] Y. D. Gong, P. Shum, D. Y. Tang, C. Lu, X. Guo, V. Paulose, W. S. Mand, and H. Y. Tam. Regimes of operation states in passively mode-locked fiber soliton ring laser. *Optics and Laser Tech.*, 36:299–307, 2004.

[66] V. S. Grigoryan and T. S. Muradyan. Evolution of light pulses into autosolitons in nonlinear amplifying media. *J. Opt. Soc. Amer. B.*, 8:1757–1765, 1991.

[67] A. B. Grudinin and S. Gray. Passive harmonic mode locking in soliton fiber lasers. *J. Opt. Soc. Amer. B.*, 14:144–154, 1997.

[68] I. Hickman. *Hickman's Analog and RF Circuits.* Newnes, Oxford, 1998.

[69] J. B. Hong, Y. B. Yeo, B. W. Lee, and B. Y. Kim. Phase sensitive detection for mode-locked fiber laser gyroscope. *IEEE Phot. Tech. Lett.*, 11(8):1030–1032, 1999.

[70] I. N. Duling III. All fiber ring soliton laser mode locked with a nonlinear mirror. *Optics Lett.*, 16:539–541, 1991.

[71] I. N. Duling III. Subpicosecond all-fiber erbium laser. *Electron. Lett.*, 27:544–545, 1991.

[72] I. N. Duling III. *Compact Sources of Ultrashort Pulses.* Cambridge Univ. Press, Cambridge, UK, 1995.

[73] M. Y. Jeon, H. J. Jeon, and B. Y. Kim. Mode-locked fiber laser gyroscope. *Opt. Lett.*, 18:320–322, 1993.

[74] H. J. Jeong, J. H. Kim, H.-W. Lee, and B. Y. Kim. Birefringence modulation in fiber-optic phase modulators. *Opt. Lett.*, 19:1421–1423, 1994.

[75] H. J. Jeong, Y. W. Koh, B. W. Lee, M. Y. Jeon, and B. Y. Kim. Analysis of polarization properties of a mode-locked fiber laser gyroscope. *Applied Optics*, 35:2206–2210, 1996.

[76] Q. Jing-ren, S. Jue, and W. Xu xu. Z. Bing. Bidirectional single-mode er-doped fiber ring laser. *Optoelectronics Letters*, 3(1):0034–0036, Jan 2007.

References

[77] H. Kanamori, H. Yokota, G. Tanaka, M. Watanabe, Y. Ishiguro, I. Yoshida, T. Kakii, S. Itoh, Y. Asano, and S. Tanaka. Transmission characteristics and reliability of pure-silica-core single-mode fibers. *J. Lightwave Tech.*, LT-4:1144–1150, 1986.

[78] U. Keller. Recent developments in compact ultrafast lasers. *Nature*, 424:831–838, 2003.

[79] R. Khosravani and A. E. Willner. System performance evaluation in terrestrial system with high polarization mode dispersion and the effect of chirping. *IEEE Phot. Tech. Lett.*, 13(4):296–298, 2001.

[80] K. Kieu and M. Mansuripur. All-fiber bidirectional passively mode-locked ring laser. *Opt. Lett.*, 33:64–66, 2008.

[81] N. Kikuchi. Analysis of signal degree of polarization degradation used as control signal for optical polarization mode dispersion compensation. *J. Lightwave Tech.*, 19:480–486, 2001.

[82] A. D. Kim, J. N. Kutz, and D. J. Muraki. Pulse-train uniformity in optical fiber lasers passively mode-locked by nonlinear polarization rotation. *IEEE J. of Quantum Elect.*, 36:465–471, 2000.

[83] S. K. Kim, H. K. Kim, and B. Y. Kim. Er3-doped fiber ring laser for gyroscope applications. *Opt. Lett.*, 19:1810–1812, 1994.

[84] R. Kiyan and B. Y. Kim. An er-doped bidirectional ring fiber laser with 90 faraday rotator as phase nonreciprocal element. *IEEE Phot. Tech. Lett.*, 10(3):340–342, 1998.

[85] E. A. Kuzin, B. I. Escamilla, D. E. Garcia-Gomez, and J. W. Haus. Fiber laser mode locked by a sagnac interferometer with nonlinear polarization rotation. *Opt. Lett.*, 26(20).

[86] K. Y. Lau and A. Yariv. Self-sustained picosecond pulse generation in a GaAlA laser at an electrically tunable repetition rate by optoelectronic feedback. *Appl. Phys. Lett.*, 42:124–126, 1984.

[87] B. W. Lee, H. J. Jeong, and B. Y.Kim. High-sensitivity mode-locked fiber laser gyroscope. *Opt. Lett.*, 22(2).

[88] L. Lefort, A. Albert, V. Couderc, and A. Barthelemy. Highly stable 68-fs pulse generation from a stretched-pulse Yb^{3+}-doped fiber laser with frequency shifted feedback. *IEEE Phot. Tech. Lett.*, 14:1674–1676, 2002.

References

[89] R. Leners and T. Georges. Numerical and analytical modeling of polarization-dependent gain in erbium-doped fiber amplifiers. *J. Opt. Soc. Amer. B.*, 12:1942–1954, 1995.

[90] I. T. Lima, R. Khosravani, P. Ebrahimi, E. Ibragimov, C. R. Menyuk, and A. E. Willner. Comparison of polarization mode dispersion emulators. *J. Lightwave Tech.*, 19:1872–1880, 2001.

[91] G.-R. Lin and Y.-L. Cheng. A delay-time tunable mode-locked erbium doped fiber ring laser system. In *CLEO, CTuX3*, page 245, Baltimore, MD, 2001. Opt. Soc. Am.

[92] Q. Lin and G. P. Agrawal. Vector theory of cross-phase modulation: Role of nonlinear polarization rotation. *IEEE J. of Quantum Elect.*, 40:958–964, 2004.

[93] J. Liu, P. F. Wysocki, M. Andrejco, and B. Palsdottir. Power conversion efficiency characterization of erbium-doped silica fibers in L-band. *Opt. Eng.*, 40:1195–1198, 2001.

[94] W. H. Loh, D. Atkinson, P. R. Morkel, M. Hopkinson, A. Rivers, A. J. Seeds, and D. N. Payne. All-solid-state subpicosecond passively mode locked erbium-doped fiber laser. *Appl. Phys. Lett.*, 63:4–6, 1993.

[95] M. Margalit, M. Orenstein, and G. Eisenstein. High-repetition-rate mode-locked Er-doped fiber lasers by harmonic injection locking. *Opt. Lett.*, 17:1791–1793, 1995.

[96] V. J. Matsas, T. P. Newson, D. J. Richardson, and D. N. Payne. Self-starting passively mode-locked fibre ring soliton laser exploiting nonlinear polarisation rotation. *Electron. Lett.*, 28:1391–1393, 1992.

[97] V. J. Matsas, T. P. Newson, and M. N. Zervas. Self-starting passively mode-locked fibre ring laser exploiting nonlinear polarisation switching. *Opt. Comm.*, 92:61–66, 1992.

[98] Xianmei Meng, Jean-Claude Diels, Dietrich Kuehlke, Robert Batchko, and Robert Byer. Ultra-short pulse OPO ring laser. In *CLEO 2000, technical digest*, volume CMW7, page 122, San Francisco, Ca, 2000. Optical Society of America.

[99] C. R. Menyuk. Nonlinear pulse propagation in birefringent optical fibers. *IEEE J. of Quantum Elect.*, QE-23:174–176, 1987.

[100] C. R. Menyuk. Pulse propagation in an elliptically birefringent Kerr medium. *IEEE J. of Quantum Elect.*, 25(12):2674–2682, December 1989.

References

[101] C. R. Menyuk. Application of multiple-length-scale methods to the study of optical fiber transmission. *J. Eng. Math.*, 36:113–136, 1999.

[102] C. R. Menyuk. Interaction of nonlinearity and polarization mode dispersion. *J. Opt. Fiber Commun. Rep.*, 1:305–311, 2004.

[103] M. D. Mermelstein, R.P. Jr., G. A. Johnson, and S. T. Vohra. Rayleigh scattering optical frequency correlation in a single-mode optical fiber. *Optics Lett.*, 26:58–60, 2001.

[104] R. Min, S. Xiao-Han, and Z. Ming-De. A modified split-step fourier method for optical pulse propagation with polarization mode dispersion. *Chinese Physics*, 12:0502–0505, 2003.

[105] M. Moenster, P. Glas, and G. Steinmeyer. Mode-locked Nd-doped microstructured fiber laser. *Opt. Express*, 12:4523–4528, 2004.

[106] P. M. Morse and H. Feshbach. *Methods of Theoretical Physics*. McGraw-Hill, New York, 1953.

[107] P. Myslinski and J. Chrostowski. Gaussian-mode radius polynomials for modeling doped fiber amplifiers and lasers. *Microwave and Opt. Tech. Letters*, 11(2):61–64, February 1996.

[108] M. Nakazawa. Rayleigh backscattering theory for single-mode optical fibers. *J. Opt. Soc. Am.*, 73:1175–1180, 1983.

[109] M. Nakazawa, E. Yoshida, and K. Tamura. Ideal phase-locked-loop (PLL) operation of a 10GHz erbium-doped fibre laser using regenerative modelocking as an optical voltage controlled oscillator. *Electron. Lett.*, 33, 1997.

[110] M. Navarro, O. Chalus, and J. C. Diels. Mode-locked ring lasers for backscattering measurement of mirror. *Opt. Lett.*, 31:2864–2866, 2006.

[111] L. E. Nelson, R. M. Jopson, H. K. Kogelnik, and J. P. Gordon. Measurement of polarization mode dispersion vectors using the polarization-dependent signal delay method. *Opt. Express*, 6:158–167, 2000.

[112] M. A. Newhouse, D. L. Weldman, and D. W. Hall. Enhanced-nonlinearity single-mode lead silicate optical fiber. *Opt. Lett.*, 15(21).

[113] R. Nietzke, J. Sacher, W. Elsasser, and E. O. Gobel. Mode locking of a semiconductor laser by self-synchronising optoelectronic feedback of the longitudinal mode beats. *Electron. Letters*, 26:1016–1018, 1990.

References

[114] R. Noe, S. Hinz, D. Sandel, and F. Wust. Crosstalk detection schemes for polarization division multiplex transmission. *J. Lightwave Tech.*, 19:1469–1475, 2001.

[115] R. Noe, D. Sandel, , V. Mirvoda, F. Wust, and S. Hinz. Polarization mode dispersion detected by arrival time measurement of polarization-scrambled light. *J. Lightwave Tech.*, 20:229–235, 2002.

[116] D. U. Noske, N. Pandit, and J. R. Taylor. Subpicosecond soliton pulse formation from self-mode-locked erbium fibre laser using intensity dependent polarisation rotation. *Electron. Letters*, 28:2185–2186, 1992.

[117] M. H. Ober, M. Hofer, and M. E. Fermann. 42-fs pulse generation from a mode-locked fiber laser started with a moving mirror. *Opt. Lett.*, 18:367–369, 1993.

[118] J. Oksanen and J. Tulkki. Coherent optical logic by laser amplifiers with feedback. *J. Lightwave Tech.*, 24:4918–4924, 2006.

[119] J. J. O'Neil. *Pulse Dynamics in Actively Modelocking Fiber Optics Lasers.* Honor thesis, University of Washington, Seattle, WA, 2002.

[120] J. Park, N. Y. Kim, W. Choi, and H. Lee N. Park. Determination of backscatter coefficient from third-order Rayleigh effect in a raman amplifier. *IEEE Phot. Tech. Lett.*, 16:1459–1461, 2004.

[121] K. H. Park, H. S. Cho, D. H. Jang, B. W. Lee, and B. Y. Kim. Mode-locked fiber laser gyroscope based on a distributed-feedback semiconductor laser amplifier. *Opt. Lett.*, 21(1).

[122] N. R. Pereira and L. Stenflo. Nonlinear Schrödinger equation including growth and damping. *Phys. Fluids*, 20:1733–1734, 1977.

[123] M. W. Phillips, A. I. Ferguson, G. S. Kino, and D. B. Patterson. Mode-locked fiber laser with a fiber phase modulator. *Opt. Lett.*, 14(13).

[124] J. E. Rothenberg. Modulational instability of copropagating frequencies for normal dispersion. *Phys. Rev, Lett.*, 64:813, 1990.

[125] G. Sagnac. L'éther lumineux démontré par l'effet du vent relatif d'éther dans un interféromètre en rotation uniforme. *Comptes Rendus*, 157:S. 708–710, 1913.

[126] G. Sagnac. Sur la preuve de la réalité de l'éther lumineux par l'expérience de l'interférographe tournant. *Comptes Rendus*, 157:S. 1410–1413, 1913.

References

[127] M. Salhi, H. Leblond, and F. Sanchez. Theoretical study of the erbium-doped fiber laser passively mode-locked by nonlinear polarization rotation. *Phys. Rev. A*, 67:013802/1–013802/7, 2003.

[128] N. H. Seong and D. Y. Kim. A new figure-eight fiber laser based on a dispersion-imbalanced nonlinear optical loop mirror with lumped dispersive elements. *IEEE Phot. Tech. Lett.*, 14:459–461, 2002.

[129] S. Y. Set, H. Yaguchi, Y. Tanaka, M. Jablonski, Y. Sakakibara, A. Rozhin, M. Tokumoto, H. Kataura, Y.Achiba, and K. Kikuchi. Mode-locked fiber lasers based on a saturable absorber incorporation carbon nanotubes. postdeadline paper PD44, Conference on Optical Fiber Communications, 2003.

[130] M. Shtaif, A. Mecozzi, M. Tur, and J. A. Nagel. A compensator for the effects of high-order polarization mode dispersion in optical fibers. *IEEE Phot. Tech. Lett.*, 12(4):434–436, 2000.

[131] A. E. Siegman. *Lasers.* University Science Books, Sausalito, CA, 1986.

[132] H. Sotobayashi, J. T. Gopinath, E. M. Koontz, L. A. Kolodziejski, and E. P. Ippen. Wavelength tunable passively mode-locked bismuth oxide-based erbium-doped fiber laser. *Opt. Comm.*, 237:399–403, 2004.

[133] K. M. Spaulding, D. H. Yong, A. D. Kim, and J. N. Kutz. Nonlinear dynamics of mode-locking optical fiber ring lasers. *J. Opt. Soc. Am.*, B-19:1045–1054, 2002.

[134] H. Sunnerud, M. Karlsson, C. Xie, and P. A. Andrekson. Polarization-mode dispersion in high-speed fiber-optic transmission systems. *J. Lightwave Tech.*, 20:2204–2218, 2002.

[135] H. Sunnerud, C. Xie, M. Karlsson, R. Samuelsson, and P. A. Andrekson. A comparison between different PMD compensation techniques. *J. Lightwave Tech.*, 20:368–378, 2002.

[136] T. R. Taha and M. I. Ablowitz. Analytical and numerical aspects of certain nonlinear evolution equations. II. numerical, nonlinear Schrödinger equation. *J. Comp. Phys*, 55(2):203–230, 1984.

[137] K. Tamura, C. R. Doerr, L. E. Nelson, H. A. Haus, and E. P. Ippen. Technique for obtaining high-energy ultrashort pulses from an additive-pulse mode-locked erbium-doped fiber ring laser. *Optics Lett.*, 19:46–48, 1994.

[138] K. Tamura, H. A. Haus, and E. P. Ippen. Self-starting additive pulse mode-locked erbium fibre ring laser. *Electron. Lett*, 28:2226–2228, 1992.

References

[139] K. Tamura, E. P. Ippen, H. A. Haus, and L. E. Nelson. 77-fs pulse generation from a stretched-pulse mode-locked all-fiber ring laser. *Optics Lett.*, 18:1080–1082, 1993.

[140] K. Tamura, L. E. Nelson, H. A. Haus, and E. P. Ippen. Soliton versus nonsoliton operation of fiber ring lasers. *Appl. Phys. Lett.*, 64:149–151, 1994.

[141] E. Tangdiongga, J. P. Turkiewicz, G. D. Khoe, and H. de Waardt. Clock recovery by a fiber ring laser employing a linear optical amplifier. *IEEE Phot. Tech. Lett.*, 16:611–613, 2004.

[142] M. Tiihonen. *Stretched Pulse Generation in Erbium-doped Fibre Ring Laser.* Master thesis, Royal Institute of Technology, Stockholm, 2002.

[143] R. Q. Torres, M. Ackerman, M. Navarro, and J. C. Diels. Scatterometer using a bidirectional ring laser. *Opt. Comm.*, 240:179–183, 2004.

[144] M. V. Tratnik and J. E. Sipe. Bound solitary waves in a birefringent optical fiber. *Phys. Rev. A*, 38(4).

[145] T. Ueda and W. L. Kath. Dynamics of coupled solitons in nonlinear optical fibers. *Phys. Rev. A*, 42:563–571, 1990.

[146] N. G. Usechak, G. P. Agrawal, and J. D. Zuegel. FM mode-locked fiber lasers operating in the autosoliton regime. *IEEE J. Quantum Elect.*, 41:753–761, 2005.

[147] A. Usman, J. Osman, and D. R. Tilley. Numerical simulation of soliton pulse propagation in doped optical fibres by finite difference method. *Turk J. Phys.*, 28:17–24, 2004.

[148] V. Uzunoglu. Synchronous oscillator outperforms the pll. *EDN*, pages 111–118, November 1999.

[149] C. Vinegoni, M. Wegmuller, B. Huttner, and N. Gisin. Measurement of nonlinear polarization rotation in a highly birefringent optical fibre using a Faraday mirror. *J. Optics A*, 2:314–318, 2000.

[150] S. Wabnitz. Modulational polarization instability of light in a nonlinear birefringent dispersive medium. *Phys. Rev. A*, 38:2018–2021, 1988.

[151] D. Wang, E. A. Golovchenko, A. N. Pilipetskii, C. R. Menyuk, and M. F. Arend. Nonlinear optical loop mirror based on standard communication fiber. *J. Lightwave Tech.*, 15:642–646, 1997.

References

[152] H. G. Winful and D. T. Walton. Passive mode locking through nonlinear coupling in a dual-core fiber laser. *Optics Lett.*, 17:1688–1690, 1992.

[153] C. Wu and N. K. Dutta. High-repetition-rate optical pulse generation using a rational harmonic mode-locked fiber laser. *IEEE J. of Quantum Elect.*, 36:145–149, 2000.

[154] S. Wu, J. Strait, R. L. Fork, and T. F. Morse. High-power passively mode-locked Er-doped fiber laser with a nonlinear optical loop mirror. *Optics Lett.*, 18:1444–1446, 1993.

[155] S. Yamashita, Y. Inoue, K. Hsu, T. Kotabe, H. Yaguchi, D. Tanaka, M. Jablonski, and S. Y. Set. 5-GHz pulsed fiber Fabry-Perot laser mode-locked using carbon nanotubes. *IEEE Phot. Tech. Lett.*, 17:750–752, 2005.

[156] C. Yan, K. P. J. Reddy, J. G. McIerney, and R. Jain. Picosecond semiconductor lasers based on regenerative feedback schemes. In *LEOS '93 Conference Proceedings*.

[157] C. C. Yang and J. S. Wang. Cross-polarization cross-phase modulation of femtosecond pulses in erbium-doped fiber amplifiers. *J. Opt. Soc. Amer. B.*, 9:682–686, 1992.

[158] X. S. Yao, G. Lutes, and L. Malek. A novel photonic clock and carrier recovery device. In *Proc. SPIE 2556*, pages 118–127, 1995.

[159] X. S. Yao and L. Malek. A light-induced microwave oscillator. TDA Technical Report 42-123, November 1995. Tracking Systems and Applications Section.

[160] X. S. Yao and L. Maleki. Converting light into spectrally pure microwave oscillation. *Opt. Lett.*, 21(7).

[161] X. S. Yao and L. Maleki. Dual microwave and optical oscillator. *Opt. Lett.*, 22(24).

[162] A. Yariv. *Optical Electronics, Fourth Ed.* Holt, Rinehart and Wiston, Philadelphia, PA, 1991.

[163] N. Yu, M. Tu, E. Salik, and L. Maleki. Opto-electronic generation of low-jitter pulsed signals. In *LEOS Conference, Invited Paper: TuBB2*. IEEE Catalog, 2002.

[164] S. C. Yun, Y. K. Tak, and H. G. Park. Regeneratively and harmonically mode-locked figure-of-eight fiber soliton laser with a stabilized repetition rate. *J. Korean Phys. Soc.*, 36(3):148–152, March 2000.

References

[165] V. E. Zakharov and A. B. Shabat. An exact theory of two-dimensional self-focusing and of one-dimensional self-modulation of waves in non-linear media. *Soviet Physics - JETP*, 34:62–69, 1972.

[166] V. E. Zakharov and A. B. Shabat. On the theory of two-dimensional stationary self-focusing of electromagnetic waves. *Soviet Physics - JETP*, 38:248–253, February 1974.

[167] B. Zhao, D. Y. Tang, P. Shum, W. S. Mand nd H. Y. Tam, Y. D. Gong, and C. Lu. Passive harmonic mode locking of twin-pulse solitons in an erbium-doped fiber ring laser. *Opt. Comm.*, 229:363–370, 2004.